Modelling and experimental characterization of an ionic polymer metal composite actuator

PJ Friend

orcid.org 0000-0003-2162-494X

Dissertation submitted in fulfilment of the requirements for the degree *Master of Engineering in Electrical and Electronic Engineering* at the North-West University

Supervisor: Dr AJ Grobler
Prof G van Schoor
Dr D Bessarabov

Graduation May 2018

Student number: 23440228

Abstract

This study is about modelling an ionic polymer metal composite (IPMC) actuator and the experimental characterization thereof. In this study a brief background on IPMCs are given to the reader and then the research that has been done in various fields that are of importance to this study was discussed. From this the equipment required to develop an experimental setup was determined. The experimental setup was designed and mainly consist of a load cell, a laser displacement sensor, a data acquisition system, and a clamp for the IPMC.

A grey box model was used that consist of an electrical equivalent circuit and an electromechanical model. The model was implemented in Simulink and was verified by using parameters and results from literature. The parameter estimation that was done in Simulink was also verified with those values. The model was developed for a Nafion N117 sample plated with a Platinum loading of 10 $mgPt/cm^2$. The model could sufficiently predict the absorbed current and the blocked force.

The behaviour of seven different samples were investigated. Samples varied in terms of the Platinum loading and the membrane thickness. The response of each sample was investigated for different input voltages. The influence of input voltage, input frequency, humidity and temperature was also investigated. It was seen that the amplitude of the input voltage, the relative humidity and the temperature affect the response of the IPMC greatly. The experimental data from the sample was used to validate the model. The model could sufficiently predict the blocked forces and the displacement for a step input.

Keywords: *Ionic polymer metal composites, actuator, equivalent circuit model*

Contents

List of Figures

List of Tables

List of Acronyms

EAP electro active polymer

FEA finite element analysis

FEM finite element method

HySA Hydrogen South Africa

IPMC ionic polymer metal composite

PCB printed circuit board

PEM proton exchange membrane

PGM platinum group metals

PID proportional-integral-derivative

RTD resistance temperature detector

SEM scanning electron microscope

TEM transmission electron microscope

List of Symbols

List of Symbols

ρ_m	Density
Y	Young's modulus
ϵ	Permittivity
ρ	Resistivity
R	Resistance
C	Capacitance
f	Force
δ	Displacement
V	Voltage
I	Current
L	Length
w	Width
h	Thickness
d	Electromechanical coefficient

Chapter 1

Introduction

This chapter is an introduction where a brief background is given to the reader. This is followed by the research objectives to show what the study is about and then the research methodology is discussed. An overview of the rest of the document is also given.

1.1 Background

An ionic polymer metal composite (IPMC) is part of the electro active polymer (EAP) group. An EAP is a polymer that expands, contracts or bends when an electric stimulus is applied. It is mainly divided into two types, electric and ionic EAP. An IPMC is an ionic EAP as ion movement causes the deformation. A typical IPMC consists of a polymer membrane (Nafion or Flemion) film which is plated with a noble metal (Platinum or Gold) on both sides to form the electrodes [2]. Inside the polymer the anions are fixed and the cations are free to move. The water inside the polymer attaches to the cation to form a hydrated cation. When a voltage is applied over the electrodes, the hydrated cations move towards the cathode. This causes the membrane to swell on the cathode side and shrink on the anode side due to the water being concentrated on

one side. This causes the membrane to bend towards the anode. Figure 1.1 illustrates this working principle of an IPMC. From this phenomenon it is clear that the IPMC needs to stay hydrated to work effectively. Due to the nature of the IPMC it can be used while submerged in a fluid. When the IPMC is physically bent it produces a small potential over the electrodes. Its electromechanical properties make it possible to use as an actuator or sensor. It has been shown that an IPMC can be constructed in such a way that it can be used as a self-sensing actuator, which means a single piece of polymer is simultaneously used as a sensor and actuator.

Some of the advantages IPMCs have is that it is lightweight and biocompatible. It is easy to miniaturize and can operate in wet environments. It also requires low voltages (up to 3 V) for large deformations with respect to the size of the IPMC. It is not perfect and has its disadvantages, namely back relaxation which is the phenomenon that occurs after it has bent towards the anode some of the water starts to move back to its original place causing the IPMC to slowly bend back to its original position. It generally has a low blocking force. The deformation is dependent on water and the IPMC exhibits water loss due to evaporation and electrolysis which decreases its performance. The properties of the IPMC make them very attractive in robotic and biomedical applications. Over the last couple of decades researchers have been looking at ways to improve the shortcomings of IPMCs, how to model and control the IPMC and real world applications.

1.2 Research objectives

The main goal of this study is to investigate the electromechanical properties of an IPMC as an actuator. This includes the modelling and characterization of an IPMC actuator. The effect of environmental conditions on the characteristics of the IPMC will also be studied.

Doing research in this field may lead to new possible applications for platinum group metals (PGM) which forms part of Hydrogen South Africa (HySA)'s goals. The elec-

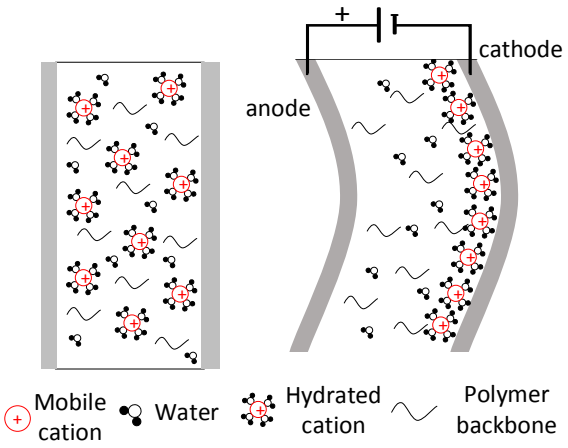

Figure 1.1: Principle of IPMC as actuator

tromechanical process is similar to proton exchange membrane (PEM) electrolysers and compressors. By doing research on sensors and actuators that are based on PEM technology there is a possibility to unlock certain fundamental relationships between degradation and performance as well as related to water management processes.

1.3 Research methodology

The research methodology that was followed in this thesis is illustrated in figure 1.2. It starts with a literature study. This is followed by developing an experimental test setup to do the various experiments. Next, the IPMC actuator needs to be modelled. Then the IPMC can be characterized through various experiments. Finally the model used can be validated with experimental results.

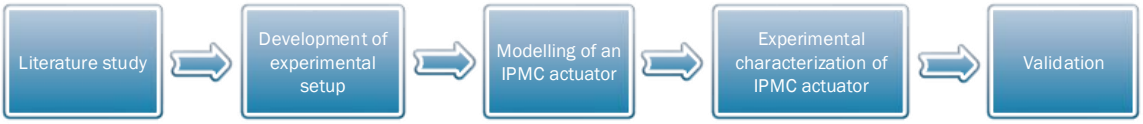

Figure 1.2: Research methodology followed

1.4 Issues to be addressed

Literature study

A comprehensive literature study needs to be done by investigating the IPMC working principle and the different variations of IPMCs that have been used. The experiments that have been done on IPMCs and the different equipment required for the experiments also need to be investigated. Where these sensors and actuators have been used and where it is possible to use them will also be looked at. Different modelling methods that have been used needs to be investigated as a model will be used in this thesis. Along with the models the methods used to validate these models will also be looked at to decide how the model will be validated in the end.

Development of the experimental setup

To determine the specifications for the experimental setup, the main characteristics that will be investigated must first be chosen. The various inputs and outputs that need to be measured can then be determined. Along with the types of measurements, it is important to know what the ranges of the measurements will be as it influences the equipment required. The environmental conditions that the experimental setup will be exposed to will be taken into consideration. From the specifications determined, the types and ranges of measurements are available and the proper measuring equipment need to be chosen. When choosing equipment the range and accuracy is very important. The test setup must be designed with the ease of use in mind, with easy and small changes when changing between experiments. The experimental setup will be designed to comply with all the specifications.

Modelling of an IPMC actuator

From the literature, the different modelling approaches need to be compared to decide what model will be used. It is also important to decide what the model must be able to predict and under what conditions. The process of building this model will start with a basic model, the model will be tested and more complexity can then be added for better accuracy or to add more features to the model. The environment in which the model will be simulated needs to be chosen. The simulated results from the model will be compared to the experimental results. The model also needs to be verified and this can be done by comparing results from the model with results found in literature.

Experimental characterization of IPMC actuator

The characteristics that will be investigated will be determined from the literature. The various experiments will be done and each experiment will be repeated multiple times to ensure better results. Different experiments can be done to study the effects that different inputs and different environmental conditions might have on the actuator. It is critical that during all the experiments that the samples used are kept hydrated to ensure the performance stays the constant during experimentations. The data from the experiments will be used to characterize the IPMC actuator.

Validation

In the validation phase, the data from the model's simulations will be compared to the experimental results to determine if the model could predict the output of the IPMC actuator sufficiently. The model can also be tested under different conditions to determine under what circumstances the model can successfully predict the behaviour of the IPMC actuator and where it fails to predict the behaviour.

1.5 Document overview

In Chapter 2 the different research that has been done in the field is discussed. There are a wide variety of categories in which research has been done on IPMCs which includes improving the IPMC properties, modelling and control of IPMCs and using them in applications. How this research was used for the purpose of this study is also discussed.

Chapter 3 explains how the experimental test setup was designed. The equipment chosen to measure the necessary inputs and outputs are discussed. The relevant hardware and software that is required to be able to take the measurements is also described. The mechanical setup and the integration of the whole setup is discussed.

Chapter 4 is about how to model an IPMC actuator. It describes the electromechanical model that was chosen and how it was implemented. Parameter estimation is done to determine the parameters from experimental values. The model is also verified in this chapter.

In Chapter 5 the experimental characterization of the IPMC actuator is done. Samples with different thicknesses and Platinum loadings were investigated. The effect of the amplitude and frequency of the input voltage was studied. The effect that humidity and temperature have on the actuator was also investigated. The model from Chapter 4 was validated with experimental results.

Chapter 6 is a conclusion of the study that was done. In this chapter some remarks on the results achieved in the study is discussed and recommendations for future work is given.

Chapter 2

Literature survey

In this chapter different types of research that has been done on IPMCs were studied. This includes what has been done to improve IPMCs, the effects that environmental conditions have on IPMC actuators and sensors, different modelling and control methods that have been used, and the applications of IPMCs actuators and sensors.

2.1 Enhancement of performance

In IPMCs there are many factors that influence its performance, like the type of membrane used, the thickness of the electrodes, the electrode surface resistance and the amount of water inside the membrane. It is also well known that IPMCs have its drawbacks, like back relaxation and water loss. Many studies have been done on minimizing these drawbacks and improving the performance of the IPMCs in general.

It is possible to change the counter ion inside the membrane and the performance of different counter ions have been compared where it was seen that Lithium (Li^+) as counter ion delivers the largest blocked force [3]. The effect of surface resistance has

also been investigated in [4] and it was seen that an increase in forces of up to 20% can be achieved when a thin layer of silver or copper is deposited on top of the platinum layer of the IPMC. The effect of the thickness of the electrode layer has also been investigated and from experimental results it was seen that there is an optimal thickness which is approximately 2 μm [5]. The experimental setup used can also influence the performance as [6] showed that there is an optimal point in the clamping pressure where best performance can be achieved.

A study on the lifetime of Ag-IPMCs was done in [7]. From literature it was found that an encapsulated IPMC will be more protected against water loss when operated in air. A parylene coating was chosen for this purpose. It was reported that IPMCs with ionic solution can operate longer in air. From specifications for the electrolyte solvents found in literature, the authors decided on propylene carbonate. $LiClO_4$ was used as electrolyte salts. The lifetime of the IPMC with water as solvent and the IPMC with ionic liquid as solvent was tested. Both IPMCs were also tested with a parylene coating. By using this ionic liquid and the coating, the lifetime of the IPMC was almost 15 times longer.

In [8] the authors study the recent advances of IPMCs and the modelling and applications thereof. In section 2 they focus on the development of high performance IPMCs. Different improvements from literature on the material are stated. This includes the using of ionic liquids as solvents, nanoparticle reinforced Nafion-IPMCs, and multi-walled carbon nanotube based electrodes. Different hydrocarbon-based polymers that could be used instead of the conventional Nafion membrane are discussed. These polymers show advantages like a larger tip displacement and no back relaxation.

2.2 Environmental conditions

2.2.1 Temperature dependence

In [9] the IPMC's capability to operate in sub-zero temperatures was investigated. The IPMC that was tested used water as a solvent. The hydration of an IPMC influences the ionic conductivity of the material. The deformation and the blocking force of the IPMC is dependent on the ionic conductivity. This investigation was done to determine how the IPMC can actuate at temperatures lower than the freezing point of water. At temperatures below 0 °C only some of the water in the IPMC had frozen. The blocking force of the IPMC was tested at different temperatures below 0 °C. The blocking force was plotted against the input voltage at −30 °C. The slope of the blocking force at −30 °C had a parabolic form where at room temperature the blocking force versus the input voltage is more linear. There is a notable decrease in the blocking force at sub-zero temperatures. The author modelled the blocking force for varying temperature based upon the ion conductivity but the behaviour of the IPMC was more complex as there was a large difference between the estimation and the actual blocking force below 0 °C. The IPMC can operate at low temperatures if the supply voltage is increased to get the desired blocking force.

2.2.2 Humidity dependence

The effect of the ambient humidity on the sensing characteristics of IPMCs was investigated in [10]. The frequency response was measured at various humidity levels. Constant-voltage charging experiments were also conducted at different humidity levels. The relative humidity range was 38% to 80%. The humidity-dependent parameters were identified. The following physical parameters change with a change in relative humidity: Young's modulus, strain-rate damping coefficient, viscous air damping coefficient, dielectric constant and the ionic diffusivity. From this a model was developed that includes the dependence on the humidity. The humidity-dependent model was

compared to the humidity-independent model and the experimental data. From the frequency response it is clear that the humidity-dependent model corresponds with the experimental data.

The electrical characteristics of a Nafion-based IPMC with ionic liquid were evaluated at different humidity levels [11]. Tests were done at 20%, 40%, 60% and 80% relative humidity (RH). An equivalent circuit model was developed which consists of a membrane resistance in series with the double layer capacitance which is then connected in parallel with the geometric capacitance. The membrane resistance decreases exponentially with an increase in relative humidity. The double layer capacitance increases with an increase in humidity. This capacitance increases more rapidly with the increase in humidity at a higher voltage.

2.3 Modelling

The modelling techniques used can be divided into three categories namely black box models, grey box models and white box models. Black box models don't contain any physical information and is solely based on system identification. These models give a good estimation of the response of the IPMC but as it doesn't contain any physical information it isn't scalable and can't be used on other IPMCs. Grey box models take the well-known physical phenomena of the polymer and represent it more graphically with equivalent circuits. These models are less complex but still contain a sufficient amount of physical information and is more practical when designing a system where an IPMC is used. White box models attempt to model the fundamental physical mechanisms that cause the actuation. The complexity of these models are much higher than the other models but it can accurately describe the behaviour of the IPMC and more complex shapes can be modelled [12].

2.3.1 Black box models

In [13] the authors developed a neural network model to model the hysteresis of an IPMC sensor. A compensator was developed based on the neural network model to reduce the effect of hysteresis. This was done to be able to get an approximately linear relationship between the input and output of the IPMC sensor. With this model it was possible to compensate for the effect of hysteresis and it achieved satisfactory results in producing a linear input-output relationship.

In [14] a model that takes hysteresis and the dynamics of an IPMC sensor into account was proposed. First they make use of a hysteretic operator to transform the multi-valued mapping of the input and output of the hysteresis in the IPMC sensor to a single valued mapping. The nonlinear dynamics of the IPMC sensor is described with a nonlinear auto-regressive and moving average model with exogenous input. A d-step-ahead nonlinear predictive scheme was used to compensate for the time delay that may exist in the IPMC sensor. A model based predictive compensator is proposed to eliminate the effect of hysteresis, the dynamics and the time delay of the sensor. The proposed model method showed better results than the neural network based strategy [14].

A nonlinear black box model was proposed to model the bending behaviour of an IPMC in [15]. A general multilayer perceptron neural network that has one input, one output and hidden layers was built. A smart learning mechanism based on an extended Kalman filter with self-decoupling ability was used to train the neural network. This model could accurately predict the tip displacement of the IPMC.

2.3.2 White box models

Samaranayake [16] used finite element method (FEM) to describe the three dimensional behaviour of an IPMC actuator. He used similarities between the electro-mechanical behaviour of an IPMC and the thermal expansion and contraction of a bi-metallic strip

to model the behaviour of the IPMC. The contraction and expansion theory was used to predict the deflection of the IPMC while the large deflection theory was used to determine the shape. From mathematical equations it was shown that the strain of the IPMC is linearly dependent on the applied voltage. The model is based on the fact that the volume change due to ion transport is the same as the deformation in a bi-metallic strip due to a temperature difference. Samaranayake stated that the advantage of this modelling approach is that it would be possible to simulate the deflection of an IPMC of any odd shape without having to construct it first. To determine the shape of the IPMC a large deflection model was used where it was assumed that the IPMC beam was under a uniformly distributed load. This model uses a strip to determine the characteristics of the IPMC which is used to refine the model. After this the model can be used to predict the behaviour of a more complex shape of IPMC. A design procedure was described. The large deflection and small deflection model was compared with experimental results where it was seen that the large deflection model determined the shape correctly. A strip was used to refine the model parameters and the model was used to predict the behaviour of a semi-circular shape. The model was able to predict the deformation of the semi-circular IPMC.

The author in [16] used the principle of the thermal expansion of a bi-metallic strip to model the large deflections of the IPMC actuator. The bending motion of an IPMC with an applied voltage is similar to the deformation of a bi-metallic strip when it is exposed to a temperature difference. It is possible to simulate the deflections of any shape IPMC before it is constructed. To achieve this a strip must first be made from the exact same material. The FEM model for this strip is then developed. From experiments the parameters of the FEM model can be refined to match the actual deflections. This model can then be used to simulate any shape of IPMC that is made from the exact material. This was tested with a semi-circular shaped actuator and the experimental data agreed with the FEM simulation.

Simpson developed a finite element analysis (FEA) model that can predict the deflection and force of an IPMC actuator [17]. The force model uses equations that are based on physics. There is one parameter that must be experimentally determined for the

specific sheet of IPMC. The model was used to determine the effect that the shape and size of the IPMC has. A rectangular and triangular shape was modelled. The force of the triangle is almost half of that of the rectangle. The deflection of the triangle was also slightly smaller than that of the rectangle. The deflection of the rectangular IPMC had an error of 2.77% and the force had an error of 23.37% whereas the deflection and force of the triangular IPMC had an error of 13.3% and 4.92% respectively. This model has a large error in the determination of the force.

2.3.3 Grey box models

An intuitive graphical representation of the governing equations of a system can be obtained by using an equivalent circuit with lumped parameters. If defined properly, the circuit elements can have clear physical interpretations that enables the user to investigate the relationship between elements without having to study the underlying equations [18].

Throughout the literature there are a few different grey box models that make use of an equivalent circuit together with a couple of mechanical equations to model the behaviour of an IPMC. These models vary in complexity and most of the current models are some sort of derivation of the model Newbury et al proposed [19].

Newbury et al proposed a linear electromechanical model for IPMCs that can be used to model a sensor or actuator in a single framework [19]. The author also wanted to use the model to compare the electrical, mechanical and electromechanical coupling properties of IPMCs with other transducers. An equivalent circuit model is used and the energy conversion between the electrical and mechanical domain is done by using an ideal linear transformer. According to the author this type of model has been used to model piezoelectric transducers, electromagnetic speakers and electrostatic devices.

Considering the IPMC as a cantilever beam, it is possible to derive an equation for the mechanical impedance due to the stiffness of the IPMC. An inertial term also represented as a mechanical impedance is used to improve the accuracy as the frequency

approaches the first natural frequency of the IPMC. The electrical circuit is made up of two components, a resistor and an impedance which represents the dc resistance and the ability to store electrical charge respectively. For simplicity the IPMC was viewed as a homogeneous material with perfectly conductive electrodes. The IPMC has a high resistance at dc and a small resistance at high frequencies with a high capacitive component at intermediate frequencies. The impedance of the electrical circuit thus consists of multiple parallel branches with a resistor and capacitor in series. The electromechanical coupling is represented the turns ratio of a linear transformer. The equations used to determine the electromechanical coupling is similar to that used in piezoelectric transducers. The various circuit elements are described through material properties and transducer dimensions. The input-output relationships can be used to compare transducer technologies and to get a better insight in how different dimensions effect the performance, which is a useful design tool.

In [20] Newbury et al looks at the parameter estimation and model validation through various experimental results. Due to various factors the experimental validation was not an easy task. Some of these factors were to keep the IPMC at a constant hydration level as it was tested in air and back relaxation when a step voltage is applied. Due to variations in performance of transducers with similar dimensions the parameter estimation and model validation was done on the same IPMC. Through experiments it was shown that between 0 - 20 Hz the IPMC acts predominantly as a linear elastic material which means viscoelasticity is not significant in the frequency range of this work. The author stated that the highest charge densities are achieved at frequencies of 0.1 Hz and below.

In [2] Bonomo et al presents a new nonlinear lumped parameter model to describe the electrical behaviour of an IPMC actuator. The author described three types of currents namely ionic, electronic, and displacement current. From this an equivalent circuit was developed. Tests were done at various frequencies and voltages. From the I-V characteristics it was seen that at low frequencies (10 mHz - 10 Hz) there is a nonlinear behaviour. At frequencies between 10 Hz and 500 Hz the behaviour is capacitive. At frequencies higher than 500 Hz the IPMC has a resistive behaviour with no deforma-

tion observed.

From this a nonlinear dynamic grey box model was developed. It uses a nonlinear electrical model to describe the absorbed current when a voltage is applied over the electrodes and then an electromechanical model is used to derive a relationship between the absorbed current and the actuation of the IPMC [18]. The model used has similarities to that of [19] as the electrical circuit was used and improved to make it able to predict the nonlinearity that would occur at voltages higher than 1.2 V. The system was mainly modelled in the time domain due to the nonlinearity of the model. IPMCs with different types, dimensions, and counter-ions were tested experimentally. The model consist of two stages, a nonlinear electrical stage that determines the absorbed current from the input voltage and a linear electromechanical stage that determines the blocked force or tip deflection from the absorbed current from the first stage. The electrical stage was improved from previous work like [19] by adding a section to represent the nonlinearly in the current due to the applied voltage and a surface resistance is also introduced. It was stated that two parallel RC branches in the equivalent circuit can predict the dynamic behaviour with less free parameters. The model proved accurate enough to predict the behaviour of the IPMC.

Various authors used the model from [18] with some changes. Authors have used simplified versions of this model like [21] who used only one RC branch with no nonlinear part in the electrical stage. In this paper the authors used the total electric charge to determine the displacement and also used the cantilever beam theory to determine the force. The model could predict the displacement for inputs 1 Hz and below. Other authors like [22] also explored a more complex version of this model. Where the clamped section of the IPMC was also modelled in the electrical stage. The clamped section looks similar to the free section with the surface resistance between the two sections. The steady state current was modelled using a third order polynomial that is dependent on the input voltage, this was done by using variable resistors for both steady state resistors. The mechanical stage was also done differently by using a segmented mechanical beam to enable more precise prediction of the bending curve by predicting the tip bending angle and the blocked torque rather than the linear displacement and

blocked force. This model was accurate for inputs up to 3 V. It is also scalable and external load as an input.

Various authors proposed equivalent circuit models that are more simplified that could predict the outputs it was designed for. Diab proposes an electro mechanical model to predict the behaviour of an IPMC when a voltage is applied over the electrodes [23]. The model consists of two integrated blocks. The first block is the electrical model that is derived from the electrical properties of the IPMC, a RC circuit with a dc voltage. The second block determines the deformation of the IPMC from any load that is applied. The electrical model was simplified to a RC circuit that consists of the capacitance and resistance of the IPMC, the applied voltage and the voltage across the capacitor. The mechanical model starts with a free body diagram of the IPMC beam attached to a fixed support. The density per unit load that is applied along the cantilever beam is derived from the electrical model and the load force is applied at the tip of the beam. From the structural analysis the displacement under a specified load with a specified applied voltage can be determined. This model is able to predict the load that the IPMC can hold at a specific applied voltage. The model can predict the load and the deflection and can be useful in applications like micro-grippers.

2.4 Control

To be able to use IPMCs in applications it must be able to give the required responses and for this some type of control is necessary. A wide variety of techniques have been used in the control of IPMCs in specific applications. These techniques include feedback and feedforward control. Some of these techniques are proportional-integral-derivative (PID), nonlinear control, robust control and iterative feedback tuning. This enables the designer to ensure that the IPMC acts as planned, as some of the drawback can be compensated for in the control. There are various methods that can be used to control the output of an IPMC and in this section a few of the methods are described to show that it is possible. Most methods are divided into feedforward or feedback

controllers where the feedback approach is the most used [8].

According to [24] the creep characteristics of IPMCs limits the further application of IPMCs in integrated systems. A control method to resist this creep effect was proposed. The authors developed and tested the feasibility of a sliding mode control controller for IPMCs with different shapes and dimensions. Force and displacement experiments were done and showed that this is an effective control method.

[25] stated that a precise and robust control scheme is required to be able to control IPMCs in a predictable manner and to minimize the effects of external disturbances. An adaptive feedforward control scheme for the control of the displacement of an IPMC was proposed. It consisted of three parts, adaptive system identification, an adaptive feedforward controller, and adaptive noise cancellation. The controller could accurately capture the dynamics of the system, had satisfactory reference-tracking, a fast convergence, and the noise cancellation provided a tolerance against sensor noise and external disturbances.

In [26] the authors propose using an artificial bee colony operator approach to achieve precise position control. A nonlinear dynamic model with uncertainties was used for the IPMC. A robust right coprime factorization approach is used to develop a robust control system for the IPMC. A PI controller was used and the artificial bee colony algorithm was used to obtain the parameters for the PI controller. It was shown that the IPMC control output tracks the desired reference.

In [27], an IPMC actuator was used in an inverted pendulum on a cart system. This was done to validate if IPMC material can be used in more complex applications where the actuator undergoes large deformations. A full-state linear quadratic optimal controller and a full-state observer was designed. Using a virtual cart position as feedback rather than the actual cart position it was possible to stabilize the pendulum repeatedly. A surgical tool using IPMC actuators was developed and tested by Fu et al. A strain gage is used to measure deflection on the cantilever beam. The output force was controlled from the feedback of the strain gage. A simple linear PI controller was used to control

the cutting depth and it maintained a cutting force of 1 gf [28].

[29] developed a control scheme to achieve constant finger-tip displacement for a two finger microgripper without making use of external sensors. The microgripper is made from two IPMCs where one is used as the actuating IPMC and one is used as the sensing IPMC. A one degree of freedom PID controller was tuned using iterative feedback tuning. The control scheme has a zero steady state error for displacements up to 0.25 mm and 15 and 20 % steady sate error for a displacement of 0.45 and 0.75 mm respectively.

2.5 Applications

2.5.1 Actuator

Lumia et al shows the design of a microgripper that aims at being used for the gripping and manipulation of micro-organisms [30]. The gripper consists of two fingers made from ionic polymer metal composite (IPMC) which is compliant and can operate in dry and wet conditions. A force model was developed. Experiments were done with different finger sizes and with rigid and flexible objects. The gripper could lift an object of 15 mg with a force of 85 μN. It was found that a IPMC microgripper is suited for manipulation of bio-materials. Various other microgrippers have been developed [31–36].

An underwater microrobot was developed as it can be used in underwater monitoring operations [37]. By making use of 10 IPMC legs the robot is capable of walking, rotating, grasping and floating motions. The IPMC actuator was modelled as a supported cantilever beam. The robot used three proximity sensors to avoid collision with objects. The robot could float by applying a very low frequency (0.05 Hz) signal to four of the legs to electrolyse the water next to these IPMC legs. The robot was able to float with a maximum payload of 0.3 g. According to the authors, grasping small objects

while walking or floating was the most important function of this microrobot. Various other types of microrobots have been developed [38–42].

Micropumps have the potential to be used as biomedical devices and micro systems [43]. A new diaphragm was designed using FEM simulations of the displacement and strain of the IPMC. The diaphragm was fabricated and tested. The displacement was tested at different voltages and different frequencies. The deformation was improved from 0.2 mm of the conventional design to 0.4 mm. The performance of the conventional design decreases rapidly after 8 min whereas the new design had a stable operation for 35 min. [44] did experimentation and characterization of an IPMC as a flat valve micropump.

Feng et al developed and tested a digitally controlled 5 x 5 tactical display [45]. Each PDMS bump was driven by two IPMC actuators. Each actuator has an individual control circuit which makes it possible to have four modes of operation. With this device it is possible to produce a normal or shear contact when the bump touches a fingertip to develop a refreshable braille display.

2.5.2 Sensor

An IPMC is used to develop a flow meter based on the vortex shredding phenomenon where the application of low cost, usability, and disposability is essential [46]. Tests were done in the range of 4 to 30 lmin^{-1}. An electronic circuit is used to measure the frequency of the IPMC output to determine the flow. It was reported that a mass flowmeter can be realized from this flowmeter.

In [47] an apparatus to measure the density and viscosity of a fluid is developed by using two IPMC's, one as actuator and one as sensor. By exploiting the vibrational characteristics of a cantilever beam immersed in a fluid, the vibrations can be measured to determine the density and viscosity of the fluid in which the beam is immersed.

The authors in [48] developed a module that generates electrical energy from the ver-

tical waves and horizontal currents in the ocean from a newly developed graphene-based IPMC. A moveable power system was designed to supply a stand-alone offshore plant. The system that consisted of 9 vertical modules and 9 horizontal modules was built and tested. The system delivered electrical energy over the target of 120 Wh up to 600 Wh for 20 days. Due to the growth of algae and barnacles the stiffness of the IPMCs were increased which lead to lower power outputs after 20 days.

In [49] Kruusame et al reviews what has been done regarding self-sensing IPMC actuators. A self-sensing actuator is a device which acts as an actuator and a sensor simultaneously. The methods to measure the sensing signal from the actuator are divided into three groups. The first is to make use of external circuitry to determine the sensing data from the input voltage or current. The second group consists of connecting extra leads for direct measurements. The last group uses a special signal that is modified for sensing purposes as the driving voltage. In all these methods electrical noise is a challenge. A different approach to making a self-sensing actuator is to pattern the electrodes to form two parts that are electrically isolated and use one part only as a sensor and the other only as an actuator. Due to the shared polymer backbone there is a good mechanical coupling. There is still cross-talk and can be successfully suppressed by implementing the following two methods. Creating an electrode between the actuator and sensor and connecting it to ground. By connecting the opposite sensor electrodes in a bridge configuration to cancel out the common mode noise. These two methods can also be used together. It is also possible to connect a sensor and actuator mechanically. It can be a combination of IPMC sensors and a IPMC actuator or IPMC actuator with PVDF sensors. A strain gage can also be bonded to the IPMC actuator.

2.6 Critical literature review

From the literature it was seen that there are many possibilities for IPMCs to be used as actuators and sensors. It was shown that it is possible to model and control the output of the IPMC. It was also seen that the temperature and humidity have an influence on

the performance of an IPMC. From this it was decided to make use of a simple model to be able to model the response of an IPMC as an actuator and investigate how the performance is effected by the environmental conditions namely humidity and temperature. The characteristics of various types of samples will also be investigated to get a better understanding of how the thickness and the electrode thickness influences the outputs. From the literature it was clear what is required in terms of the experimental setup.

Chapter 3

Experimental setup

From the literature survey it was clear that there are a few key aspects to building the experimental setup. The current drawn, the displacement, and the force of the IPMC must be measured. Some kind of clamp to hold the IPMC, and also apply a voltage over the electrodes, is required. In this chapter the equipment chosen, the relevant hardware and software that will be used, the mechanical setup and the integration of the whole setup will be discussed.

3.1 Hardware selection

To investigate the electromechanical properties of an IPMC there are a few measurements that must be taken. The first is to measure how much the tip of the IPMC bends under an applied voltage. In the literature it was seen that the two most common methods to measure this displacement of the IPMC is with a camera or a laser displacement sensor. Each of these methods have their advantages and the best option for this specific study must be chosen. The camera can give more information than just the tip displacement, like the curve of the bending. The laser sensor usually has a much higher resolution and will be able to measure smaller displacements than the

camera. To get accurate readings from the camera the correct software is required. The camera also works better for large displacements as the curl can cause the IPMC to bend out of the line of the laser. For the purposes of this study a laser displacement sensor was chosen. The IPMCs that are going to be used in this study are similar to that found in literature and the authors measured the displacement with the laser sensor. As similar displacements were expected the laser sensor would be sufficient. The laser sensor had to have a small form factor as the entire setup has to be small enough to fit inside an environmental chamber (Espec SH-262). The chosen sensor, optoNCDT1420-25 from micro-epsilon, has a range of 25 mm which gives 12.5 mm in each direction. This sensor has a resolution of 1.25 μm. It has a built-in controller and the output can be measured with a data acquisition system.

To measure the force of the IPMC a load cell was required. In the literature the most authors used a 10 gf load cell as the forces to be measured are very small. When looking for a load cell the 10 gf was the smallest that was available. A few load cells were compared and the GSO-10 from transducer techniques was chosen. This specific load cell was also used by many authors. Its nominal resistance is 350 Ω and has a rated output of 1 mV/V and a 10 V excitation voltage which means for 10 gf the output will be 10 mV. An amplifier is required to amplify this signal to a signal that is more readable. The LCA-RTC load cell amplifier was used to give an excitation voltage to the load cell and to amplify the signal to a more readable value. This amplifier can be used with various load cells with different properties and it had to be set up. It was set up for a 10 V excitation voltage, an 0 to $\pm$10 V output, and a 1 mV/V signal sensitivity.

The current that the IPMC draws must also be measured. A 1 Ω resistor was placed in series with the IPMC and the voltage over the resistor was measured to determine the current drawn. More detail of the electrical connection can be seen in section 3.2.

A data acquisition system was required to be able to log and plot the different measured values. A National Instruments cDAQ-9174 was used. To measure voltages the NI 9205 module was used. The NI 9263 module was used to generate a voltage signal to power the IPMC. The NI 9217 module is an resistance temperature detector (RTD)

module that was used to implement the four probe method as it supplies a small current and measures the voltage. This is discussed in more detail in Section 3.2.

To measure the dry and hydrated weight of the different samples a scale (Adam PGW 253e) with a resolution of 0.001 g was used.

3.2 Electrical system

Some basic hardware components were still required to finish the test setup. A diagram to illustrate all the major components and how they are connected and the expected signals was drawn in Figure 3.1. This was used to help integrate all the components as it made it clear what inputs or outputs between components were required.

A 24 V power supply was used to power the load cell amplifier and the laser displacement sensor. One channel on the NI 9263 was used for the input signal to the IPMC. The current that the module can deliver is 1 mA and the IPMC can have a peak current in the range of 200 mA depending on the IPMC and the input signal. A current amplifier that could deliver 300 mA, was used to be able to supply the IPMC with sufficient current.

The laser displacement sensor's output is $4 - 20$ mA and to make use of less data acquisition modules this output had to be converted to a voltage output. This was done by using a 500 Ω resistor and measuring the voltage over it. This changes the output of the sensor to $2 - 10$ V which can be read with the NI 9205. The output from the load cell amplifier can be ± 10 V but as only compression will be measured with the load cell a value between 0 and 10 V is expected. This is read on one of the channels of the NI 9205. The voltage applied to the IPMC is also measured by the NI 9205.

To measure the current that the IPMC draws, a 1 Ω resistor was placed in series with the IPMC and the voltage over it is measured. As a maximum of 200 mA was expected the expected voltage would be ± 200 mV. The reference voltages of the channel can be

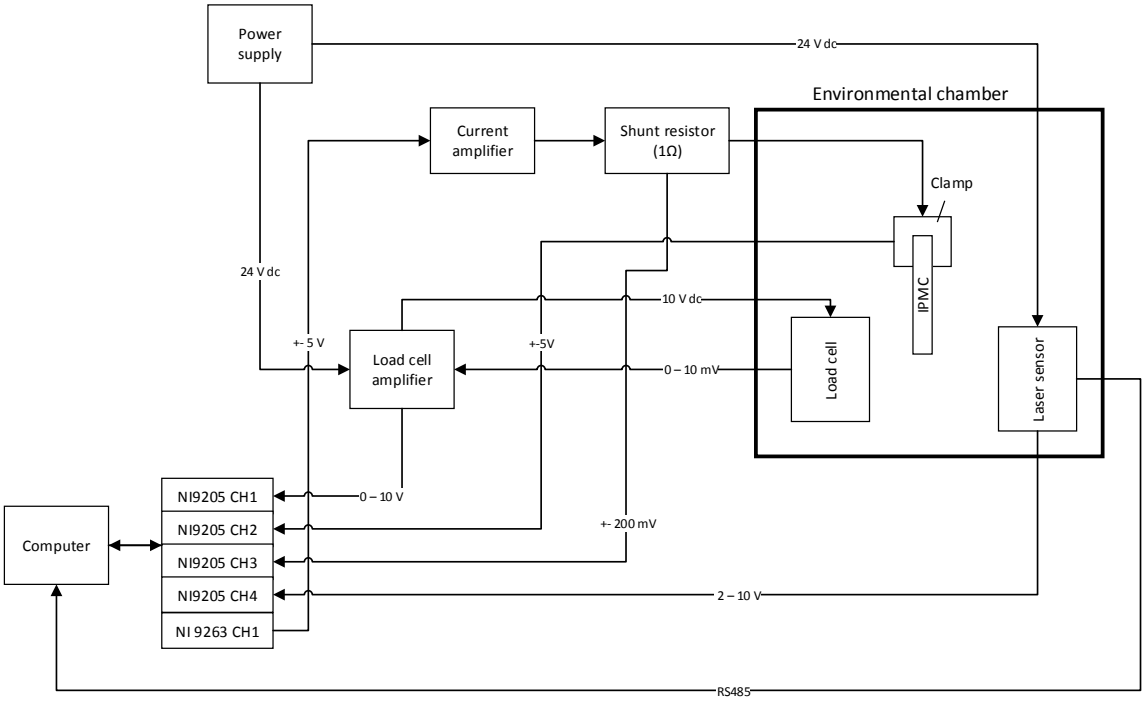

Figure 3.1: Overview of electrical integration

adjusted to 0.2, 1, 5 and 10 V to be able to measure more accurately by making use of most of the readable range.

The laser displacement sensor has the capability of communicating to a computer via RS485. A RS485 to USB converter circuit was made to be able to use this functionality. As the measurements are done with the data acquisition system, this extra feature was mainly included to be able to easily set the middle point and set up the sensor. It can also be done without the computer interface. A printed circuit board (PCB) had to be designed for this circuit, the current amplifier, the current sensing resistor and the resistor for the laser sensor. A schematic of the electrical connection of all hardware components can be seen in Figure 3.2.

To accurately measure the surface resistance of the IPMC the four probe method has to be used. For this method a small constant current must be supplied to two points on the IPMC surface and then the voltage must be measured on the surface. Figure 3.3a shows how it must be measured and the dimensions for the contact points were

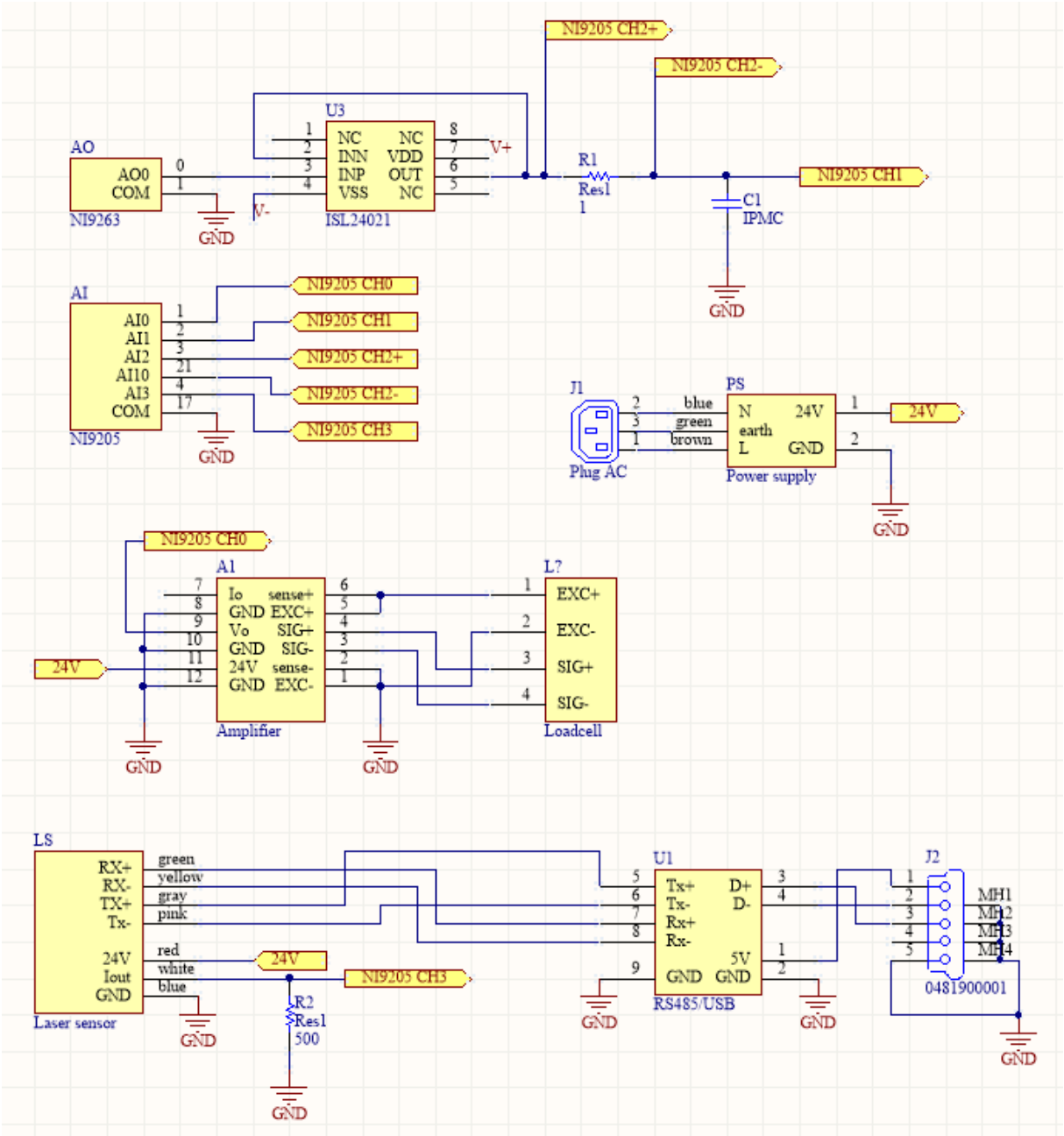

Figure 3.2: Electrical diagram of experimental setup

included. The dimensions were chosen to be able to measure directly on the sample that was going to be investigated. The resistance is then used to calculate the surface resistance of the specific sample. To implement this, pieces of copper sheet was cut into the correct sizes for the contact points and was fixed to a piece of plastic to make sure they are always the correct distances apart, and this setup can be seen in Figure 3.3b.

3.3 Mechanical setup

To organize the hardware neatly, a box was made where all the hardware components that don't fit inside the environmental chamber can be placed. A basic box was made from Perspex and the power supply, load cell amplifier, data acquisition system, and the designed PCB was placed inside. Plugs were added to easily connect and disconnect the main power, the load cell and the laser displacement sensor. A photo of this hardware setup is shown in Figure 3.4.

For the setup the load cell, laser displacement sensor, and a clamp for the IPMC must be placed inside the environmental chamber. The load cell must be movable as it must be against the IPMC when used and away from it when displacement experiments are done. A setup was designed where it is possible to move the laser sensor and the load cell while the IPMC clamp stays at a fixed place. This was done by using two rails and making two platforms that move on it. The idea behind it was also to make it possible add a few components later to change the setup to be able to test the sensor properties of the IPMC. This can be done by adding a stepper motor, a screw and fixing a nut to one platform. The platform can then be moved to displace the IPMC and the voltage can be measured.

The clamp was designed to be able to change the clamping force as this can influence the performance of the IPMC. The clamp was made with two Aluminium contacts. One is fixed to the structure and the other is pressed towards it with a cylinder. The air pressure is used to change the clamping pressure. The clamp is fixed in such a way that the IPMC would be orientated in a vertical position which was done to minimize

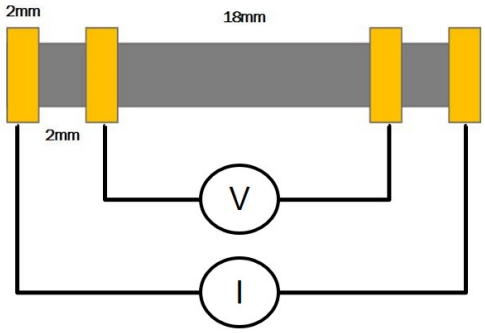

(a)

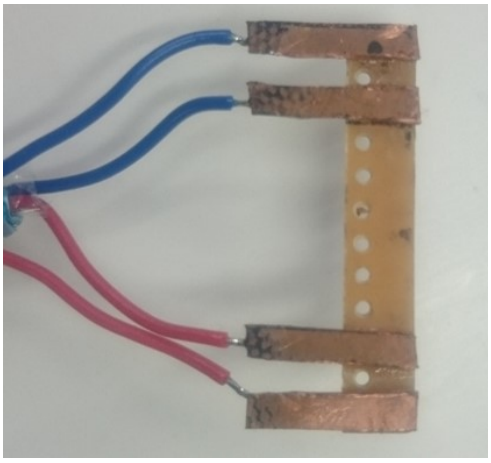

(b)

Figure 3.3: (a)An illustration of how the four probe method works and (b)a photo of how the four probe method was implemented for this study

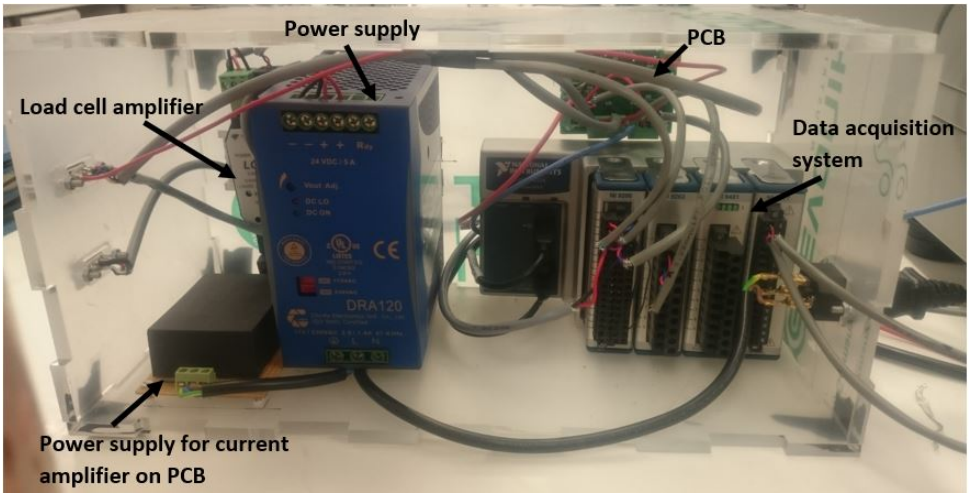

Figure 3.4: Photo of hardware setup

the effect that gravity would have on the displacement. This entire setup is then placed inside the environmental chamber and can be seen in Figure 3.5

3.4 Software for data acquisition

This data acquisition system is mostly used with its own software, namely LabView. It was difficult to achieve the outputs required with this software but would be possible with much more experience in using the program. Due to this issue Matlab was used instead of LabView. A script was written that sets up each module and channel of the data acquisition system in Matlab. It then generates the output signal and measures all the inputs, and saves the data in a file. The data can then be retrieved from the file at any time and be used to plot all relevant data.

3.5 Experimental method

The following steps were used in most of the experiments done:

Step 1: Remove IPMC from water

Step 2: Remove all excess water by tapping surface with tissue paper

Step 3: Clamp IPMC in the setup at a specific clamping pressure

Step 4: Turn environmental chamber on and set to specific temperature and humidity

Step 5: Wait approximately 30 minutes for the IPMC to be in equilibrium with the set humidity

Step 6: Turn environmental chamber off to reduce the vibration effect on the IPMC

Step 7: Do experiment

Step 8: Hydrate sample before next experiment

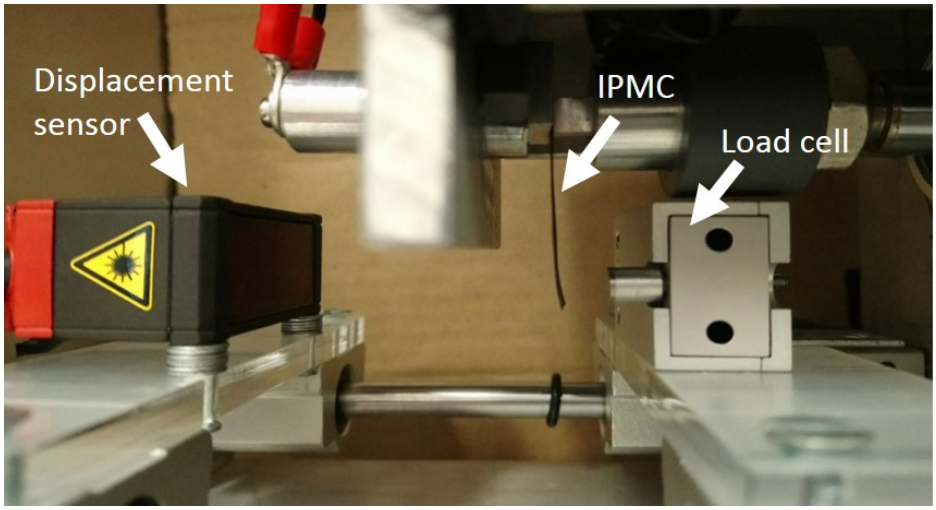

Figure 3.5: Experimental setup inside the environmental chamber

For experiments done at room temperature steps 4, 5 and 6 were ignored. This was a guideline for all experiments and any deviations from this will be discussed with the specific experiment. Short experiments were done to ensure that the environment inside the chamber won't deviate while it is switched off. It was switched off when doing the experiments because the fan blowing causes the IPMC sample to move slightly. It would be possible to filter out this high frequency movement. It was decided to rather eliminate this effect as it might still have an influence on the displacement even when the high frequency movement is removed. Due to the effect that the clamping pressure has on the performance of an IPMC as seen in [6], all the experiments were done at a constant clamping pressure.

3.6 Conclusion

In this chapter the design of the experimental setup was discussed. The main components are a data acquisition system, a load cell, a laser displacement sensor and the IPMC clamp. The laser sensor used is a optoNCDT1420-25 from micro-epsilon. The load cell used is the GSO-10 from transducer techniques that is used together with the LCA-RTC load cell amplifier. A clamp was manufactured from Aluminium. A NI cDAQ-9174 was used with the NI 9205, NI 9263 and NI 9217 modules. The experimen-

tal setup is placed inside the Espec SH-262 environmental chamber to be able to test at various temperatures and humidities.

One of the main challenges of the setup was to build the setup in such a way that it fits inside the environmental chamber. All components used were small and with the setup assembled inside the chamber there was little room left. Due to an air cylinder being used to control the clamping pressure the clamping mechanism took a lot of space inside the chamber. Alternative clamping techniques can be investigated to create more open space in the chamber after the setup is inserted.

The laser sensor measures in a straight line and when the IPMC bends too much the distance measured is not on the same point on the actuator anymore. When conducting tests at higher voltages where large displacements occur, there is a time where the actuator tip is no longer in the sight of the sensor due to the bent shape. This will limit the experiments to lower voltages or smaller displacements. Other technologies that can give an indication of the bending might deliver more accurate results in these conditions. A combination of sensors could also be tested but due to the limited space this would be difficult to achieve.

The setup was easy to assemble and to adjust. Care must be taken when inserting the IPMC into the clamp, as the contact area is small it could happen that the contact area is smaller than required due to a miss-alignment with the clamp. The setup is easy to use and met all necessary requirements.

Chapter 4

Modelling

In this chapter the model used is explained in more detail. A linear model was developed. The implementation of the model and the parameter estimation for the model is discussed. The model is also verified by using data from literature and a model is developed for a specific IPMC sample.

4.1 Modelling approach

To have a model is important as it can help designers to decide on the properties and dimensions of an IPMC that will achieve the desired performance. From the literature survey it was seen that grey box models are simple and also contain some physical information of the phenomena inside the IPMC. As discussed in Chapter 2, many authors use a similar model which ranges in complexity. It was decided to follow this approach as it delivers good results with less complexity than other approaches.

4.2 Electromechanical model

From these models it was decided to use a model similar to that presented in [18]. This model consists of two sections namely, a non linear electrical equivalent circuit and a linear mechanical section. A similar approach was followed and the model consists of a linear electrical equivalent circuit where the input is the applied voltage and the output is the absorbed current. This output is then used as an input to the electromechanical section and the output is either the free tip displacement ($\delta(t)$) or the blocked force($f(t)$) as seen in Figure 4.1.

According to [18] black box models can't easily be used for other IPMCs and white box models are mostly too complex for practical use or too simple to deliver accurate predictions. Thus a grey box model is used as it can deliver good results from simple equations that describe the understood phenomena.

The model is based on an IPMC beam that is clamped of the one side where the electrical signal will be applied over the thickness of the actuator. This beam can be seen in Figure 4.2 along with all the parameters that is required for the model. The parameters of interest are: f the force that is applied to the sample, L_c the length of the clamped section of the IPMC, L_f the length of the free section of the IPMC, L_s the point where the force is applied, w the width of the IPMC and h the thickness of the membrane.

In the electrical section of the model, an equivalent circuit model is used to determine the absorbed time-varying current for a time-varying voltage input. The current produces the bending of the IPMC due of the water distribution it causes. Thus it is

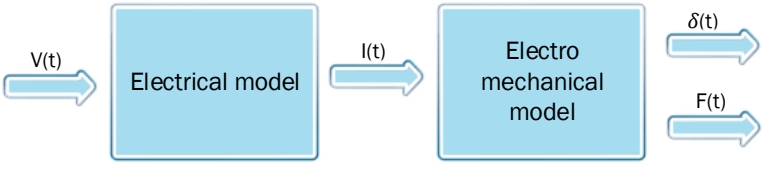

Figure 4.1: An overview of how the two sections of the model fit together

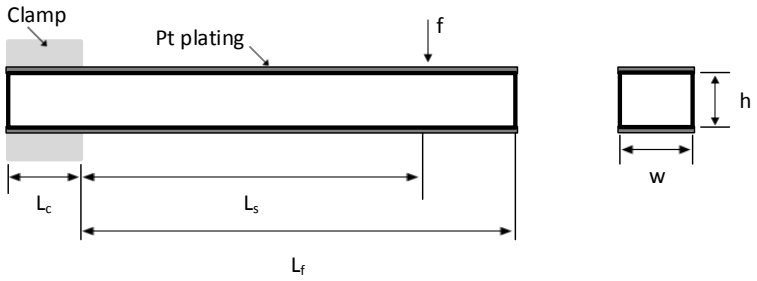

Figure 4.2: A drawing of a clamped IPMC with the relevant parameters that was used in the model

important to be able to accurately predict the absorbed current to be able to predict the mechanical response. The current consists of a non linear static part and a dynamic part due to the capacitive nature of an IPMC [18]. The nonlinearity is only seen at input voltages higher than 1 V and the cause of this considered to be due to water electrolysis which occurs at approximately 1.23 V.

For the purpose of this study the nonlinear part of the model from [18] was ignored and the equivalent circuit used can be seen in Figure 4.3. In the model, R_{dc} is the dc resistance of the IPMC, R_e is the resistance of the electrode surface, $R_{C1}C_1$ is the branch that reflects the fast phenomena and $R_{C2}C_2$ is the branch that reflects the slow phenomena of the capacitive nature of the IPMC. For simplicity it was assumed that the surface resistance of both electrodes are the same.

The circuit elements were introduced by physical considerations thus it is possible to scale the lumped elements by multiplying some coefficient with the geometrical properties of the actuator. If the electrode is studied as a layer, the surface resistance can be written in terms of the length and width of the IPMC actuator. R_e was scaled by introducing a resistance R_s and is written as

$$R_e = \frac{R_s L_t}{w} \,. \tag{4.1}$$

R_s can be experimentally determined and the method is discussed in Section 3.2. The

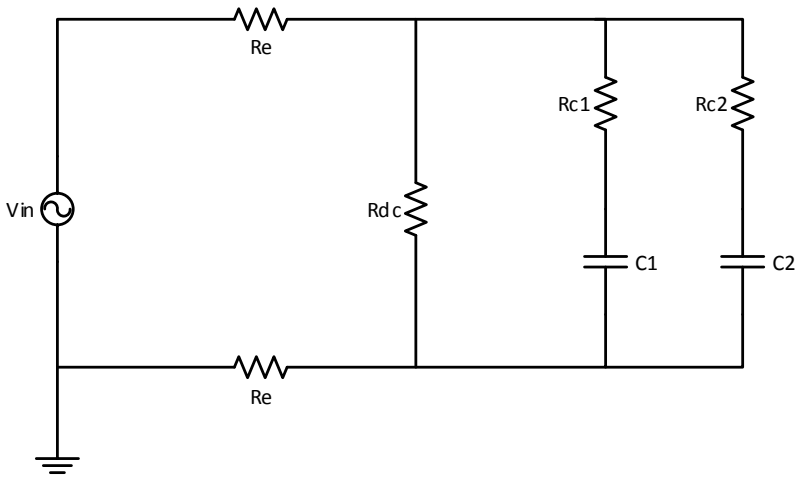

Figure 4.3: A schematic representation of the equivalent circuit that is used to model the electrical response of the IPMC

resistance R_{dc} which is the resistance of the actuator against a dc input and represents the dc resistivity of the actuator (ρ_{dc}) and the geometrical properties of the actuator as

$$R_{dc} = \frac{\rho_{dc} h}{(L_f + L_c) w} \,. \tag{4.2}$$

The value for ρ_{dc} can be calculated from experimental values and is explained in Section 4.5. The resistance of the actuator against the charges involved in the fast phenomena, R_{C1} can be described as the resistivity against charges of the fast phenomena (ρ_1) and the dimensions of the actuator

$$R_{C1} = \frac{\rho_1 h}{(L_f + L_c) w} \,. \tag{4.3}$$

The capacitor of the same branch (C_1) can be described as

$$C_1 = \frac{\epsilon_1 (L_f + L_c) w}{h} \,. \tag{4.4}$$

Using a similar method, the resistance against the charge of the slow phenomena (R_{C2})

can be described as

$$R_{C2} = \frac{\rho_2 h}{(L_f + L_c)w} \tag{4.5}$$

and the capacitance of this branch (C_2) can be described as

$$C_2 = \frac{\epsilon_2 (L_f + L_c)w}{h} \,. \tag{4.6}$$

The permittivity (ϵ_1 and ϵ_2) and the resistivity (ρ_1 and ρ_2) are found through experimental investigation. In order to make accurate predictions there must be a sufficient number of RC branches. This determines the degrees of freedom available to describe the dynamics of the actuator. In [18] it was found that two RC branches can give a good prediction of the dynamic behaviour with a small number of parameters that need to be identified experimentally.

The current absorbed by the IPMC causes the mechanical reaction due to the redistribution of the water molecules inside the IPMC [19]. The current flowing through the capacitive branches produce the bending of the actuator. The relationship between the current in the RC branches (I_C) and the displacement (δ) can be written as

$$\frac{\delta}{I_C} = \frac{1}{s}\left(\frac{3dL_s^2}{\eta(L_f + L_c)wh} \right)\left(\frac{1}{1 + s^2 \frac{12L_f^4 \rho_m}{\Gamma^4 Y h^2}} \right) \tag{4.7}$$

where d represents the coupling between the electrical and mechanical domain and is similar to the piezoelectric coefficient used in piezoelectricity. It can be determined by using the expressions for the free deflection and the blocked force. Γ is the solution of the characteristic equation of a clamped beam for the first mode and its value is known from literature as 1.875 and ρ_m is the density of the IPMC. The equivalent permittivity (η) is the electrical impedance of the RC branches and can be described as

$$\eta = \frac{\epsilon_1}{1 + s\epsilon_1\rho_1} + \frac{\epsilon_2}{1 + s\epsilon_2\rho_2}\,. \tag{4.8}$$

The blocked force depends on the applied voltage and the relationship between the blocked force (f) and the input voltage can be written as

$$\frac{f}{V_{appl}} = \frac{f}{V_{in} - 2R_e I_{in}} = \frac{3dhwY}{4L_s} \tag{4.9}$$

where V_{appl} is the voltage across the capacitive branches, V_{in} is the is the input voltage applied over the actuator and I_{in} is the current absorbed by the actuator. Y is the Young's modulus of the IPMC and as Nafion is a viscoelastic material it is not a constant value and can be approximated by using the Golla-Hughes-McTravish model as

$$Y = Y_c\left(\, 1 + k\,\frac{s^2 + 2\zeta\omega s}{s^2 + 2\zeta\omega s + \omega^2}\,\right) \tag{4.10}$$

where Y_c is the static Young's modulus, k is a real constant value, ζ is the damping coefficient and ω is the natural frequency. It was shown in [19] that the Young's modulus can be seen as a constant when working at low frequencies (up to 20 Hz). IPMCs are generally used with low frequency inputs as the water distribution is a slow response and at higher frequencies it will have very little movement. As the frequencies that are going to be used in this study are far below 20 Hz, the Young's modulus was assumed to be a constant in this model.

4.3 Simulink model

To implement the model presented in the previous section, Simulink was used as the electrical section and the electromechanical section can be simulated in a single environment. To create the model the electrical circuit was built in Simulink and it was used together with (4.7) and (4.9). The model used is shown in Figure 4.4 and the com-

ponents and Simulink blocks were all described with variables. This makes the model easy to use for any IPMC actuator as long as the variables are declared for that specific actuator. A script was used to set up all these parameters for a specific actuator. It was also described in variables as the program for the parameter estimation must be able to adjust the variables.

4.4 Verification of Simulink model

Before this model can be used in the rest on the study it is necessary to verify that the model delivers correct results. To verify the model it was decided to use data from literature and see if the results are similar. For this purpose the work of [1] was used. The authors used the model from [18] and tested linear an nonlinear least square methods for parameter identification. This was one of the papers with the most information regarding the parameters and could thus be used to test this model. The parameters from [1] was inserted into the model and the absorbed current, the displacement and force output was plotted and compared to that of [1]. The results were similar, the form was correct and values differed slightly but could be due to not having all the correct parameters that was used.

The next part that must also be verified is the ability to determine the model parameters from experimental data. The steps that are used in the parameter estimation are discussed in Section 4.5 and will not be discussed here as this section is solely for the purpose of verifying the technique before it is used in the model. For this the simulated output data from the model with the parameters from [1] was saved and used as experimental data and will be referred to as the experimental data for the rest of this section. The parameters were changed to random values to create a difference between the simulated output and the experiment values. First the electrical parameters are estimated and the difference between the simulated and experimental absorbed current can be seen in Figure 4.5. The parameter estimation program inside Simulink was used to estimate the parameters and the results from the parameter estimation can be seen

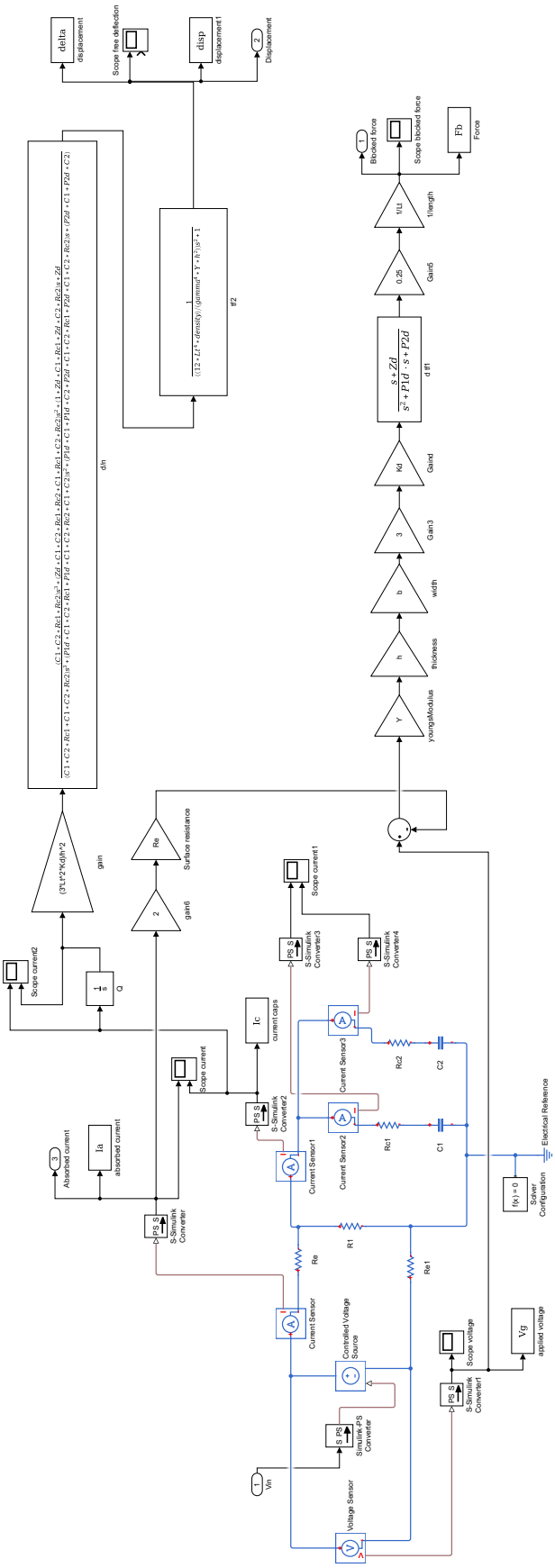

Figure 4.4: Implementation of both the electrical and electromechanical section modelled in Simulink

in Figure 4.6. From this figure it is clear that the program can successfully estimate the parameters to match the simulated data to the experimental data.

The next step is to determine the electromechanical coupling coefficient (d). Figure 4.7 illustrates the difference between the simulated and experimental force before the parameter estimation is done. The parameter estimation was done and is illustrated in Figure 4.8 and it could successfully determine the parameters to match the simulated blocked force with the experimental blocked force. This verifies that the technique used to estimate the parameters of the model from the experimental values is sufficient. This is a perfect scenario that was tested and it is expected that the real experimental values won't be fitted with the same accuracy as there exists difficulties such as noise, back relaxation, etc. The model can now be used and tested with real experimental values.

4.5 Parameter estimation

The next step in creating the model is to determine the parameters of the IPMC. Some of the parameters are properties of the material that can be measured and other properties are determined experimentally. Figure 4.9 illustrates the process that must be followed to determine all the parameters. It starts with determining all the electrical parameters and then the mechanical parameters. The first step is to measure the surface resistance of the IPMC. This is done by using the four probe method which is explained in Section 3.2. The second step is to determine the dc resistance, which is done by applying a dc voltage and using it together with the steady state current drawn to calculate the dc resistance.

The third step is to use parameter estimation to determine the values of ϵ_1, ϵ_2, ρ_1 and ρ_2 by making use of various experiments. To do this the built in parameter estimation toolbox in Simulink was used. This allows the user to give various inputs with the outputs measured to the program and the parameters that must be estimated are selected. The program then runs the simulation with the defined inputs and compares the outputs to the experimental ones. Parameters are adjusted until the simulated out-

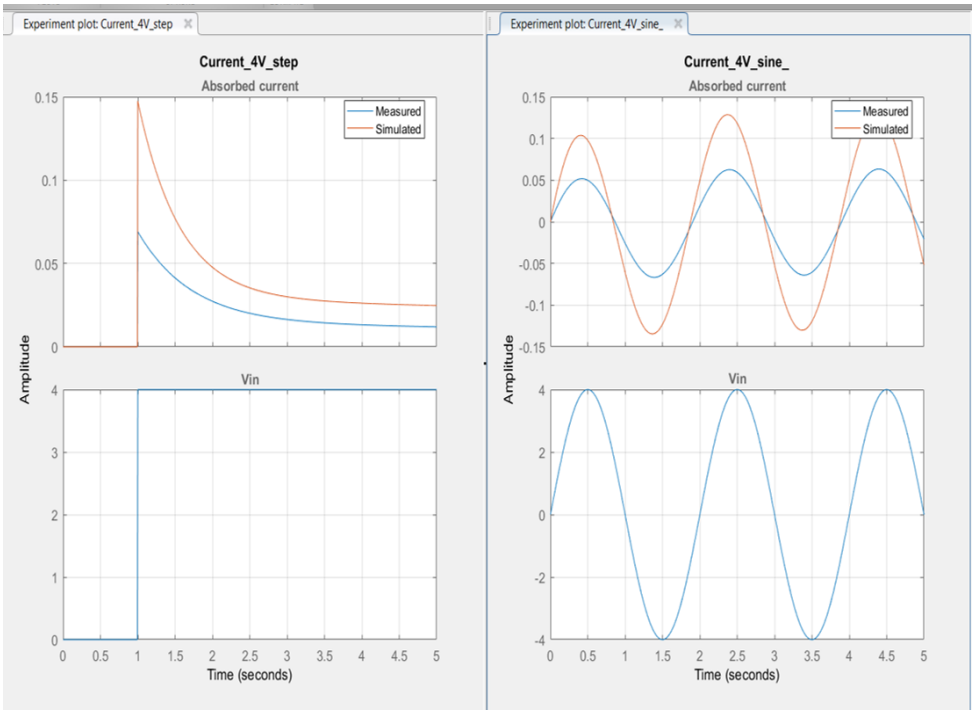

Figure 4.5: Simulated and experimental absorbed current generated with values from [1] before parameter estimation

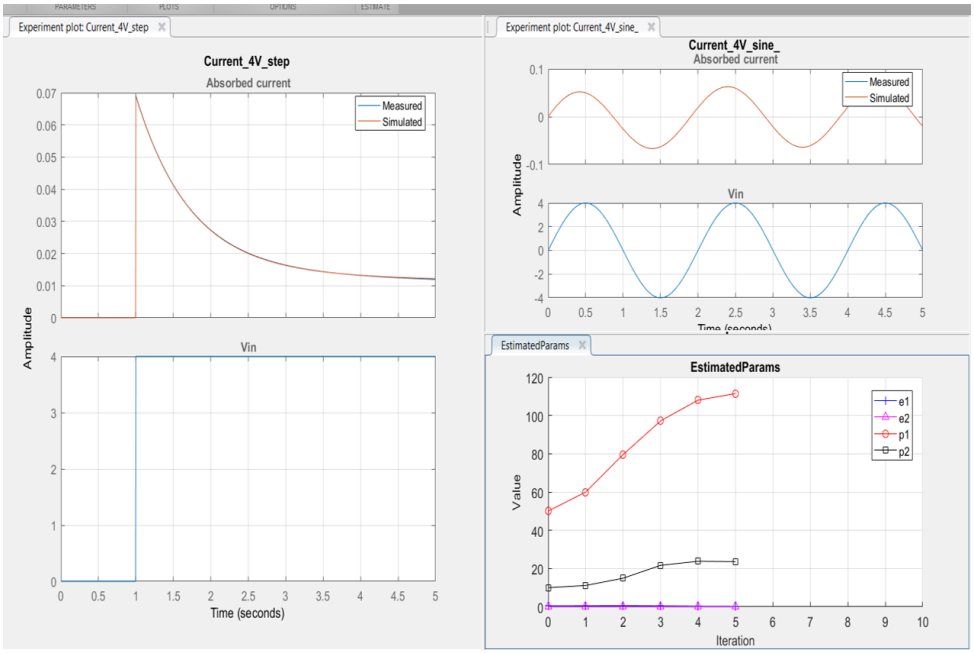

Figure 4.6: Simulated and experimental absorbed current generated with values from [1] after parameter estimation

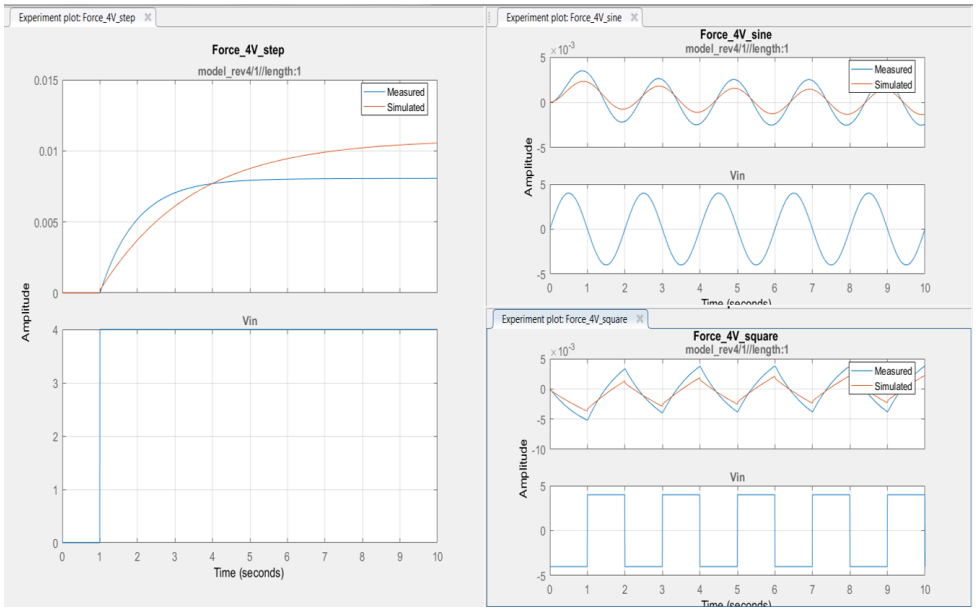

Figure 4.7: Simulated and experimental blocked forces generated with values from [1] before parameter estimation

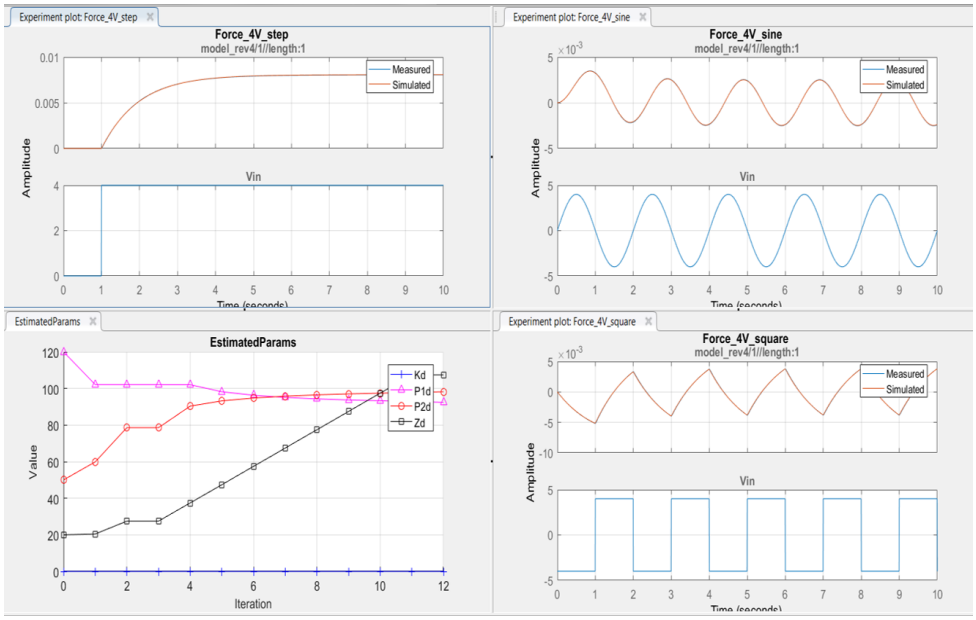

Figure 4.8: Simulated and experimental blocked forces generated with values from [1] after parameter estimation

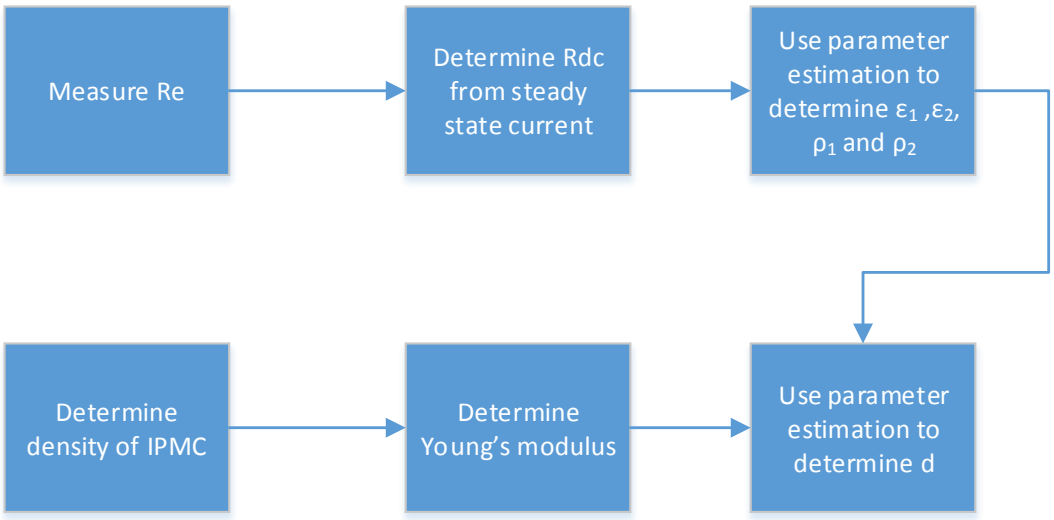

Figure 4.9: Process to determine all the required parameters for the model

put matches the experimental one or the error doesn't change with more than a pre-set value. A 1 V step and 1 V 0.1 Hz sine wave was used for the estimation. The program also allows the user to select experiments to validate the data. Which will be used later. For these experiments the absorbed current was the output.

The model was developed for the Nafion N117 IPMC with a loading of 10 $mgPt/cm^2$ in room conditions. Figure 4.10 illustrates the simulated and the experimental values of the model when incorrect parameters were given to the model as a starting point. Figure 4.11 illustrates the simulated and experimental outputs of the model after the parameters were estimated. Table 4.1 shows the parameters determined.

Table 4.1: Electrical parameters for sample 2

Parameter	Value
R_e	8
R_{dc}	70.92
ρ_1	0.35734
ρ_2	24.2415
ϵ_1	0.11998
ϵ_2	0.48106

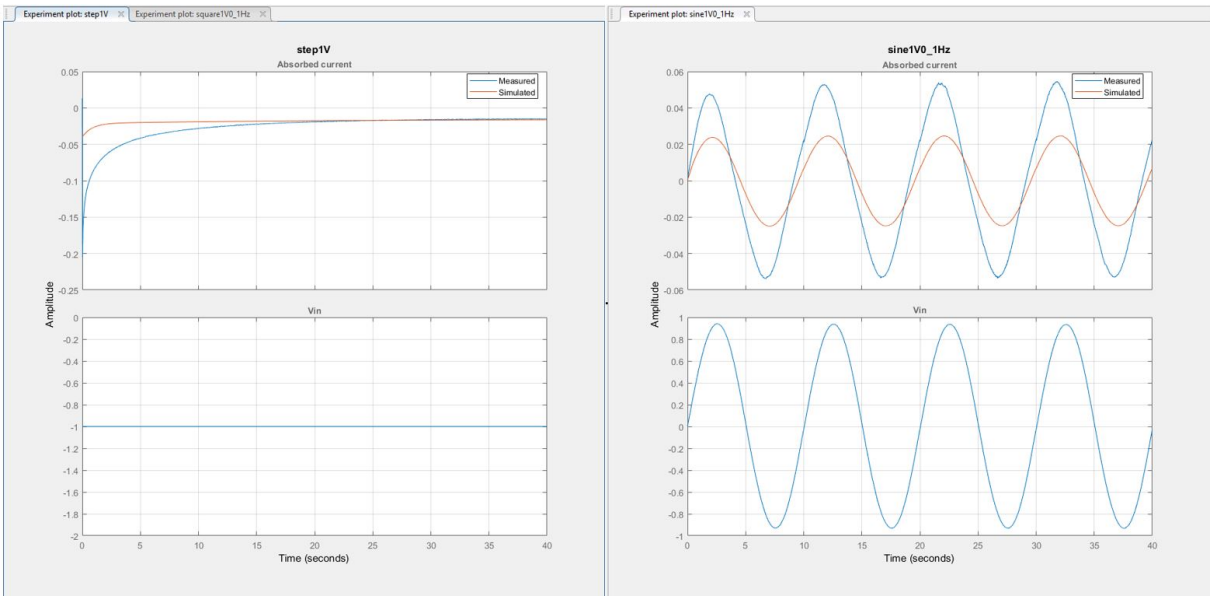

Figure 4.10: Simulated and experimental current outputs before parameter estimation was done

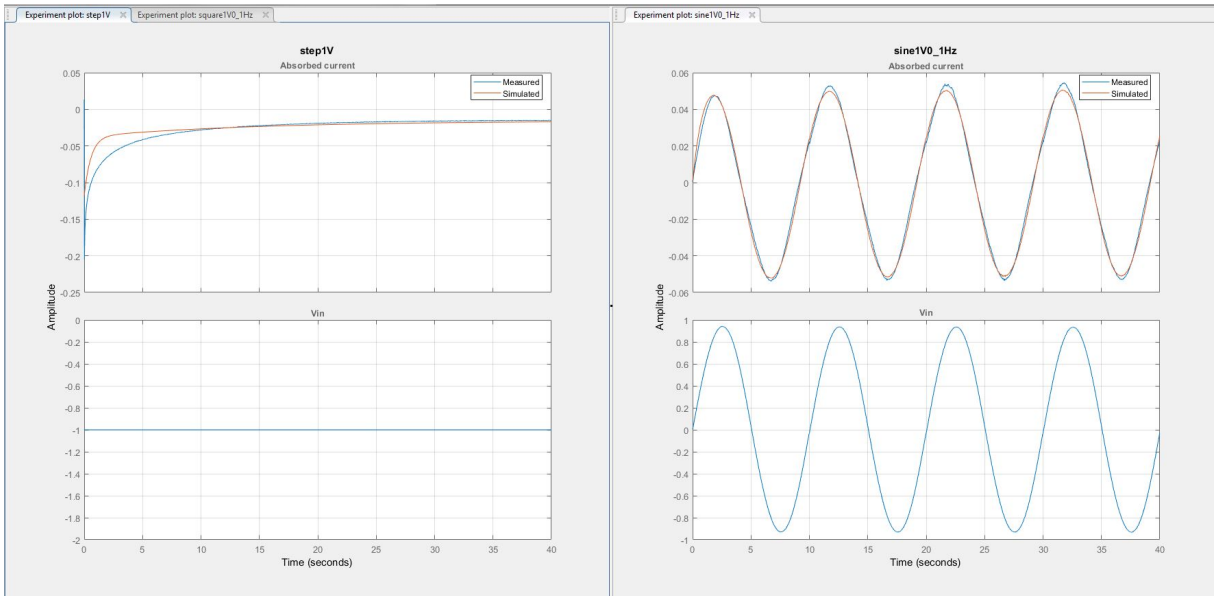

Figure 4.11: Simulated and experimental current outputs after parameter estimation was done

To determine the electromechanical parameters, the density of the IPMC must be determined. This is done by measuring the weight of the IPMC and using it together with the volume of the IPMC to calculate the density as seen in [20]. The Young's modulus is also determined from experimental values where the force of the IPMC is measured when it is displaced at a specific distance. To do this the load cell was moved against the membrane to displace it. The force and displacement was measured and used to determine the stiffness of the actuator. From this the Young's modulus was calculated. A method similar to this was used in [20] where the load cell was used to displace the actuator at a fixed distance. Young's modulus can be calculated as

$$Y = \frac{4L_s^3}{wh^3}\frac{f}{\delta}\,. \tag{4.11}$$

After all these parameters have been determined the electromechanical coupling coefficient d can be estimated. According to [18] the structure of d that delivers the best results is

$$d = K_d \frac{s + Z_d}{s^2 + P_{1d}s + P_{2d}}\,. \tag{4.12}$$

To estimate the parameters in d, the force was measured as the output and the inputs used for experiments were 1 V step, 1 V, 0.1 Hz sine wave. Figure 4.12 shows the simulated and experimental output when incorrect values were used as a base. The parameters were estimated by using the blocked force as output. Figure 4.13 shows the simulated and experimental outputs with the estimated parameter values. The parameters for the electromechanical section are listed in Table 4.2.

4.6 Conclusion

In this chapter the grey box model that was used to predict the behaviour of an IPMC was described. The model consists of two parts, an electrical equivalent circuit and

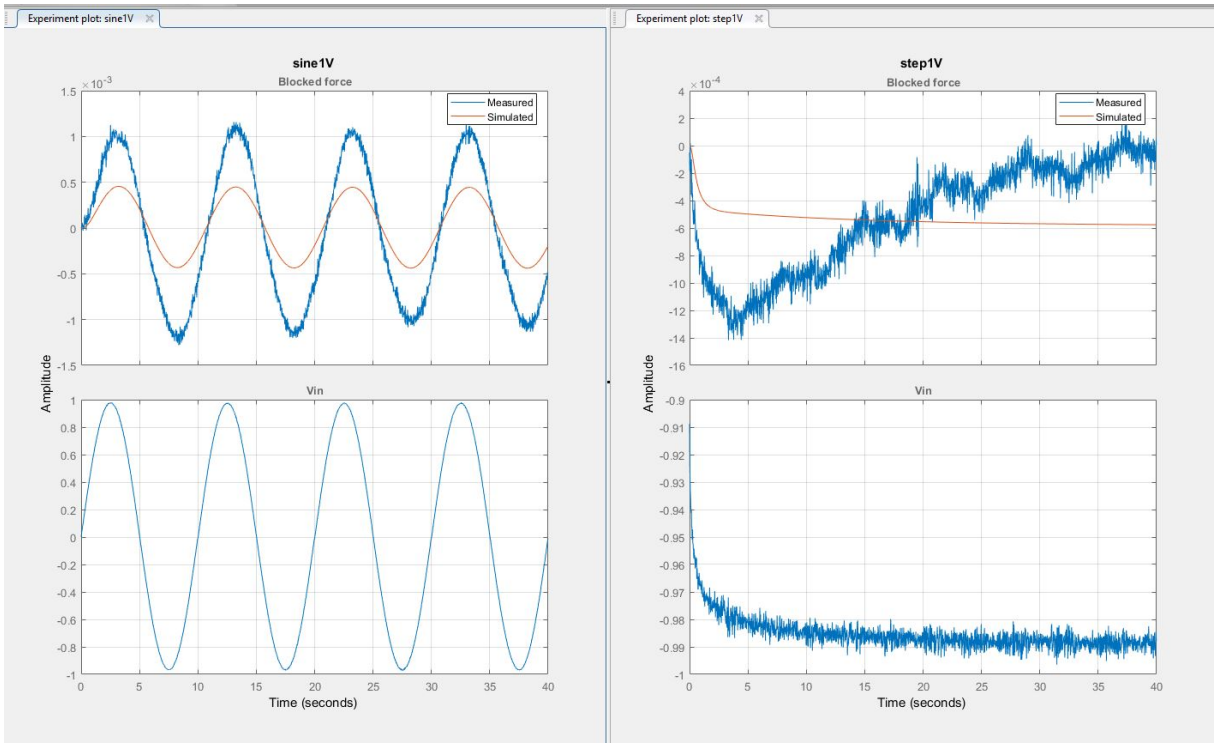

Figure 4.12: Simulated and experimental force outputs before parameter estimation was done

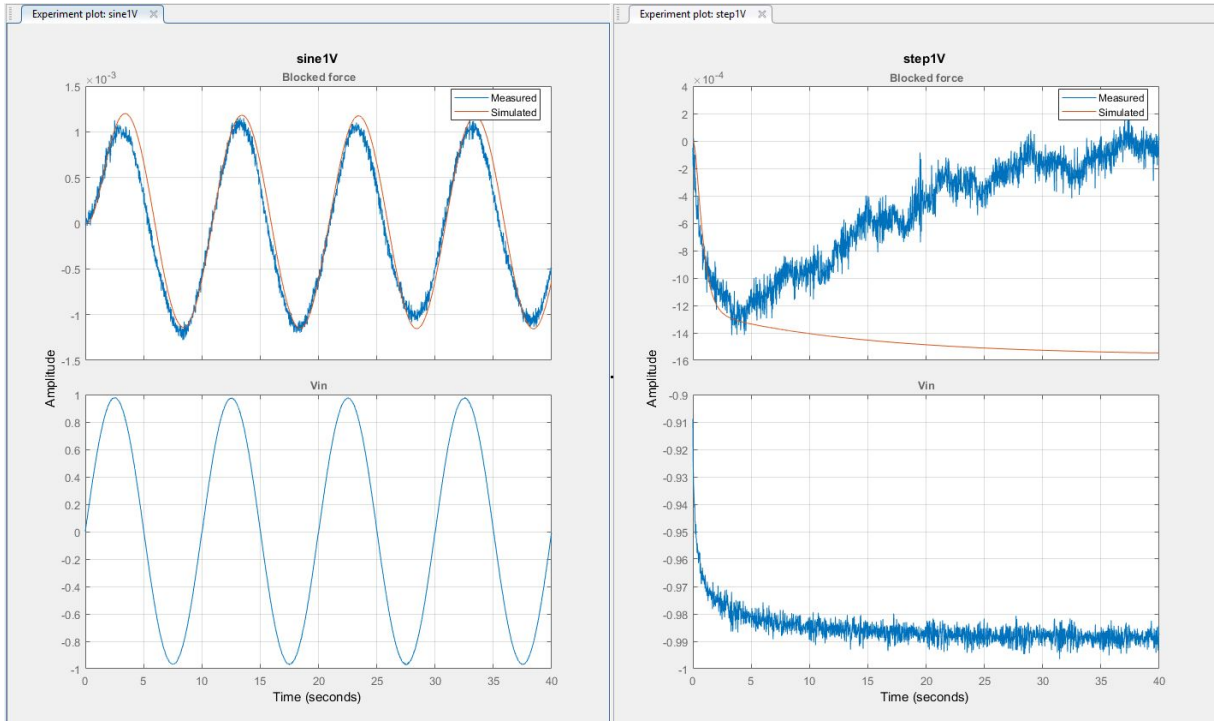

Figure 4.13: Simulated and experimental force outputs after parameter estimation was done

Table 4.2: Mechanical parameters for sample 2

Parameter	Value
ρ_m	3.965×10^3
Y	1.45×10^9
K_d	6.79×10^{-9}
P_{1d}	15.897
P_{2d}	41.097
Z_d	210.5

an electromechanical model. The model was implemented in Simulink and was verified with data from [1] which used a similar model. Some parameters in the model had to be determined from experimental data and for this the parameter estimation in Simulink was used. Simulated data was used as to verify that the parameter estimation delivers sufficient results. From this the model was developed for a 30 mm x 5 mm N117 sample with a platinum loading of 10 mgPt/cm^2 (see Section 5.1.2).

The model could successfully determine the electrical parameters. The model could fit the data sufficiently to the blocked force. In Figure 4.13 the output force for a step input follows the ramp of the simulated force and then it starts to deviate. This phenomena is known throughout literature as back relaxation which can be seen in the force and displacements of IPMC actuators under step voltages. When the force reaches a maximum all the water inside the membrane finished moving to the one side. After this some water starts to diffuse back to its original state causing the force or displacement to decrease gradually. As the model does not include back relaxation this deviation was expected.

Chapter 5

Experiments

In this chapter the behaviour of various samples were investigated. The response of each sample was investigated for different input voltages. The influence of input voltage, input frequency, humidity and temperature was also investigated. Comparisons between the different samples are made in terms of their outputs and absorbed current. The model discussed in the previous chapter is validated with experimental results.

5.1 Characterizing IPMC

In this section different samples of IPMCs were investigated. The samples used in this study are made from Nafion N117 and N1110. There were membranes with different Platinum loadings (Pt thickness) namely 5, 7 and 10 mgPt/cm^2. The N117 and N1110 membranes were plated with these loadings. A sample of Nafion N117 plated with 2 mgPt/cm^2 supplied by HySA was also investigated. Seven different samples were investigated in the study. First, each sample was sent for scanning electron microscope (SEM) and transmission electron microscope (TEM) imaging to be able to determine the thickness of the Pt electrodes. Various experiments were done on each sample to

be able to make a comparison between samples and investigate the effect of the Pt loading and thickness of the membranes on the behaviour. The information about the samples that are tested can be found in Table 5.1.

5.1.1 HySA sample (sample 1)

The first sample that was investigated is a sample made from Nafion N117 and plated with a loading of 2 mgPt/cm^2 and was produced by HySA. In Figure 5.1 the surface of the membrane can be seen. In the TEM image (Figure 5.3) the Pt electrode can be seen and it is clear from this image that the Pt on this sample is very dense.

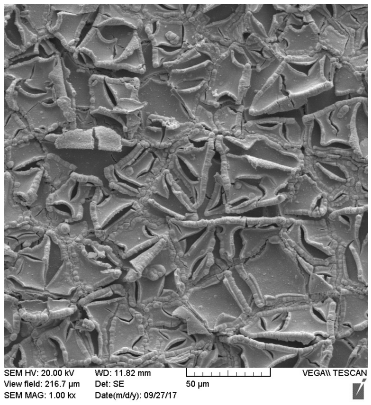

Figure 5.1: Typical Pt morphology by SEM on the surface of the membranes produced by HySA

From the cross-section in Figure 5.2 the Nafion layer with Platinum electrodes can be seen. For all the following experiments a sample of 30 mm x 5 mm was used. The dry

Table 5.1: Description of each sample that will be tested

Sample number	Membrane type	Pt loading
1	Nafion N117	2 mgPt/cm^2
2	Nafion N117	10 mgPt/cm^2
3	Nafion N117	7 mgPt/cm^2
4	Nafion N117	5 mgPt/cm^2
5	Nafion N1110	10 mgPt/cm^2
6	Nafion N1110	7 mgPt/cm^2
7	Nafion N1110	5 mgPt/cm^2

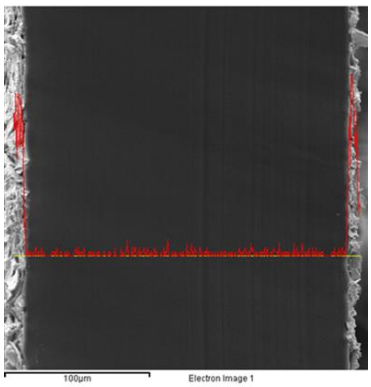

Figure 5.2: Typical Pt morphology by SEM of the membrane cross-section produced by HySA

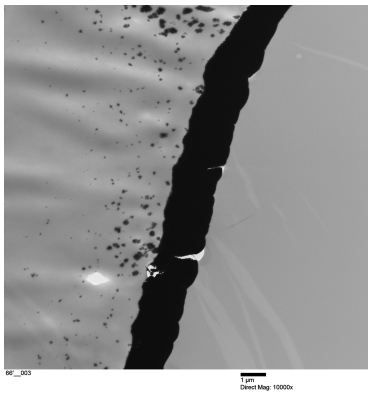

Figure 5.3: Typical Pt morphology by TEM of the membrane cross-section produced by HySA

weight of the sample was measured as 90 mg and was then submerged in deionized water for 24 hours before experiments were done. After this the weight of the hydrated sample was measured as 107 mg.

The experiments were first done in room conditions and it was seen that the IPMC starts to curl even with no voltage applied. A test was done to determine the rate of this curl and create a baseline in room conditions. Figure 5.4 shows how the IPMC curls when just clamped in the test setup. From this it was decided that the tests won't be done in room conditions for this sample.

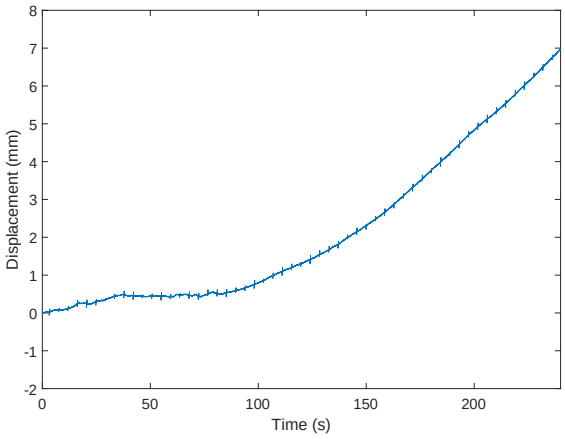

Figure 5.4: Baseline in room conditions for HySA sample

A similar approach was used to see if this effect also appears when the IPMC is kept in a high humidity environment. Figure 5.5 shows that it is much more stable in a high humidity and doesn't bend significantly over a long time period. From this it was assumed that this curl phenomenon was due to the IPMC losing water. This phenomenon was not fully investigated and tests were done in a high humidity to eliminate this effect from the experiments.

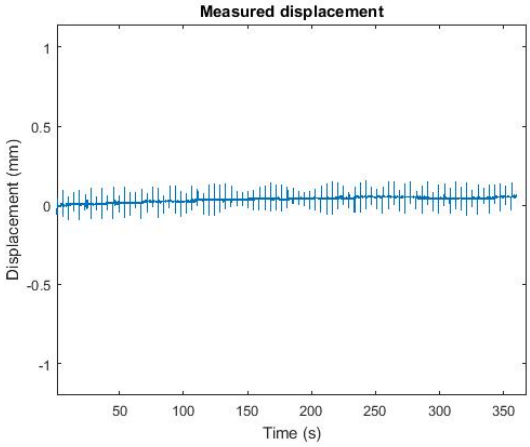

Figure 5.5: Baseline in 20°C 80 %RH for HySA sample

The experiments were all done in a high humidity, namely 20°C 80 %RH to be certain the displacement and force is the result of the applied voltage. It is known that clamping pressure can influence the performance of the IPMC thus it was kept constant throughout all the experiments. The displacement for different input signals was

investigated first. Figure 5.6 shows the applied voltage, the absorbed current and the tip displacement of the IPMC for a 1 V step input. The sample has a maximum tip displacement of 0.55 mm and draws a peak current of 89.88 mA and a steady state current of 3.5 mA.

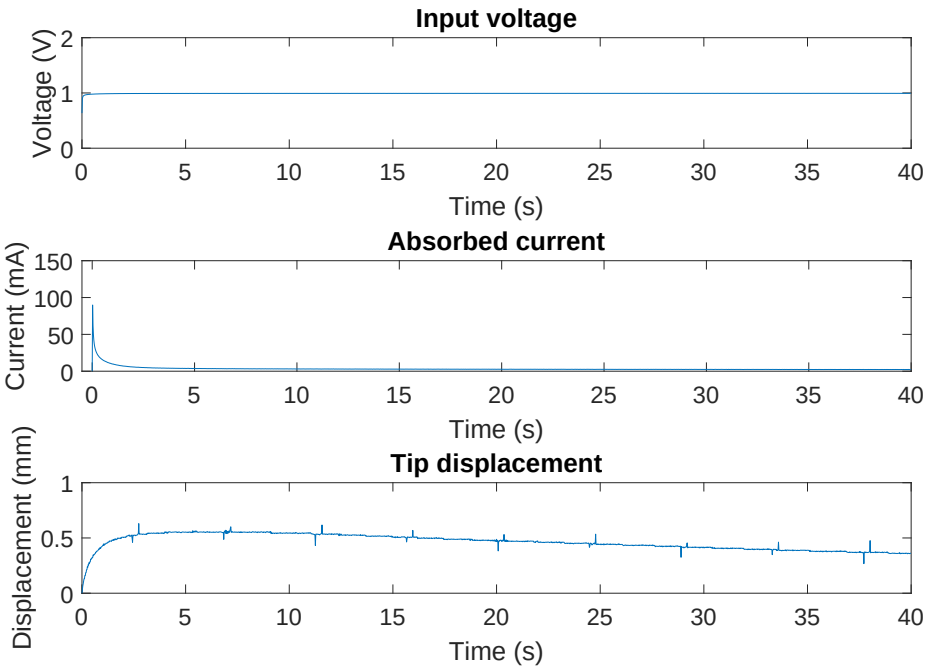

Figure 5.6: Displacement for 1 V step input for HySA sample

Figure 5.7 shows the applied voltage, the absorbed current and the tip displacement of the IPMC for a 1 V sine wave with a frequency of 0.1 Hz input. The displacement's amplitude was 0.23 mm and it draws a maximum of 8.5 mA to achieve that displacement. The frequency 0.1 Hz was chosen as it has a larger displacement than higher frequencies. Throughout this chapter most of the experiments that were done with ac signals had a frequency of 0.1 Hz. The current absorbed doesn't have a pure sinusoidal waveform. It is uncertain what the cause of this is. It was not seen in the other samples that was tested. A similar waveform was seen with the 5 mgPt/cm^2 samples discussed later in this section. It might be that the lower the Platinum loading is, the more the sinusoidal waveforms deforms.

Figure 5.8 shows the applied voltage, the absorbed current and the tip displacement of the IPMC for a 1 V square wave with a frequency of 0.1 Hz input. The maximum

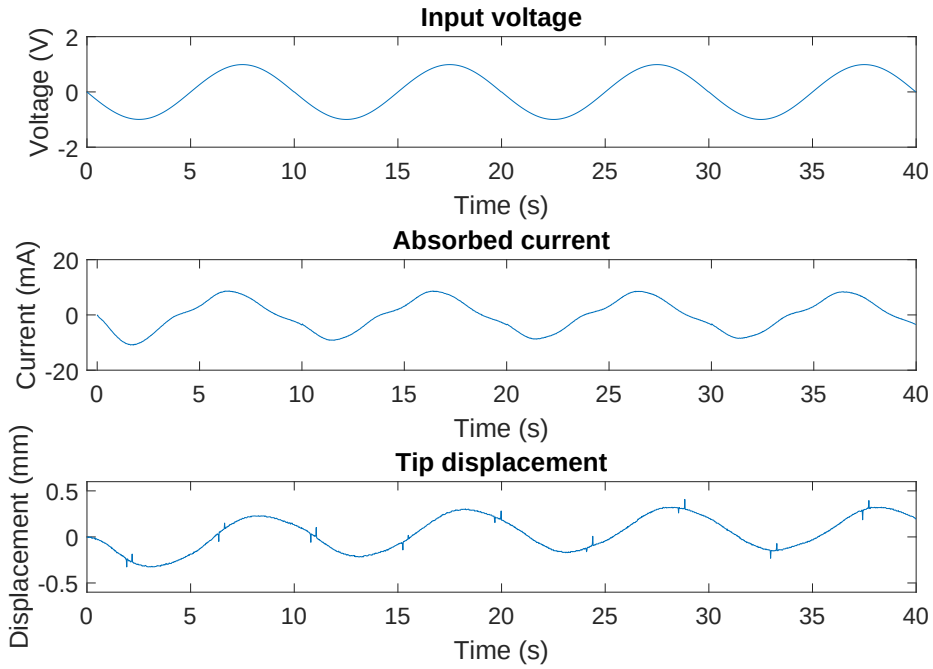

Figure 5.7: Displacement for 1 V sine input for HySA sample

displacement was 0.28 mm and the current had a peak of 86 mA which drops to a value of 3.3 mA.

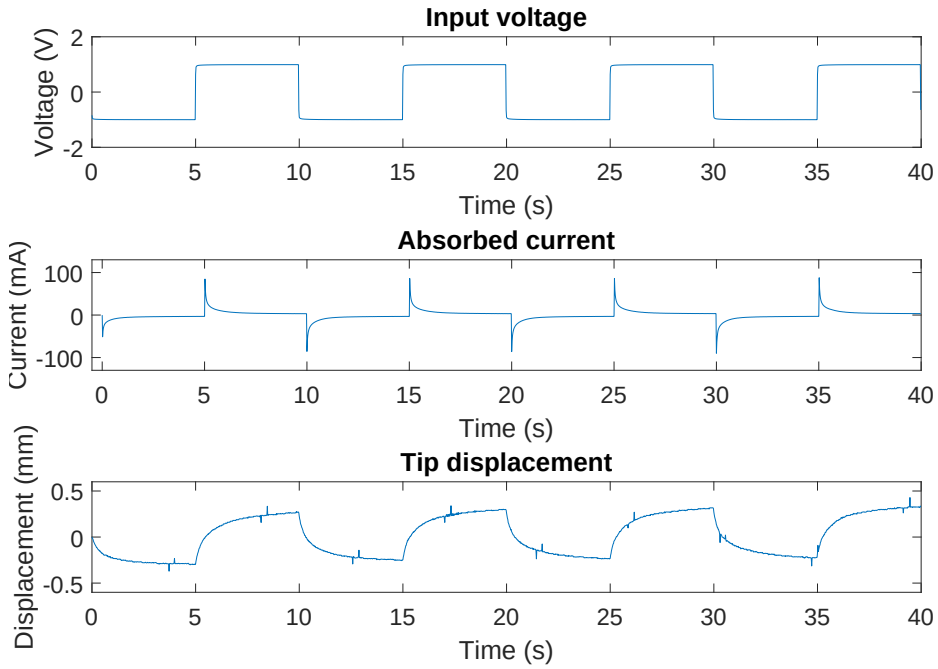

Figure 5.8: Displacement for 1 V square input for HySA sample

The blocked force of the IPMC was investigated next and various input signals were tested. From this it was seen that this sample exhibits a very low force and was difficult to measure and to use for comparisons thus the force was measured at a higher voltage. Figure 5.9 shows the input voltage, the absorbed current and the blocked force for a 3 V step input signal. It had a maximum value of 4 mN and the current drawn had a peak value of 174.5 mA and a steady state value of 110 mA.

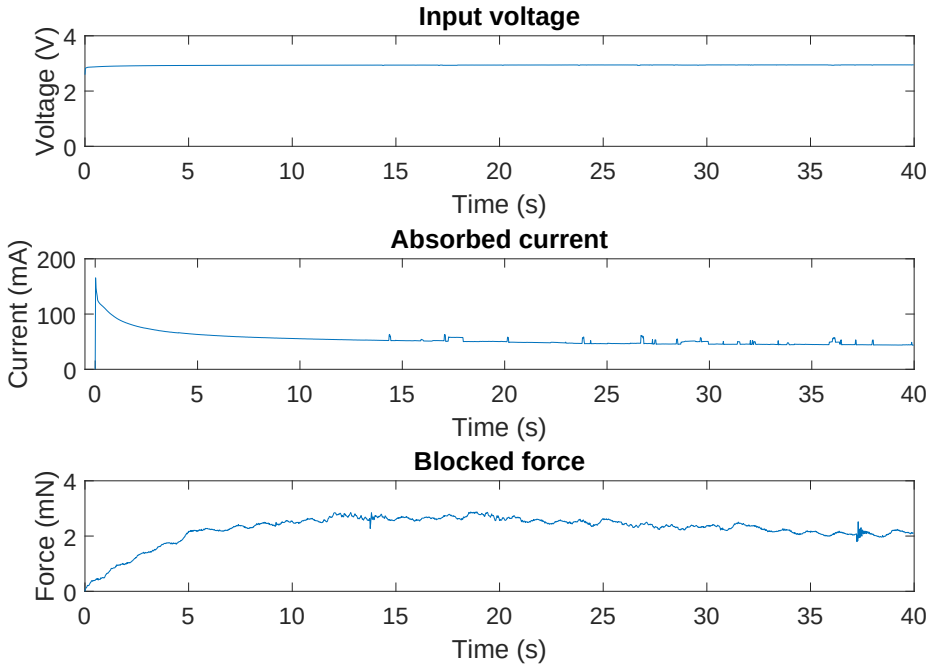

Figure 5.9: Force for 3 V step input for HySA sample

5.1.2 N117 10 mgPt/cm^2 (Sample 2)

The next sample that was investigated was a Nafion N117 membrane plated with a loading of 10 mgPt/cm^2 and was produced by an OEM. In Figure 5.10 shows the Pt on the surface of the membrane. The thickness of the Pt electrode can be seen in Figure 5.11 which shows the cross-section of the IPMC. The TEM image in Figure 5.12 shows the Pt layer and that it is more disperse than the sample produced by HySA.

The sample used for experiments was 30 mm x 5 mm. The surface resistance was measured as 8Ω with the four probe method. The dry weight of this sample was 103

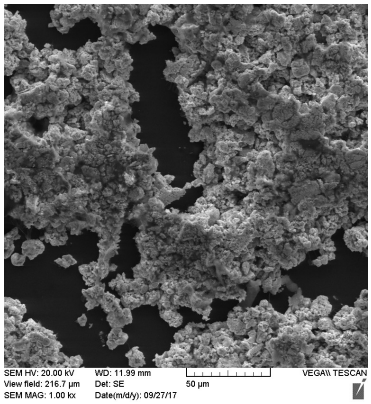

Figure 5.10: Typical Pt morphology by SEM on the surface of the N117 10 mgPt/cm^2 membrane

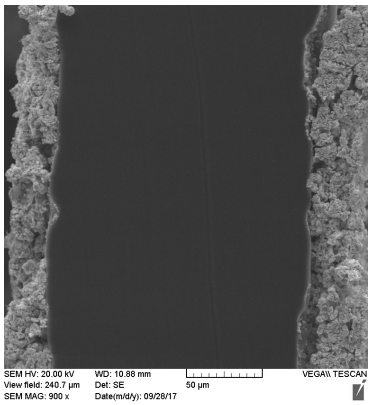

Figure 5.11: Typical Pt morphology by SEM of the cross-section of the N117 10 mgPt/cm^2 membrane

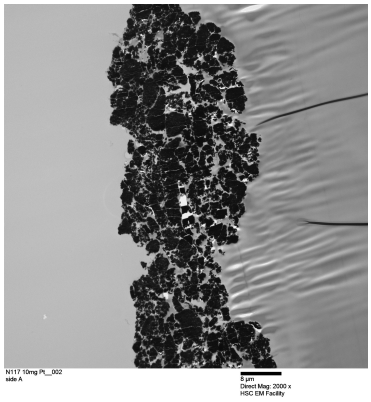

Figure 5.12: Typical Pt morphology by TEM of the cross-section of the N117 10 mgPt/cm^2 membrane

mg and after it was hydrated in deionized water its weight was 113 mg. To determine if this sample also curls in room temperature the displacement when no voltage was applied, was measured to create the baseline shown in Figure 5.13. It does start to curl but at a much slower rate than the previous sample. From this it was decided that tests can be done in room conditions if the tests are kept short and the sample hydrated between each test.

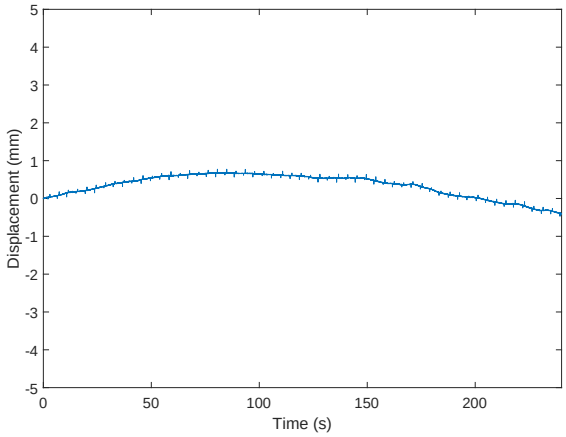

Figure 5.13: Baseline in room conditions for N117 10 mgPt/cm^2 sample

An experiment to determine the baseline in a high humidity was also done. The result can be seen in Figure 5.14 where there is a small displacement and then the displacement doesn't change significantly. Tests can be done in this region.

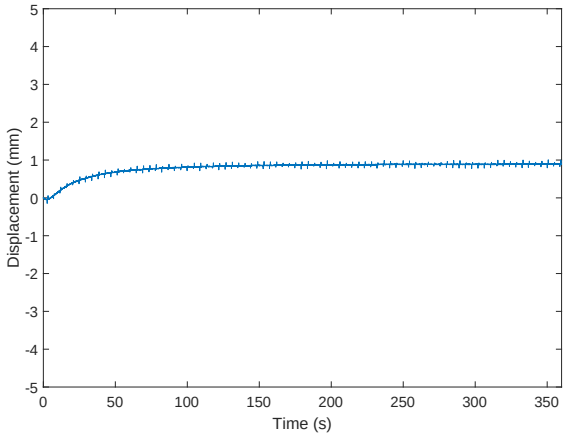

Figure 5.14: Baseline in 20°C 80%RH for N117 10 mgPt/cm^2 sample

Experiments to investigate the displacement when a voltage is applied was tested in

room conditions first and then in a more humid environment later. This was mainly done to be also be to create and test the model discussed in Chapter 4. In all the experiments the clamping pressure was kept constant. Figure 5.15 shows the applied voltage, absorbed current and tip displacement when a 1 V step input was applied. The displacement was 3.7 mm and the peak current drawn was 204.8 mA and the steady state current was 15 mA. This sample draws significantly more current than the HySA sample with a 2 mgPt/cm^2 loading. It has a much larger displacement which makes sense as the current reflect the ion movement which determine the displacement. The samples will be compared in Section 5.1.8 after all samples are investigated.

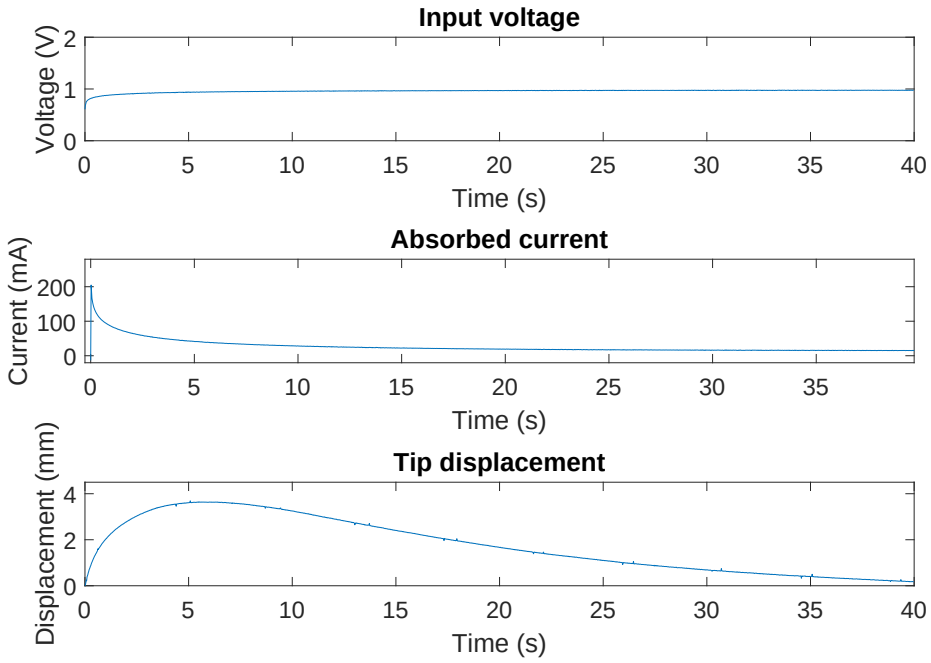

Figure 5.15: Displacement for 1 V step input for N117 10 mgPt/cm^2 sample

Figure 5.16 illustrates the applied voltage, absorbed current and tip displacement when a 1 V sine wave with a frequency of 0.1 Hz input was applied. The maximum displacement was 1.43 mm and the maximum current drawn was 52.5 mA.

Figure 5.17 illustrates the applied voltage, absorbed current and tip displacement when a 1 V square wave with a frequency of 0.1 Hz input was applied. The maximum displacement was 1.8 mm and the current drawn has a peak of 180 mA and then drops to 30 mA.

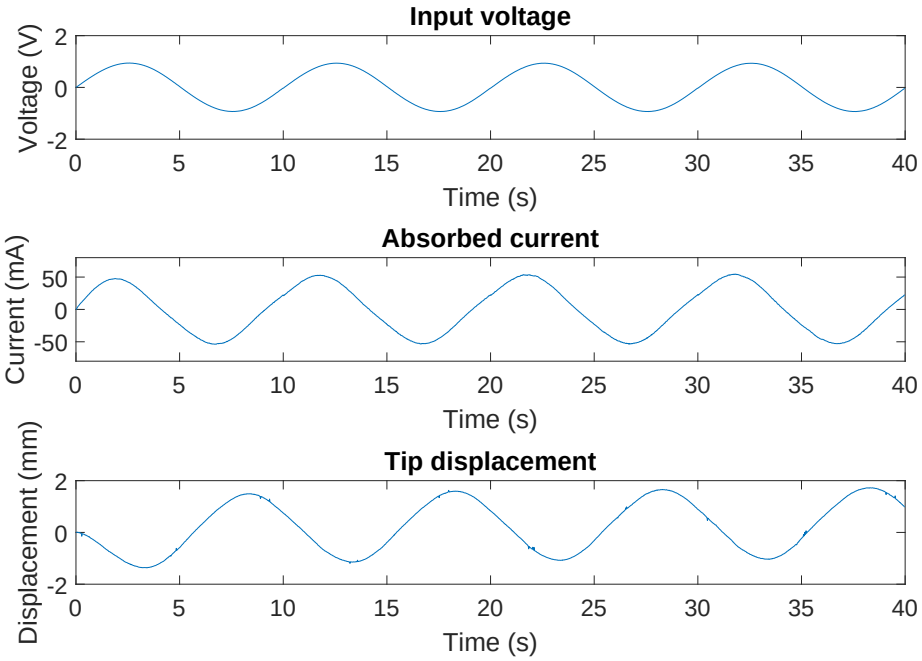

Figure 5.16: Displacement for 1 V sine input for N117 10 mgPt/cm^2 sample

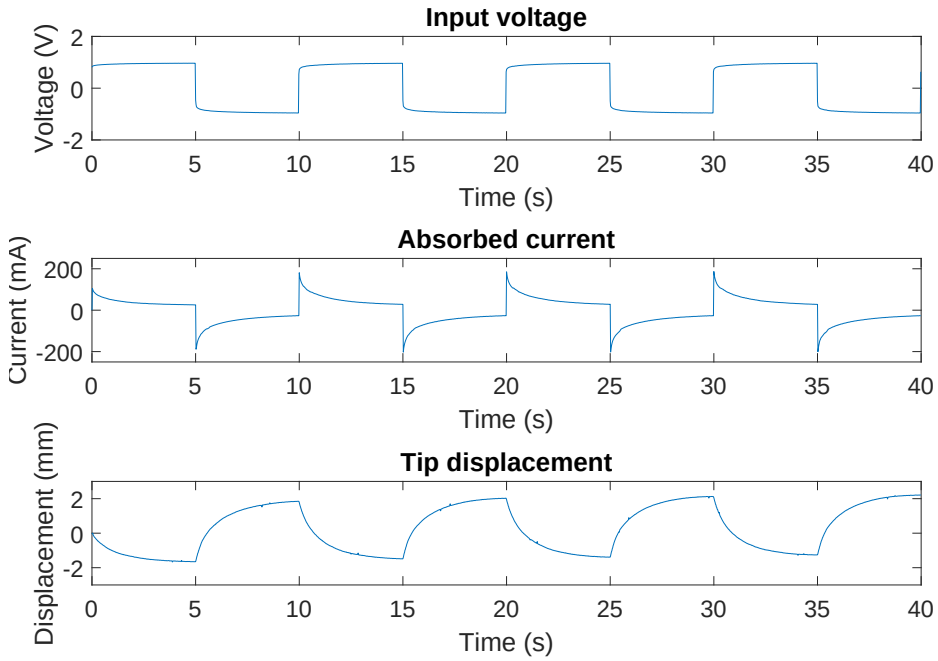

Figure 5.17: Displacement for 1 V square input for N117 10 mgPt/cm^2 sample

The blocked force for various inputs was investigated. In order to be able to measure both positive and negative forces with a load cell that can only measure compression a small preload was applied. This was also done in [20]. This preload differed between

samples as it must be large enough that the IPMC makes contact with the load cell at all times during the experiment. The following experiments were done in room conditions, mainly for modelling purposes as previously stated. Figure 5.18 illustrates the applied voltage, absorbed current and blocked force for a 1 V step input. The blocked force of 1.3 mN was achieved while the current drawn had a peak value of 67.01 mA and a steady state value of 7 mA.

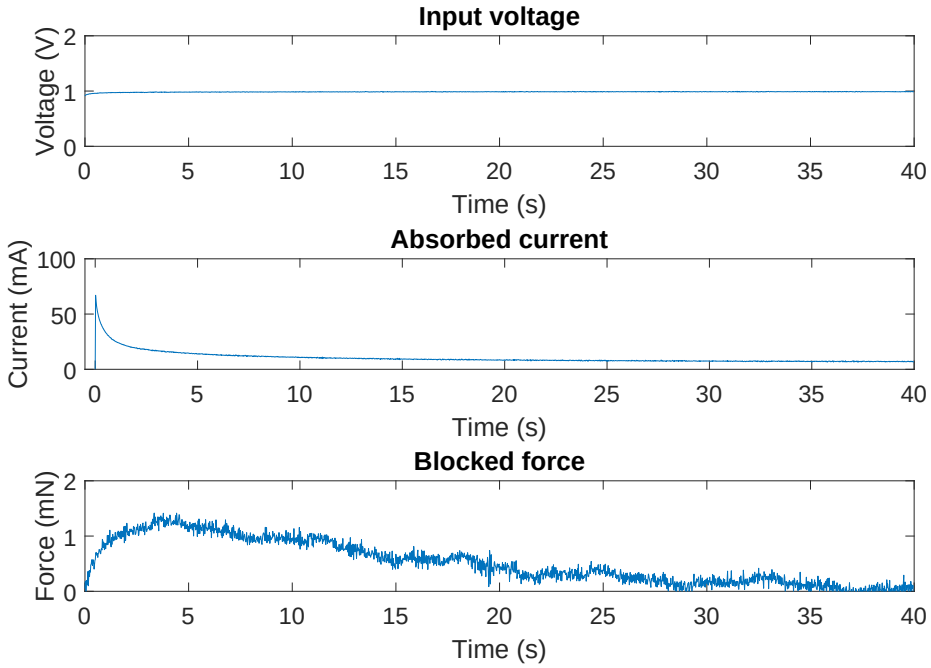

Figure 5.18: Force for 1 V step input for N117 10 mgPt/cm^2 sample

Figure 5.19 illustrates the applied voltage, absorbed current and blocked force for a 1 V sine wave with a frequency of 0.1 Hz input. The maximum force was 1.1 mN and the maximum current drawn was 30 mA.

Figure 5.20 illustrates the applied voltage, absorbed current and blocked force for a 1 V square wave with a frequency of 0.1 Hz input. The maximum force was 1.2 mN and the current drawn had a peak value of 105 mA and then dropped to 15 mA.

To investigate the effect that humidity has on the IPMC performance, tests were done at different humidities and the displacement was measured. The temperature was kept at a constant of 20°C and the humidity was set to 60 %RH, 70 %RH and 80 %RH. Figure

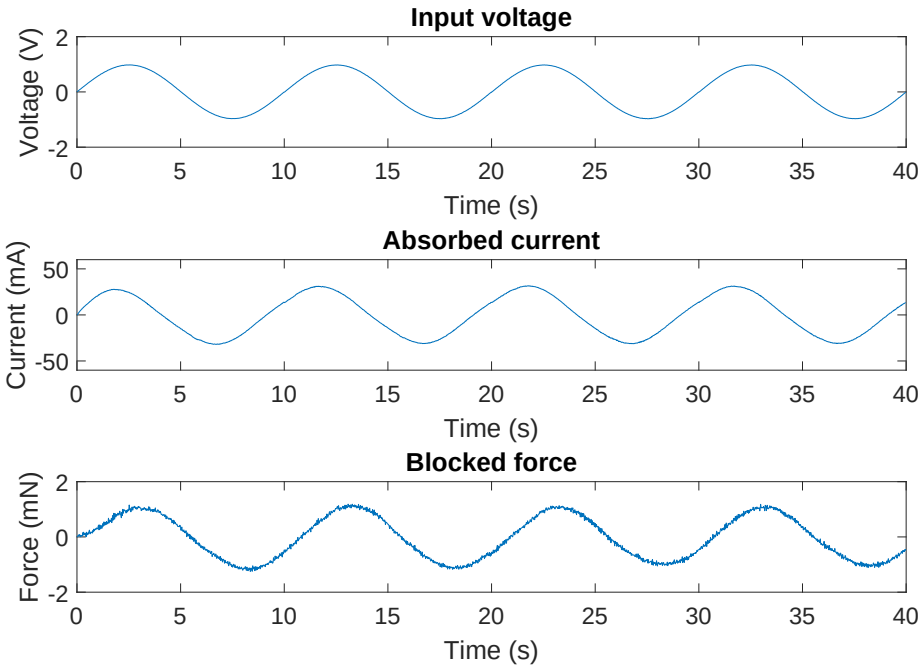

Figure 5.19: Force for 1 V sine input for N117 10 mgPt/cm^2 sample

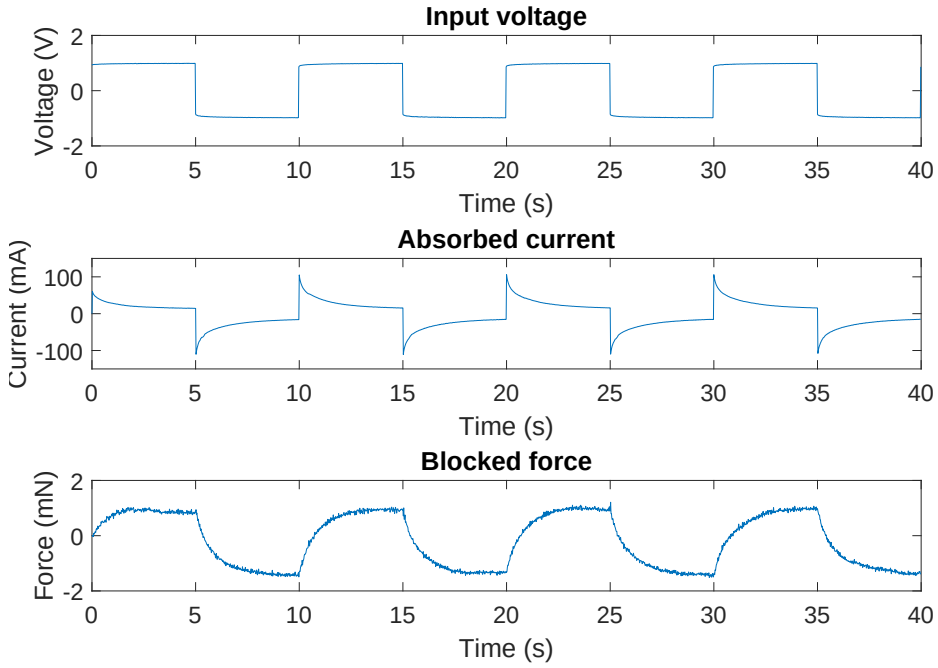

Figure 5.20: Force for 1 V square input for N117 10 mgPt/cm^2 sample

5.21 illustrates the displacement at each humidity point. The input voltage was a 1 V step input. This figure shows that the humidity has a large effect on the displacement between 80 %RH and 70 %RH and there is a small difference between the displace-

ments at 70 %RH and 60 %RH. The maximum displacements at 80 %RH, 70 %RH and 60 %RH were 3.83 mm, 1.27 mm and 1 mm respectively. The exponential increase in performance with an increase in %RH corresponds with work done in [11].

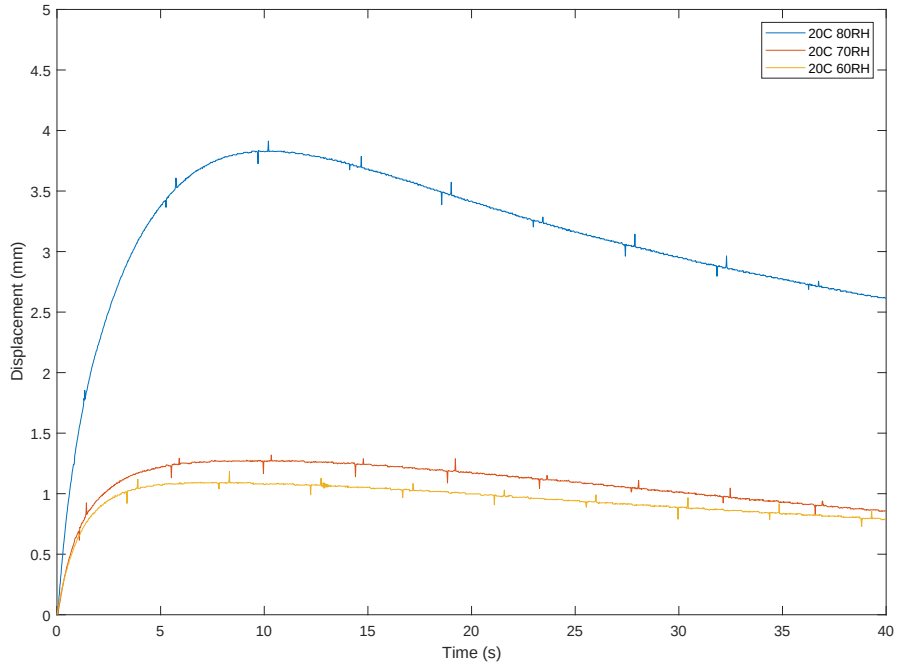

Figure 5.21: Displacement at different humidities with 1 V step input for N117 10 mgPt/cm^2 sample

As the performance of the IPMC also includes the blocked force a similar experiment was done. In this case the blocked force was measured at each humidity point and plotted in Figure 5.22. The input signal used was a 1 V step. Similar to what was seen in the effect of humidity on displacement the force is significantly larger at 80 %RH and only slightly differs between 70 %RH and 60 %RH. The maximum blocked force at 80 %RH, 70 %RH and 60 %RH was 2.5 mN, 1.2 mN and 1 mN respectively.

The effect of voltage on the performance of the IPMC was also investigated and plotted in Figure 5.23. In this experiment all the tests were done at 20°C 80 %RH. The input signals were a 1, 2 and 3 V step. The displacement increases from 1 to 2 V and 3 V has a much larger displacement. This shows that the displacement increases exponentially with the input voltage. This relates with what was seen in the literature.

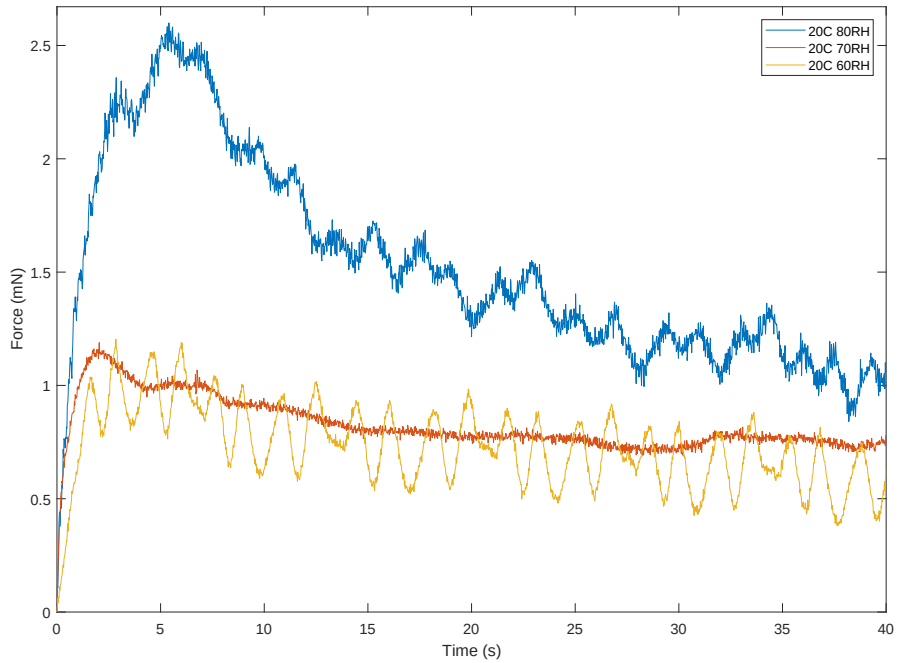

Figure 5.22: Force at different humidities with 1 V input for N117 10 mgPt/cm^2 sample

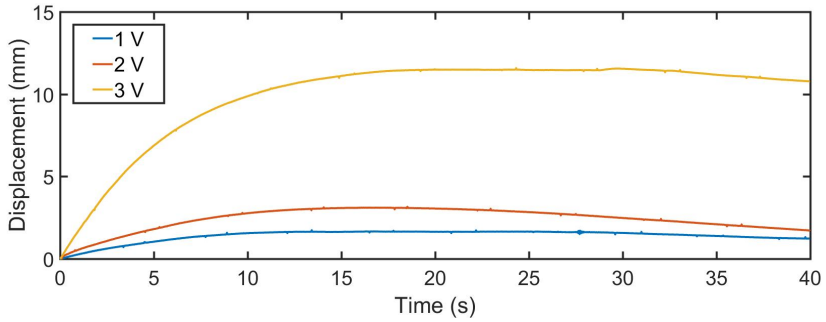

Figure 5.23: Displacement in room conditions at different voltages for N117 10 mgPt/cm^2 sample

To investigate the effect that temperature has on the displacement of the IPMC the displacement for a 1 V step input was measured at 20, 30 and 40°*C*. The humidity was kept constant at 80 %RH. From 20 and 30 °*C* there was a large decrease in displacement. From 30 to 40°*C* the decrease was much smaller. This shows that the temperature does not have a linear effect on the displacement

The effect of the frequency on the displacement was investigated as it has a significant

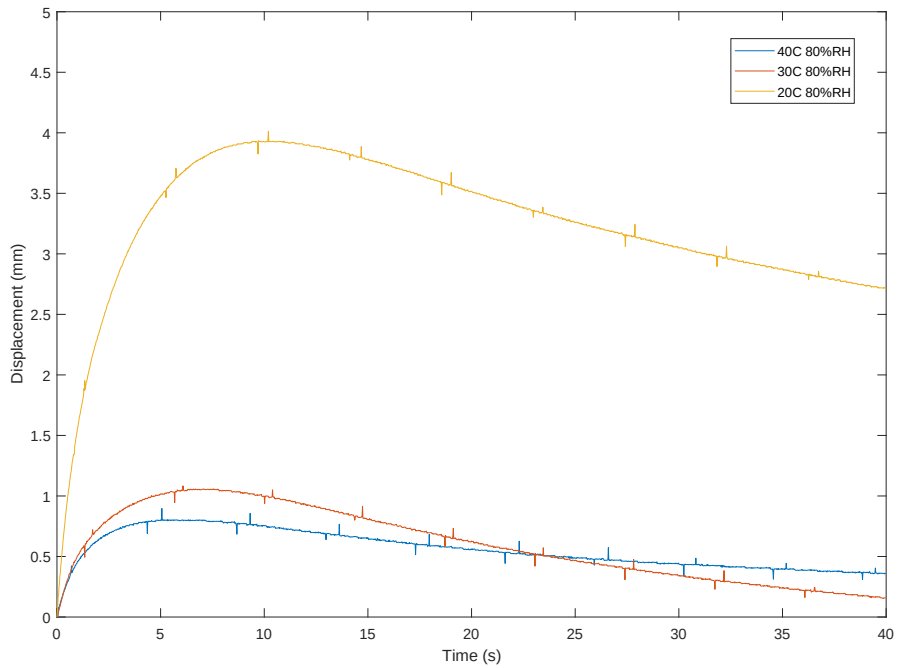

Figure 5.24: Displacement at different temperatures with 1 V step input for N117 10 mgPt/cm^2 sample

role in the amplitude of the displacement because the water inside the membrane requires time to move from one side to the other. These experiments were done in a 20°C 80%RH environment and all the input signals were 1 V sine waves with frequencies varying from 0.05 Hz to 1 Hz. The amplitude of the displacement was plotted against the signal frequency in Figure 5.25. The maximum displacement decreases exponentially with an increase of frequency.

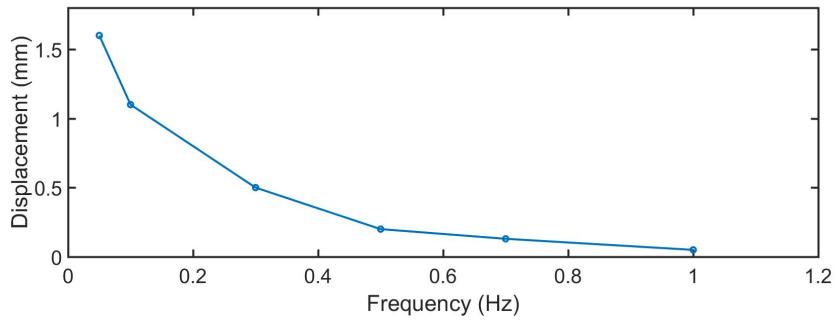

Figure 5.25: Displacement in room conditions for 1 V sine inputs with different frequencies for N117 10 mgPt/cm^2 sample

5.1.3 N117 7 mgPt/cm^2 (Sample 3)

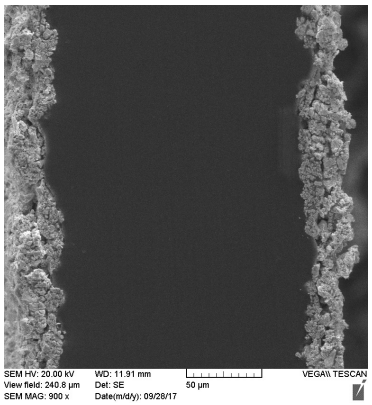

Figure 5.26: Typical Pt morphology by SEM of the cross-section of the N117 7 mgPt/cm^2 membrane

This sample is based on Nafion N117 and is plated on both sides with 7 mgPt/cm^2 and Figure 5.26 shows the cross-section of the sample through a SEM photo. The sample's dimensions are 30 mm x 5 mm and the measured dry weight is 89 mg and weighs 101 mg after it was submerged in deionized water for 24 hours. First the displacement was measured when no voltage was applied in room condition and was plotted in Figure 5.27. From this it was seen that the displacement changes to much to do the experiments in room condition. This experiment was repeated in an environment of $20°C$ 80 %RH and is illustrated in Figure 5.28. This baseline is shows that experiments can be done in this environment knowing that the displacement is only caused by the voltage applied.

The first set of tests are to investigate the displacement under different input signals. These experiments were all done at $20°C$ 80 %RH and at a constant clamping pressure. The input voltage, absorbed current and tip displacement for a 1 V step input signal can be seen in Figure 5.29. The maximum displacement was 1.82 mm and the peak current drawn was 88 mA and the steady state current was 7 mA. This is approximately half of the current of the sample with the 10 mgPt/cm^2 loading.

The input voltage, absorbed current and tip displacement for a 1 V sine wave with a frequency of 0.1 Hz can be seen in Figure 5.30. The maximum displacement was 0.58

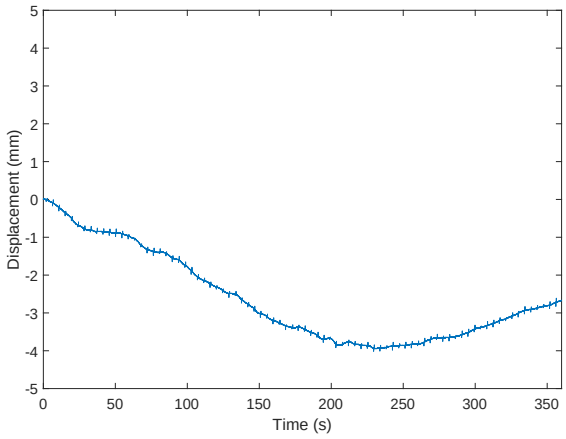

Figure 5.27: Baseline in room conditions for N117 7 mgPt/cm^2 sample

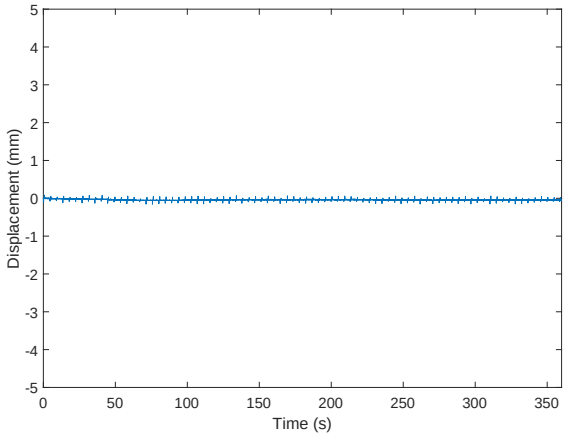

Figure 5.28: Baseline in 20°C 80 %RH for N117 7 mgPt/cm^2 sample

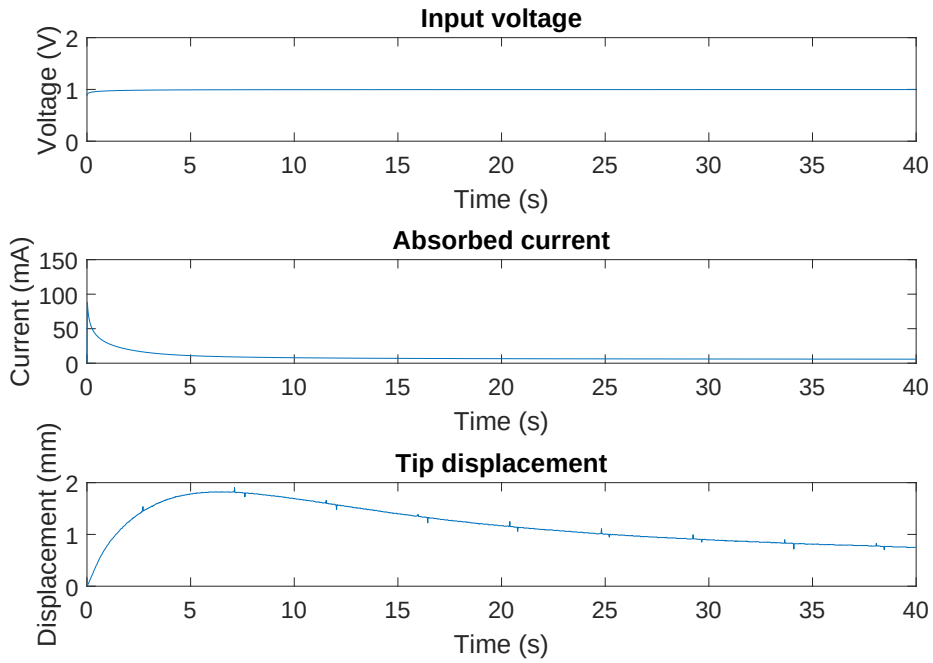

Figure 5.29: Displacement for 1 V step input for N117 7 mgPt/cm^2 sample

mm and the maximum current drawn was 17.7 mA.

The input voltage, absorbed current and tip displacement for a 1 V square wave with a frequency of 0.1 Hz can be seen in Figure 5.31. The maximum displacement was 0.8 mm and the peak current drawn was 78.71 mA and then it drops to 9.2 mA.

The blocked force was measured in 20°C 80 %RH by setting the load cell against the tip of the IPMC with a small preload to ensure that it makes contact the entire time. Figure 5.32 illustrates the input voltage, absorbed current and blocked force for a 1 V step input signal. The maximum force was 1.15 mN and the peak current was 90.7 mA and the steady state value was 6 mA. This experiment was repeated for a 3 V step input signal to be able to better compare it with the other samples later as some of the samples have a too low force at 1 V. The input voltage, absorbed current and blocked force is shown in Figure 5.33. With a 3V input it has a maximum blocked force of 2 mN and the maximum current was 113.2 mA with a steady state value of 50 mA.

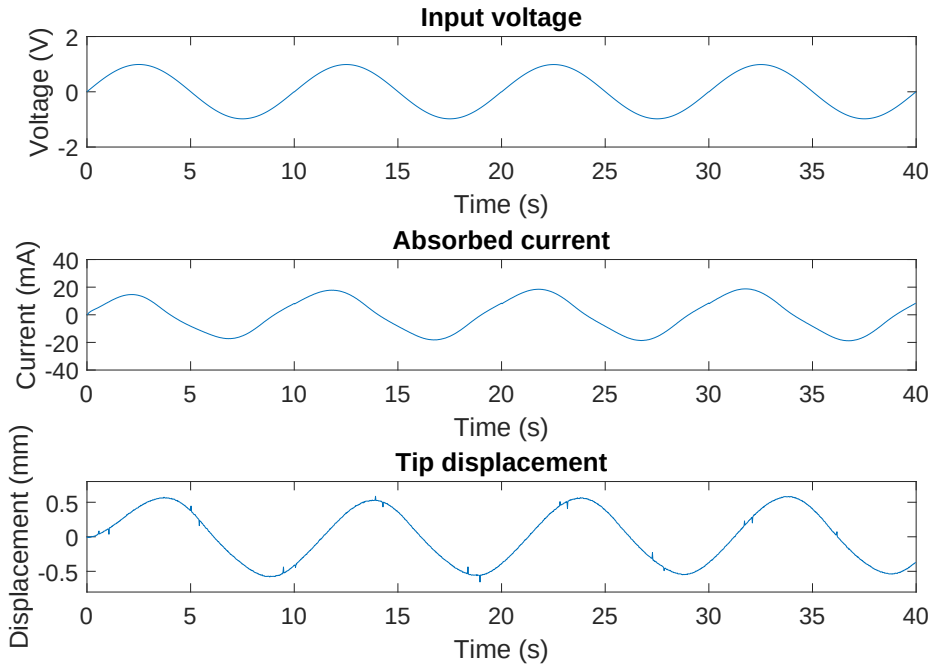

Figure 5.30: Displacement for 1 V sine input for N117 7 mgPt/cm^2 sample

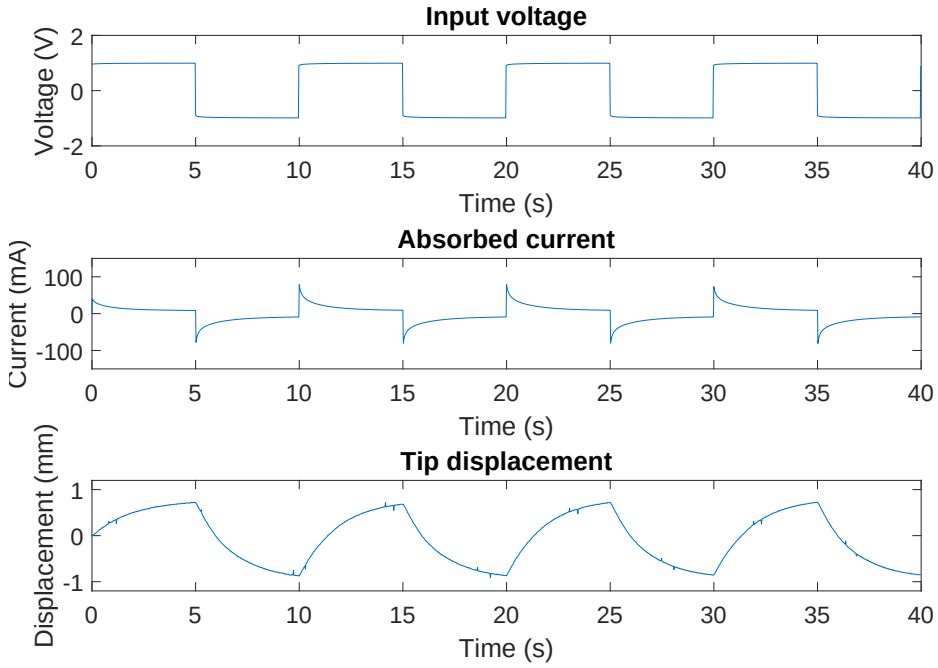

Figure 5.31: Displacement for 1 V square input for N117 7 mgPt/cm^2 sample

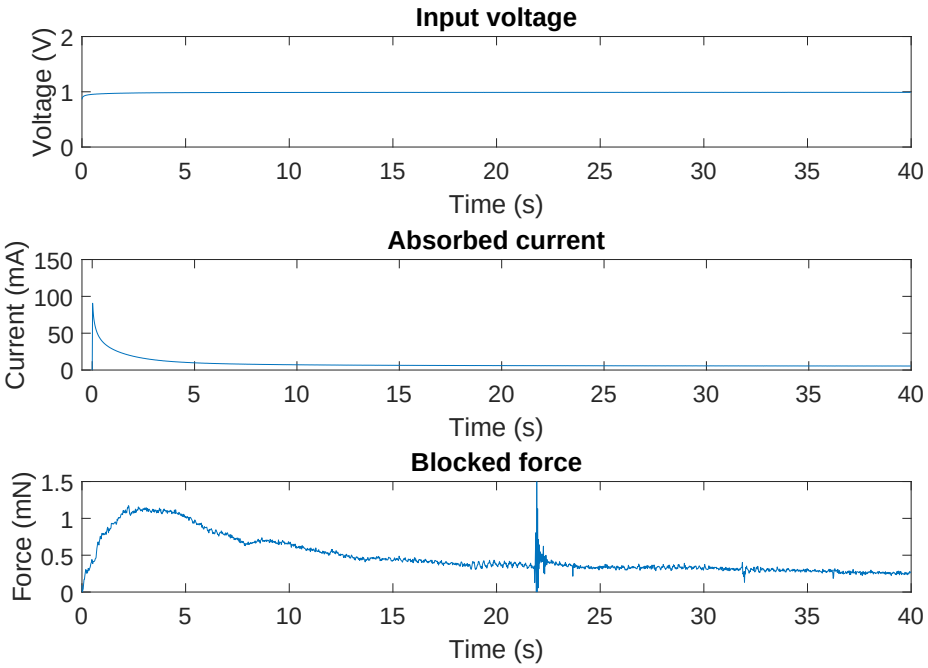

Figure 5.32: Force for 1 V step input for N117 7 mgPt/cm^2 sample

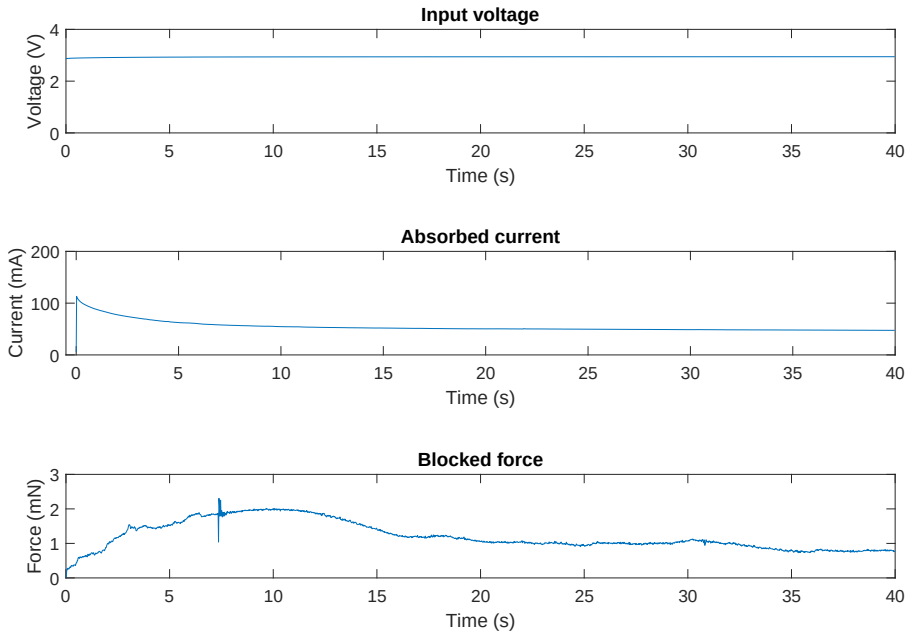

Figure 5.33: Force for 3 V step input for N117 7 mgPt/cm^2 sample

5.1.4 N117 5 mgPt/cm^2 (Sample 4)

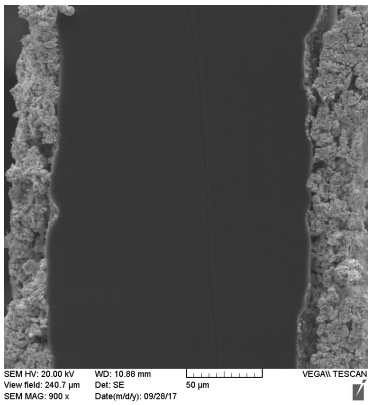

Figure 5.34: Typical Pt morphology by SEM of the cross-section of the N117 5 mgPt/cm^2 membrane

The sample that was used in the experiments in this section has a Nafion N117 base with a Pt loading of 5 mgPt/cm^2. Figure 5.34 shows the cross-section of the sample. The sample dimensions are 30 mm x 5 mm. Its dry weight was 86 mg and after it was hydrated in deionized water for 24 hours it weighed 99 mg.

As seen from the other samples a test to determine a baseline for the curl in room conditions when no voltage is applied was tested. The baseline can be seen in Figure 5.35. This experiment was then repeated in an environment of 20°C 80 %RH and plotted in Figure 5.36. All experiments done on this sample was in an environment of 20°C 80 %RH. All experiments were done at a constant clamp pressure to ensure that it does not influence the performance.

The tip displacement was measured for various input signals. Figure 5.37 illustrates the input voltage, absorbed current and tip displacement for a 1 V step input signal. The maximum displacement was 0.81 mm and the peak current was 81.98 mA with a steady state value of 4.5 mA. The current values are similar to that of the HySA sample and will be more suitable to compare performance between these two samples than with the samples with a high Pt loading. Although the current drawn looks similar the N117 5 mgPt/cm^2 sample has significantly larger maximum tip displacement.

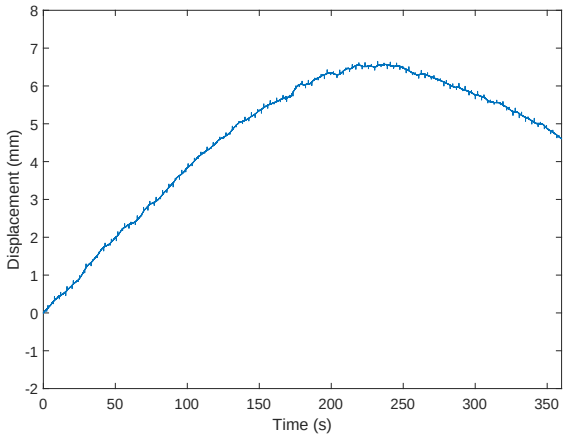

Figure 5.35: Baseline in room conditions for N117 5 mgPt/cm^2 sample

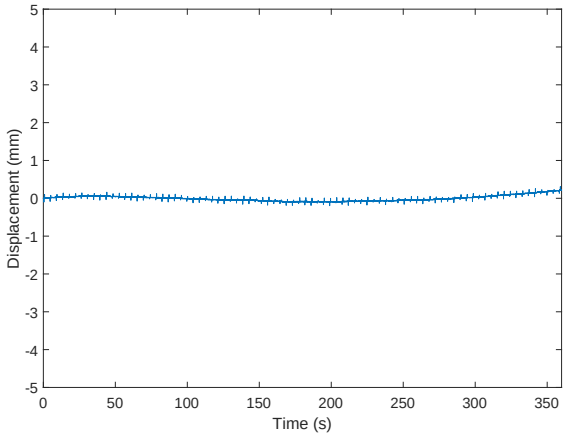

Figure 5.36: Baseline in 20°C 80 %RH for N117 5 mgPt/cm^2 sample

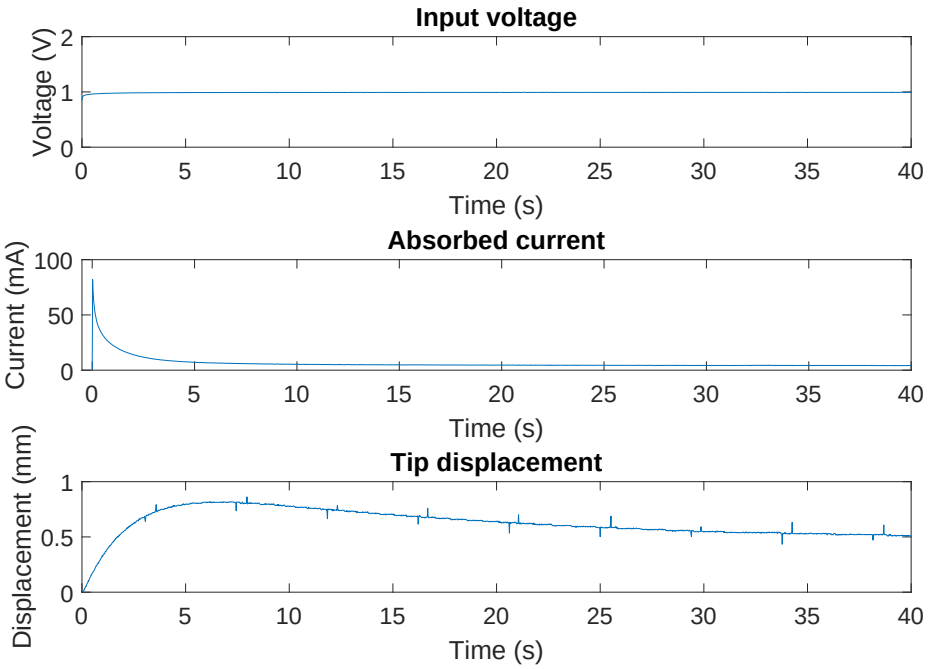

Figure 5.37: Displacement for 1 V step input for N117 5 mgPt/cm^2

Figure 5.38 shows the input voltage, absorbed current and tip displacement for a 1 V sine wave with a frequency of 0.1 Hz. The maximum displacement was 0.28 mm and the maximum current drawn was 17 mA. The displacement is only slightly larger than the HySA sample.

Figure 5.39 shows the input voltage, absorbed current and tip displacement for a 1 V square wave with a frequency of 0.1 Hz. The maximum tip displacement was 0.32 mm and the peak current has a value of 79.4 mA and drops to a value of 7 mA.

The effect that humidity has on the tip displacement was determined by measuring the displacement for a 1 V sine wave with a frequency of 0.1 Hz at the different humidities. The humidities where experiments were done are 60 %RH, 70 %RH and 80 %RH and the displacements are plotted in Figure 5.40. From this figure it is seen that the displacement is larger at a higher humidity and between 70 %RH and 80 %RH there is a more significant change in displacement than between 60 %RH an 70 %RH. This is similar to what was seen with the 10 mgPt/cm^2 sample.

The blocked force was measured in 20°C 80 %RH and with a 1 V step input the force

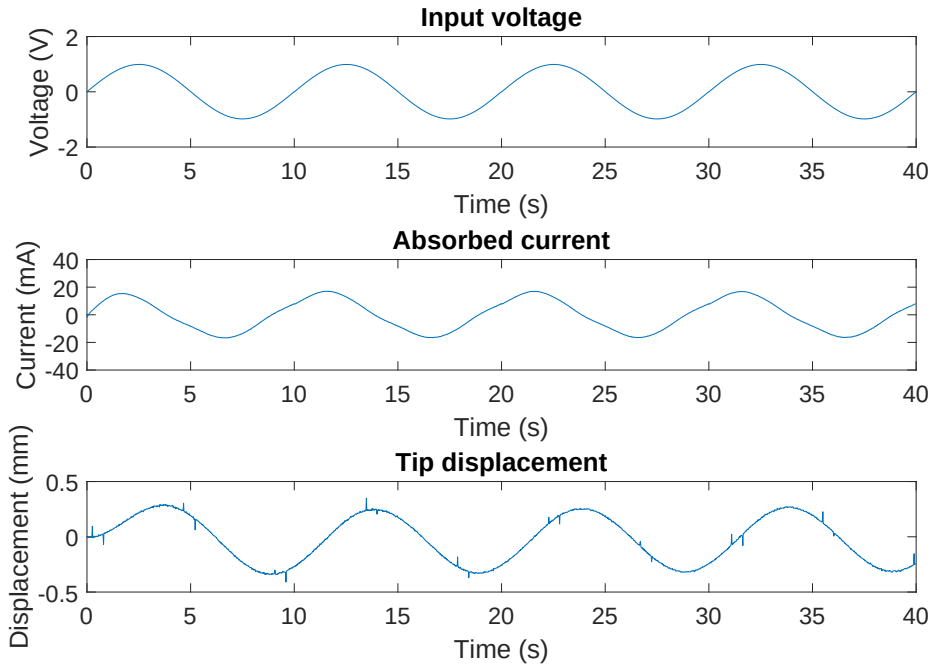

Figure 5.38: Displacement for 1 V sine input for N117 5 mgPt/cm^2

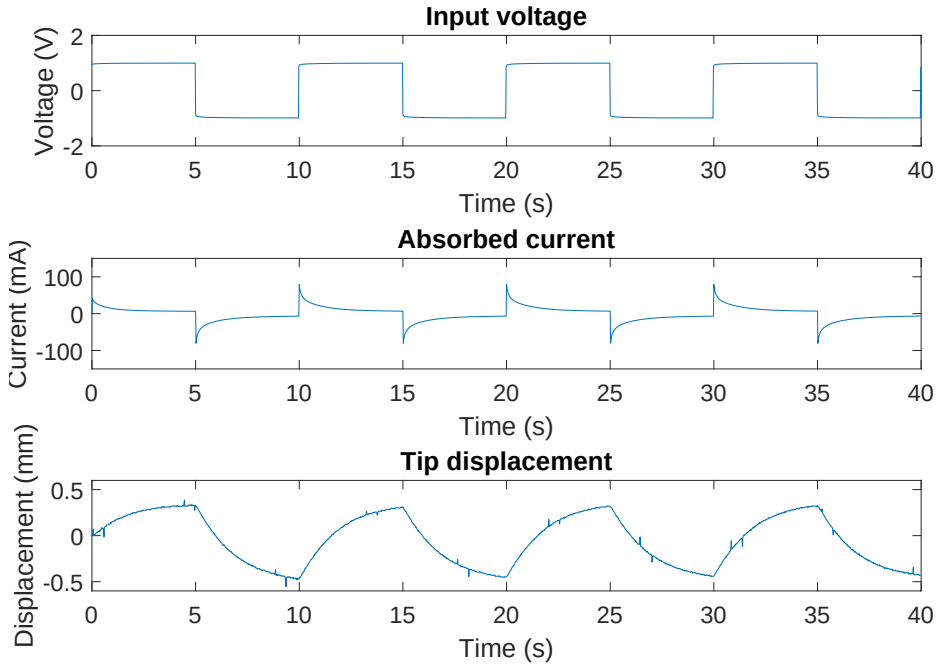

Figure 5.39: Displacement for 1 V square input for N117 5 mgPt/cm^2

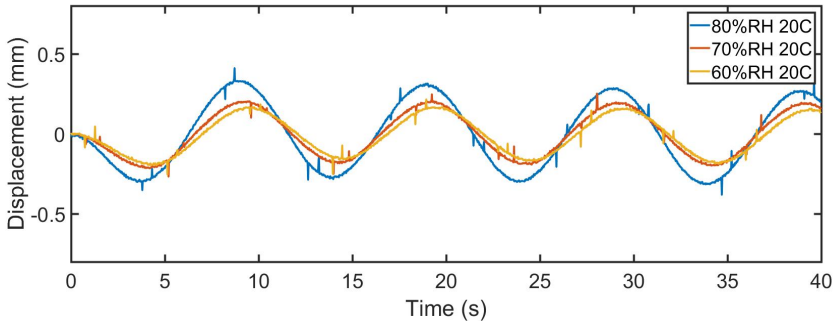

Figure 5.40: Displacement for 1 V input at different humidities for N117 5 mgPt/cm^2

was too low to see between the noise. Figure 5.41 shows the input voltage, absorbed current and blocked force for a 3 V step input. From this it is clear that this sample has a very small blocked force even at high voltages. It had a maximum blocked force of 0.5 mN and the current drawn had a peak value of 112.5 mA and a steady state value of 24 mA.

5.1.5 N1110 10 mgPt/cm^2 (Sample 5)

In this section the sample made from Nafion N1110 plated on both sides with a loading of 10 mgPt/cm^2 was investigated. The sample used was 30 mm x 5 mm and its dry weight was 120 mg. It weighed 128 mg after it was submerged in deionized water for 24 hours. As seen from the experiments on previous samples the displacement when no voltage is applied must first be measured in room conditions to see if the sample can be tested in room conditions. Figure 5.42 shows this displacement. The experiment was repeated at 20°C 80 %RH and the displacement plotted in Figure 5.43. As seen from these two figures the displacement of 2 mm happens over a time of 6 minutes in room conditions and in 20°C 80 %RH the displacement stays approximately the same. Thus all the experiments were done in 20°C 80 %RH.

The displacement was tested for different input voltages in 20°C 80 %RH with a constant clamping pressure. The input voltage, absorbed current and tip displacement for a 1 V step input can be seen in Figure 5.44. The maximum displacement was 1.27

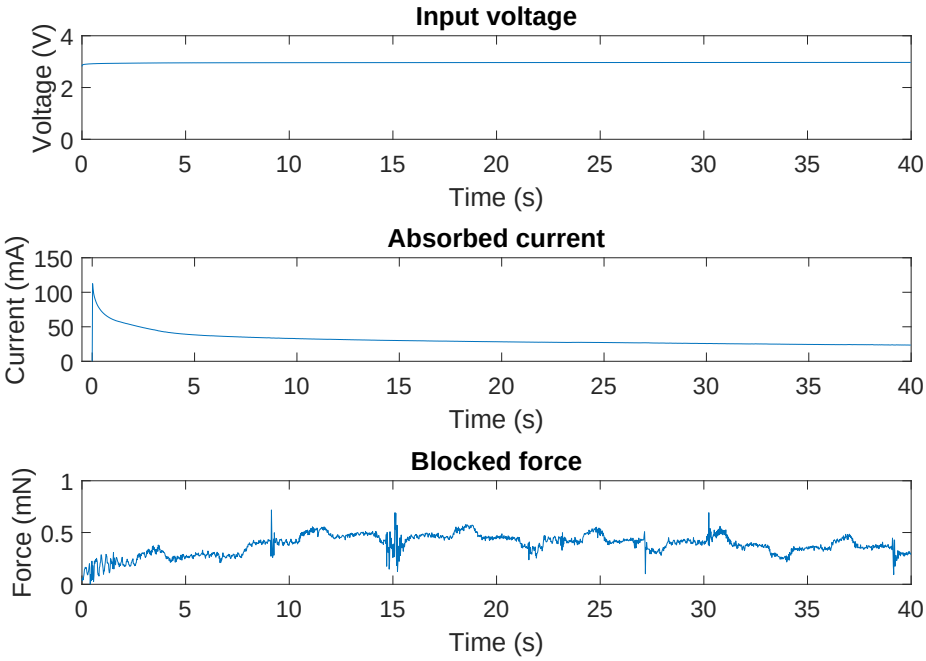

Figure 5.41: Force for 3V step input for N117 5 mgPt/cm^2

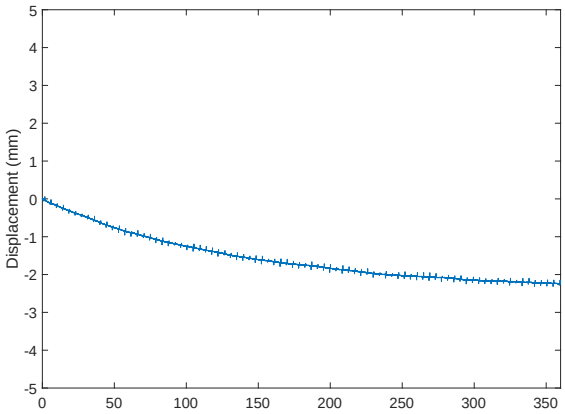

Figure 5.42: Baseline in room conditions for N1110 10 mgPt/cm^2 sample

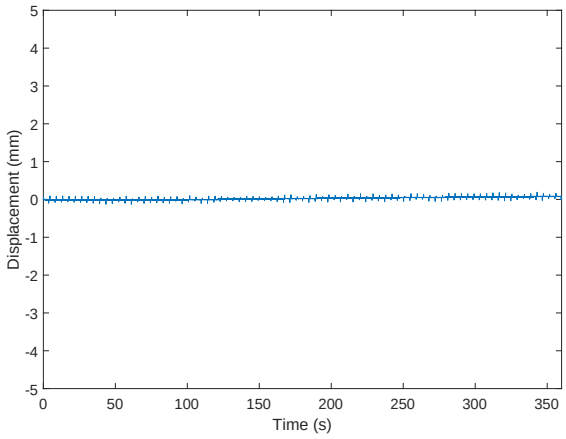

Figure 5.43: Baseline in 20°C 80 %RH for N1110 10 mgPt/cm^2 sample

mm and the peak current drawn was 100 mA and the steady state current was 14.1 mA. The N117 sample with the same loading has a larger displacement. The steady state current is similar but the N1110 sample has a lower peak current than the N117 sample.

The input voltage, absorbed current and tip displacement for a 1 V sine wave with a frequency of 0.1 Hz can be seen in Figure 5.45. The maximum displacement was 0.85 mm and the maximum current drawn was 27.5 mA

The input voltage, absorbed current and tip displacement for a 1 V square wave with a frequency of 0.1 Hz can be seen in Figure 5.46. The maximum displacement was 1.1 mm and the peak current was 178.5 mA and then drops to 22 mA. The maximum displacements are lower than that of the N117 sample which was as expected because the thicker sample having an increased stiffness.

The blocked force for different input signals were measured in 20°C 80%RH also with a constant clamping pressure. Figure 5.47 illustrates the input voltage, absorbed current and blocked force for a 1 V step input. The maximum blocked force was 3.7 mN and the current drawn has a peak value of 160.4 mA and a steady state value of 13 mA.

The input voltage, absorbed current and blocked force for a 1 V sine wave with a frequency of 0.1 Hz is shown in Figure 5.48. The maximum force was 1.1 mN and the

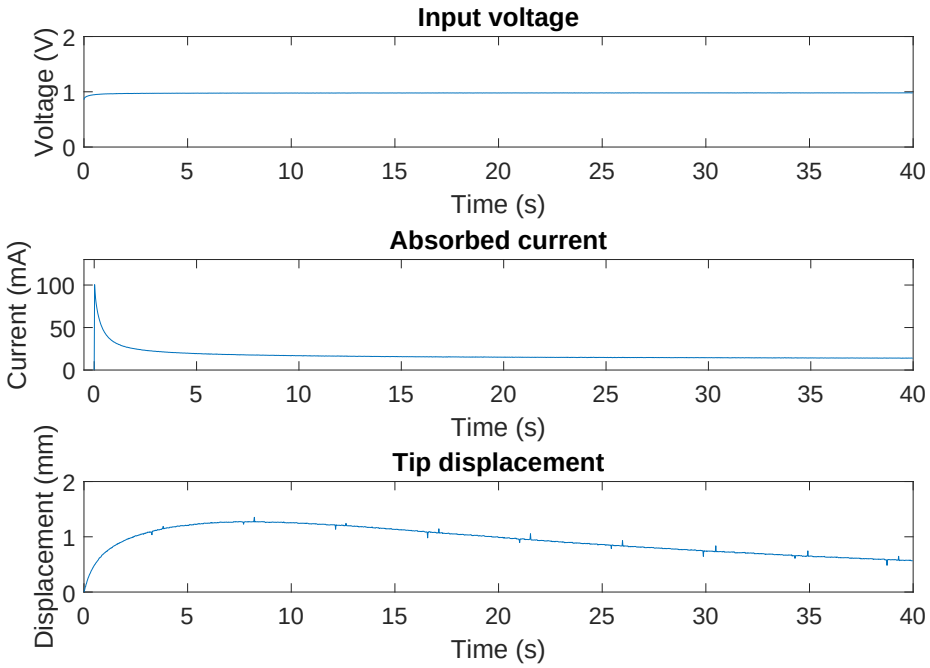

Figure 5.44: Displacement for 1V step input for N1110 10 mgPt/cm^2

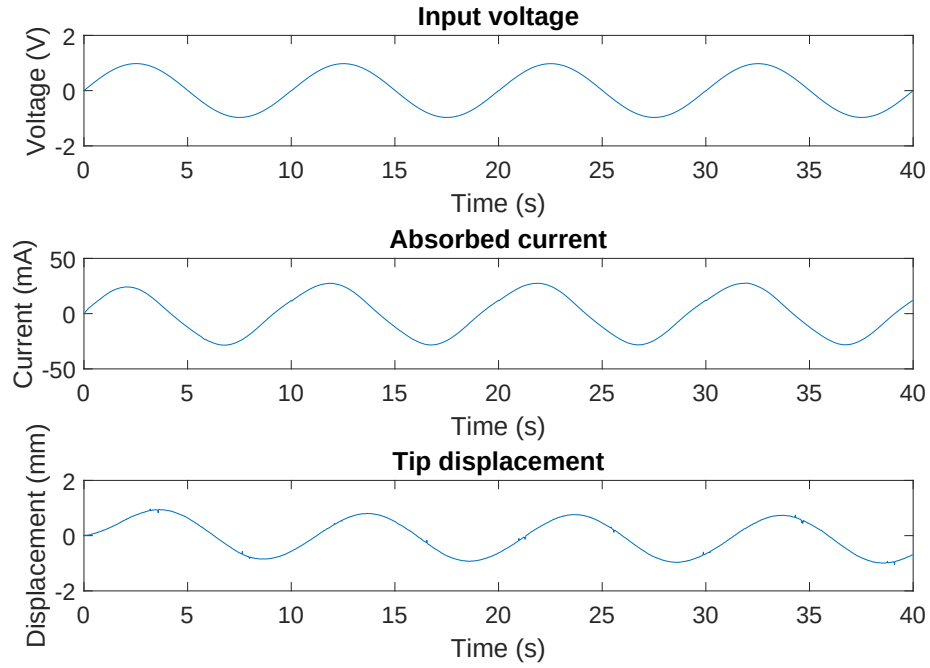

Figure 5.45: Displacement for 1V sine input for N1110 10 mgPt/cm^2

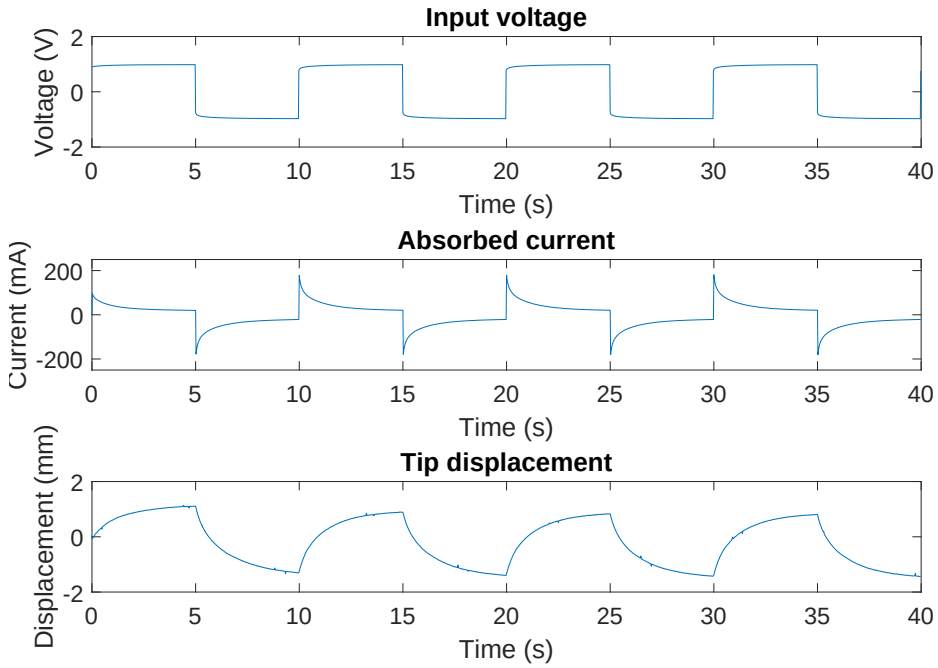

Figure 5.46: Displacement for 1 V square input for N1110 10 mgPt/cm^2

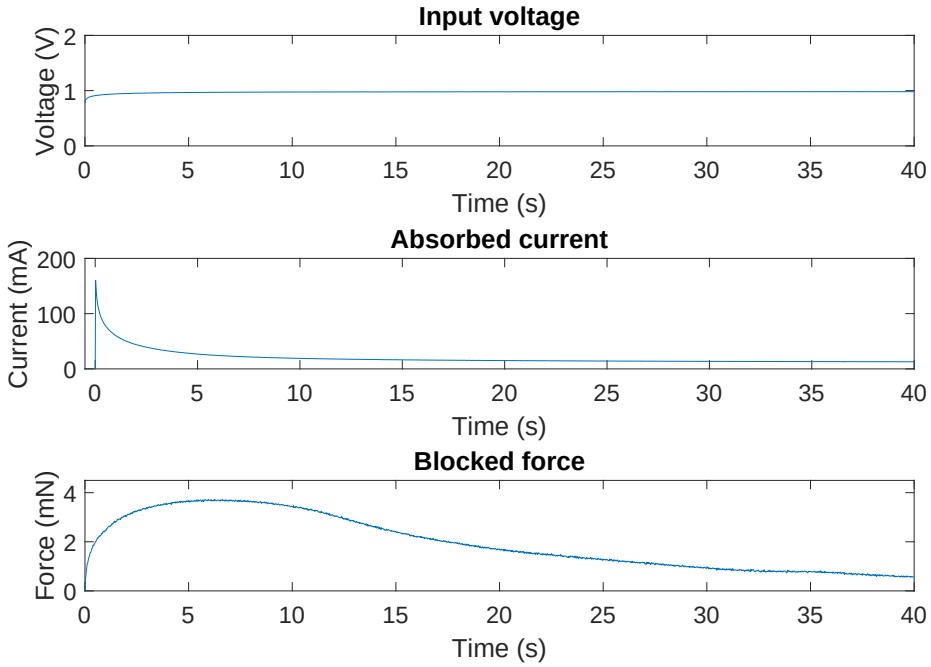

Figure 5.47: Force for 1 V step input for N1110 10 mgPt/cm^2

maximum current was 30 mA.

The input voltage, absorbed current and blocked force for a 1 V square wave with a frequency of 0.1 Hz is shown in Figure 5.49. The maximum force was 1.6 mN and the peak current was 170.9 mA and dropped to 19 mA.

The relationship between the input voltage and the blocked force was investigated. The blocked force was measured in $20°C$ 80 %RH for step inputs of 1, 2 and 3 V. The maximum force for each input voltage was plotted in Figure5.50. From this it is clear that the input voltage has a significant effect on the force. The exponential relationship seen with the displacement is visible in these results. More voltage points and testing it on various samples would confirm the exact relationship between the voltage and force.

5.1.6 N1110 7 mgPt/cm^2 (Sample 6)

This sample consists of Nafion N1110 and was plated on both sides with a loading of 7 mgPt/cm^2 and was cut into a 30 mm x 5 mm sample. The thickness of the electrodes can be seen in Figure 5.51. The dry weight was 105 mg and weighed 120 mg after it was submerged in deionized water for 24 hours. As seen from previous samples the baseline in room conditions must be measured to determine if is is possible to do experiments in room conditions. This baseline is illustrated in Figure 5.52 and from this it is seen that experiments must rather be done in a high humidity. This experiment was then repeated at $20°C$ 80 %RH and the baseline was plotted in Figure 5.53. From this it is clear that all the experiments must be done in $20°C$ 80 %RH. All experiments were done with a constant clamping pressure to ensure this does not affect the measurements.

The displacement in $20°C$ 80 %RH was measured for various input signals. Figure 5.54 shows the input voltage, absorbed current and tip displacement for a 1 V step input. The maximum displacement was 0.44 mm and the current had a peak value of 41.47 mA and a steady state value of 5 mA.

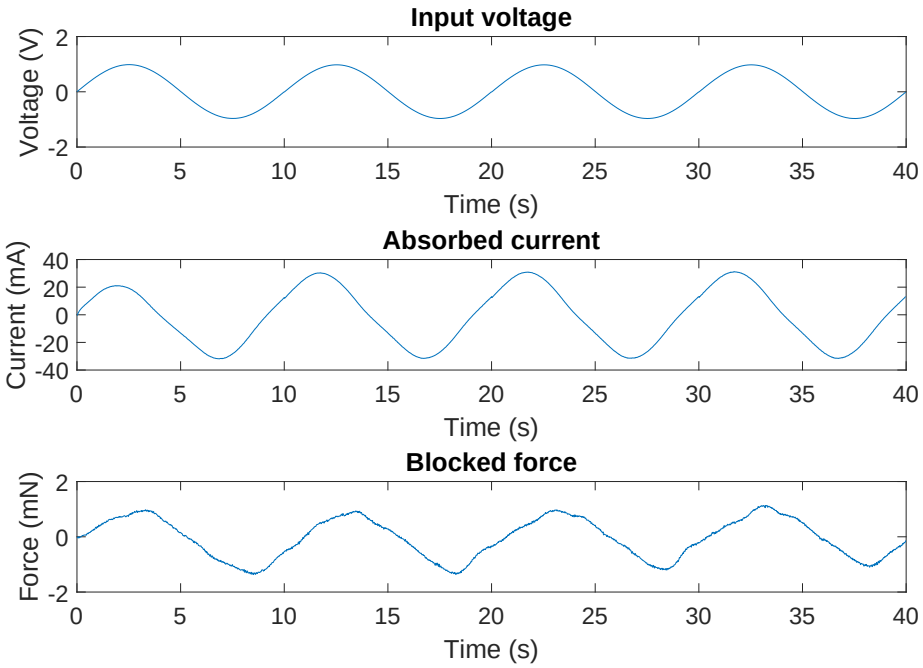

Figure 5.48: Force for 1 V sine input for N1110 10 mgPt/cm^2

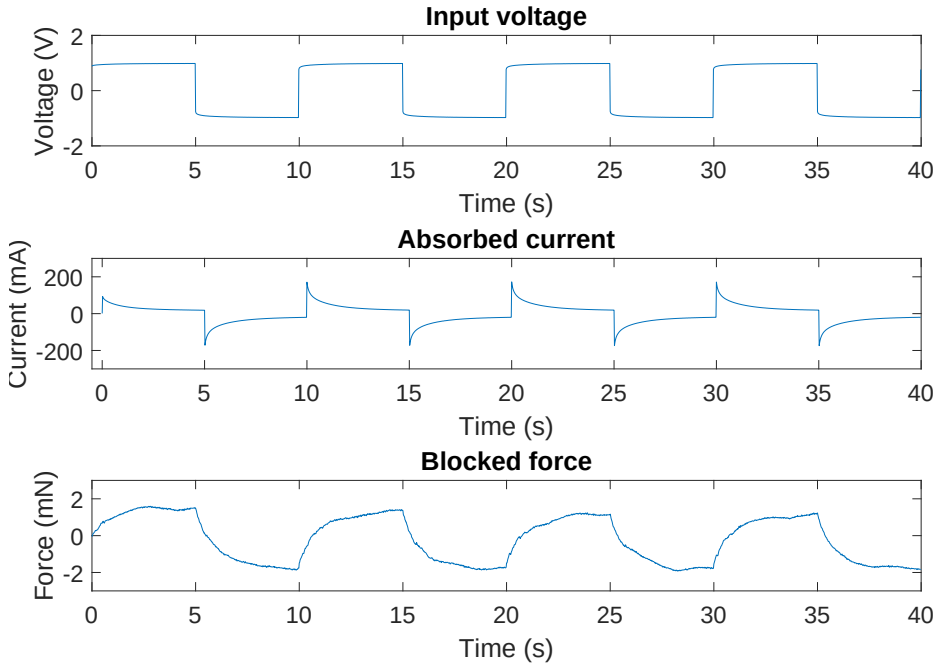

Figure 5.49: Force for 1 V square input for N1110 10 mgPt/cm^2

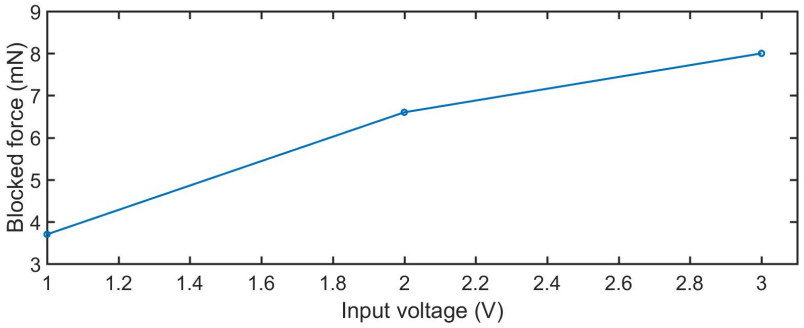

Figure 5.50: Force at different voltages for N1110 10 mgPt/cm^2

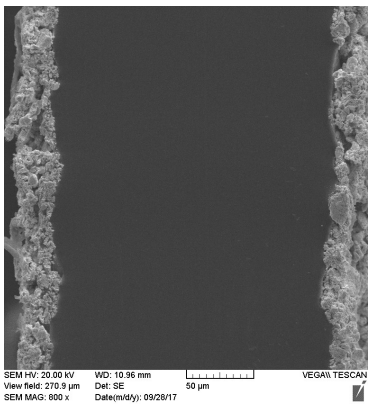

Figure 5.51: Typical Pt morphology by SEM of the cross-section of the N1110 7 mgPt/cm^2 membrane

Figure 5.55 shows the input voltage, absorbed current and tip displacement for a 1 V sine wave with a frequency of 0.1 Hz. The maximum displacement was 0.2 mm and the absorbed current had a maximum of 15.1 mA.

Figure 5.56 shows the input voltage, absorbed current and tip displacement for a 1 V square wave with a frequency of 0.1 Hz input. The maximum displacement was 0.28 mm and the absorbed current peaked at 78.97 mA and then dropped to 6.89 mA.

The blocked force was measured in 20°C 80 %RH. Due to the small blocked force of some of the samples the blocked force for a 3 V step input was measured to better compare the force of the different samples. The input voltage, absorbed current and blocked force for a 3 V step input was plotted in Figure 5.57.

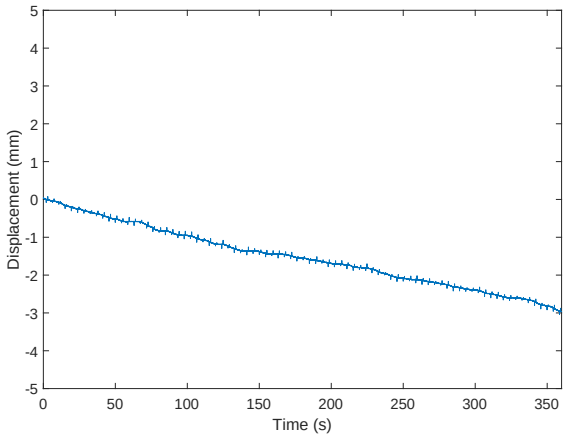

Figure 5.52: Baseline in room conditions for N1110 7 mgPt/cm^2 sample

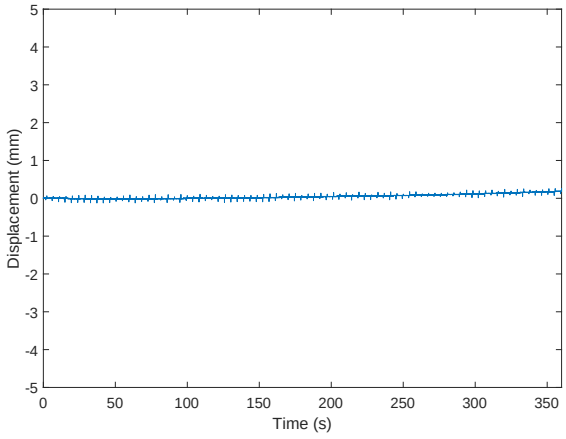

Figure 5.53: Baseline in 20°C 80 %RH for N1110 7 mgPt/cm^2 sample

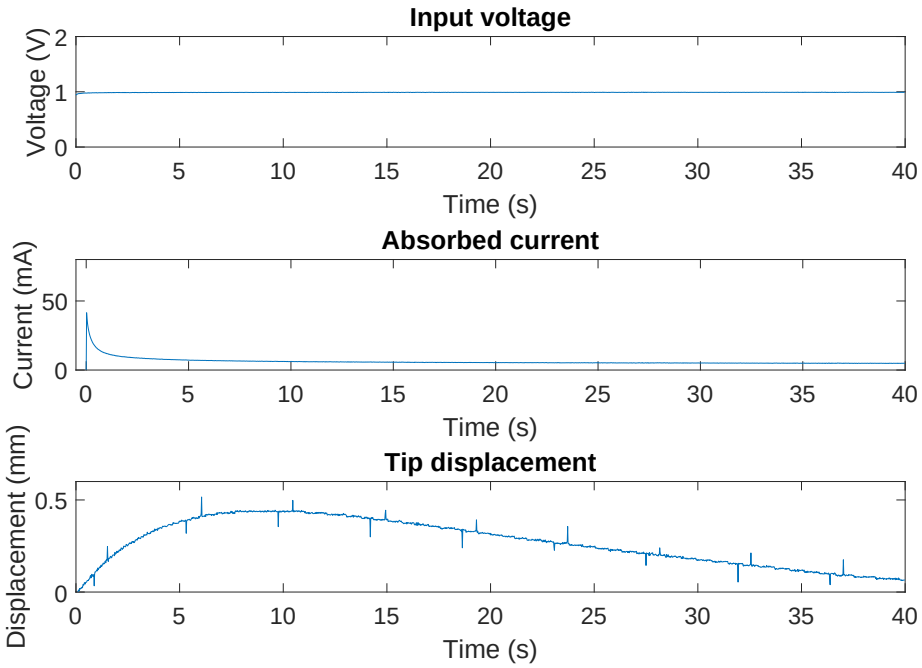

Figure 5.54: Displacement for 1 V step input for N1110 7 mgPt/cm^2 sample

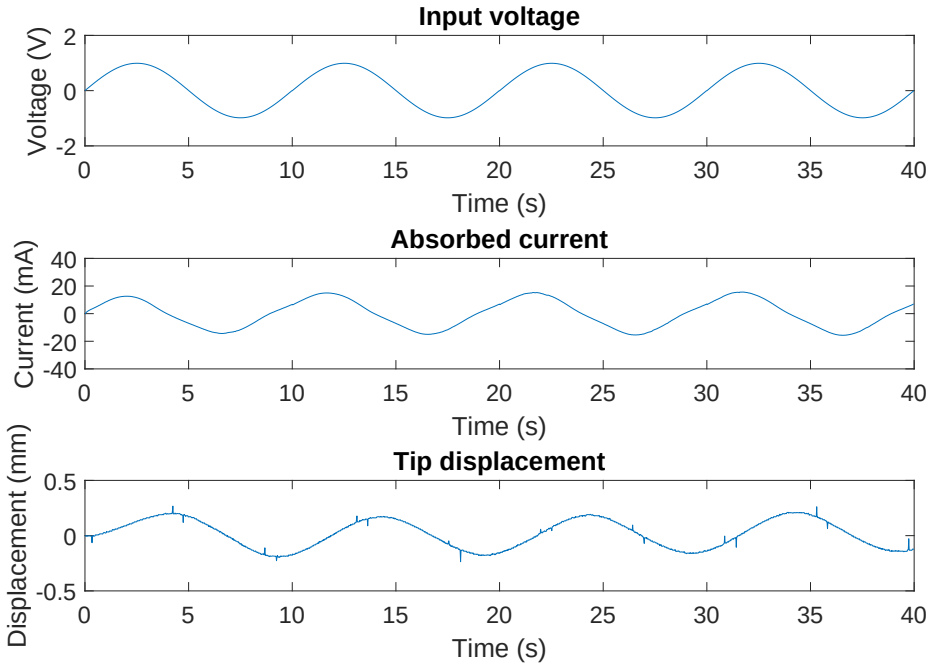

Figure 5.55: Displacement for 1 V sine input for N1110 7 mgPt/cm^2 sample

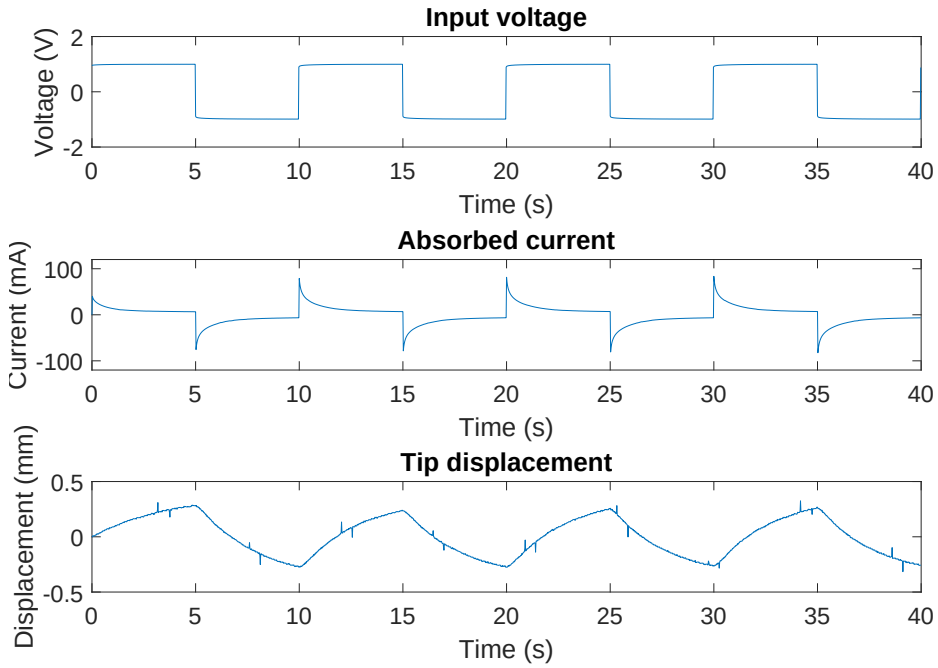

Figure 5.56: Displacement for 1 V square input for N1110 7 mgPt/cm^2 sample

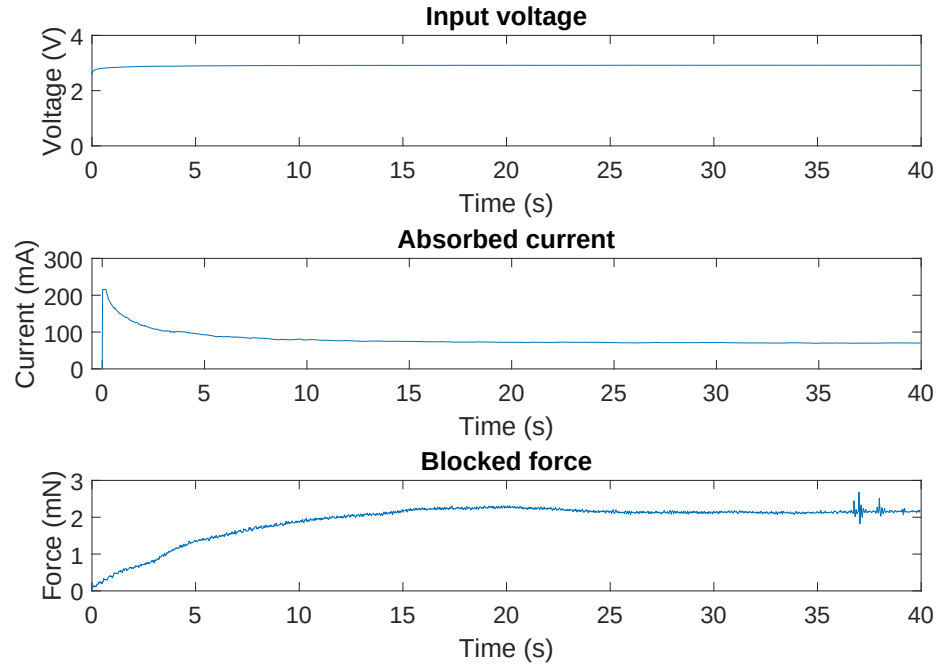

Figure 5.57: Force for 3V step input for N1110 7 mgPt/cm^2 sample

5.1.7 N1110 5 mgPt/cm^2 (Sample 7)

The last sample to be investigated was made from Nafion N1110 and was plated with 5 mgPt/cm^2. It was cut into a sample of 30 mm x 5 mm for the following experiments. The dry weight of the sample was 87 mg and after it was submerged in deionized water for 24 hours it weighed 101 mg. To determine if the sample can be used in room conditions the displacement was measured when no voltage was applied and was plotted in Figure 5.58. The experiment was repeated in 20°*C* 80 %RH and the displacement was plotted in Figure 5.59. All the experiments were done in 20°*C* 80 %RH and with a constant clamping pressure.

The displacement for different input signals was measured. In Figure 5.60 the input voltage, absorbed current and tip displacement for a 1 V step input is illustrated. The maximum displacement was 0.37 mm and the current drawn had a peak of 57.96 mA and a steady state value of 2.8 mA.

Figure 5.61 shows the input voltage, absorbed current and tip displacement for a 1 V sine wave with a frequency of 0.1 Hz. The maximum displacement was 0.08 mm and the maximum current drawn was 11.6 mA. This sample has a very small displacement as the N117 5 mgPt/cm^2 loading also had a small displacement and the higher stiffness makes it even smaller.

Figure 5.62 shows the input voltage, absorbed current and tip displacement for a 1 V square wave with a frequency of 0.1 Hz. The maximum displacement was 0.12 mm and the peak current was 58.6 mA and then it drops to 4.77 mA.

The blocked force was measured for a 3 V step input as the force at 1 V is very small and difficult to measure. Figure 5.63 illustrates the input voltage, absorbed current and blocked force for a 3 V step input. The maximum blocked force was 2.1 mN and the peak current drawn was 120.4 mA with a steady state value of 26 mA.

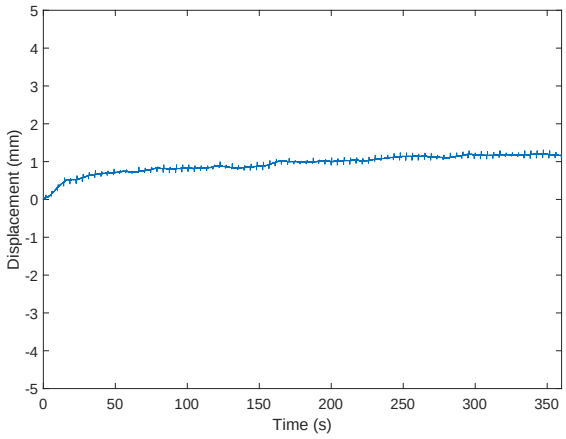

Figure 5.58: Baseline in room conditions for N1110 5 mgPt/cm^2 sample

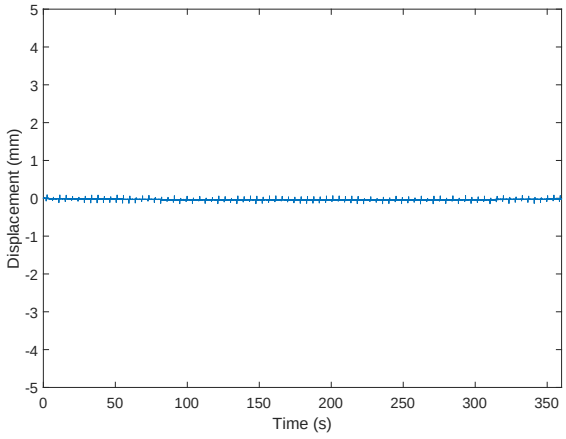

Figure 5.59: Baseline in 20°C 80 %RH for N1110 5 mgPt/cm^2 sample

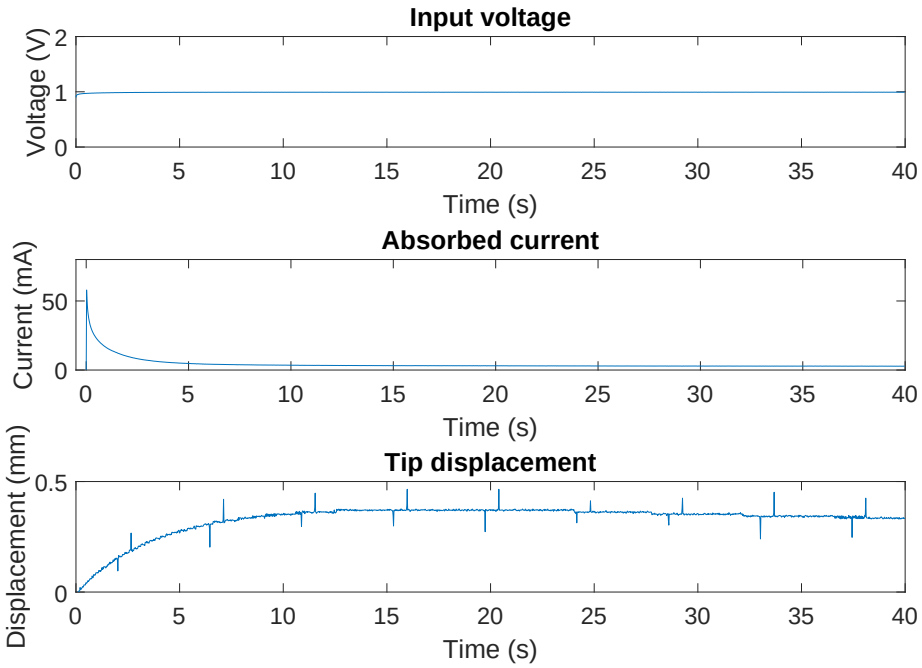

Figure 5.60: Displacement for 1 V step input for N1110 5 mgPt/cm^2

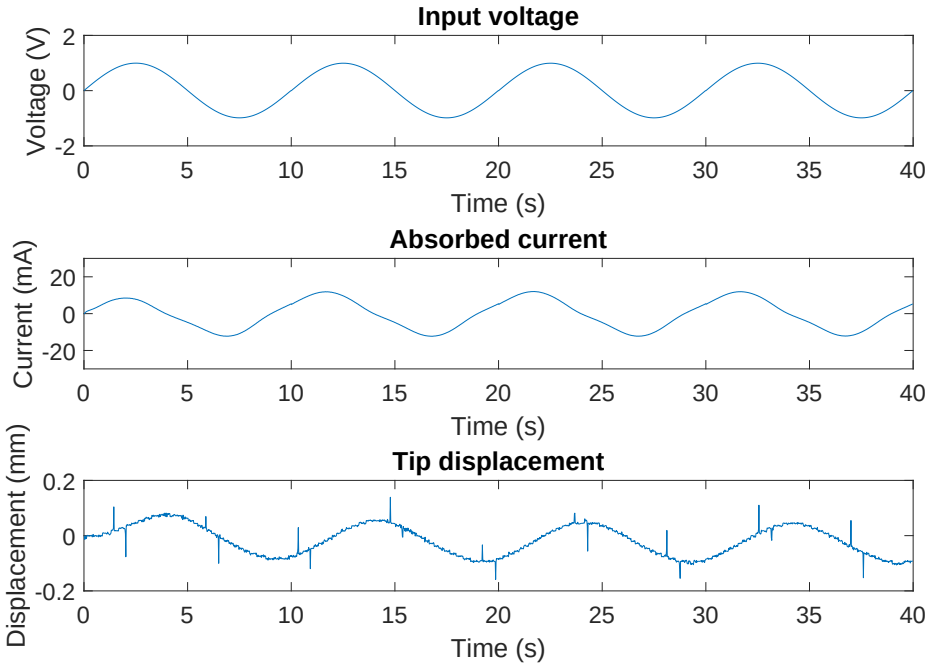

Figure 5.61: Displacement for 1 V sine input for N1110 5 mgPt/cm^2

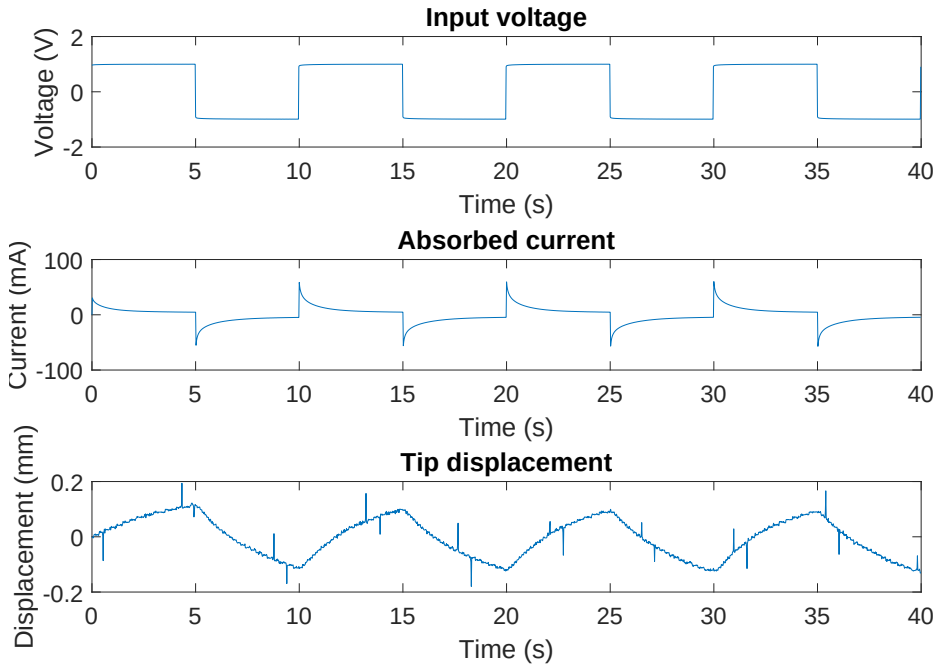

Figure 5.62: Displacement for 1 V square input for N1110 5 mgPt/cm^2

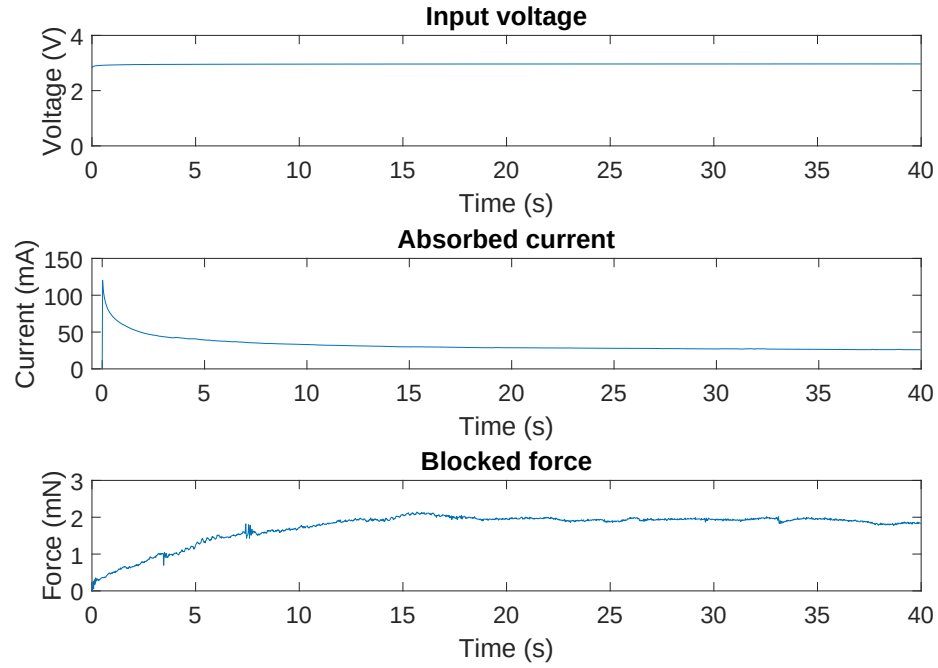

Figure 5.63: Force for 3V step input for N1110 5 mgPt/cm^2

5.1.8 Comparisons

The effect of the membrane thickness can be seen when comparing results from IPMCs with the same Platinum loading and different thicknesses. Figure 5.64 shows the effect that the thickness has on the free displacement. Figure 5.65 shows the effect of the membrane thickness on the blocked force. The IPMC samples used have a Platinum loading of 10 mgPt/cm^2. It is clear that a thicker membrane has a higher blocked force and a lower displacement than a thinner membrane. This result was expected as the thicker membrane makes the IPMC more stiff. Similar results are expected with the IPMCs with a lower Platinum loading. The rate at which the displacement decreases with an increase in membrane thickness is similar to the rate at which the force increases with an increase in membrane thickness.

To determine the effect that the Platinum loading has on the performance of the membrane, the displacement of all the different loadings of the same membrane thickness are plotted in Figure 5.66. For this comparison the N117 samples were compared as they have larger displacements. With the different Platinum loadings under investigation the higher loadings had larger displacements. It is expected that when the Platinum electrode layer is too thick the trend of an increase in displacement won't be there anymore. It has been shown in literature that there exists an optimal electrode thickness. The increase in displacement between the different Platinum loadings seem linear with the exception of the difference between the 2 and 5 mgPt/cm^2 samples. This can be due to the fact that the 2 mgPt/cm^2 sample has a more dense layer of Platinum than the other samples. To confirm this it could be tested with a sample that has the same amount of loading.

5.2 Validation

To validate the model the response of the model was tested for inputs that were not a part of the parameter estimation. The parameters were estimated by using a 1 V

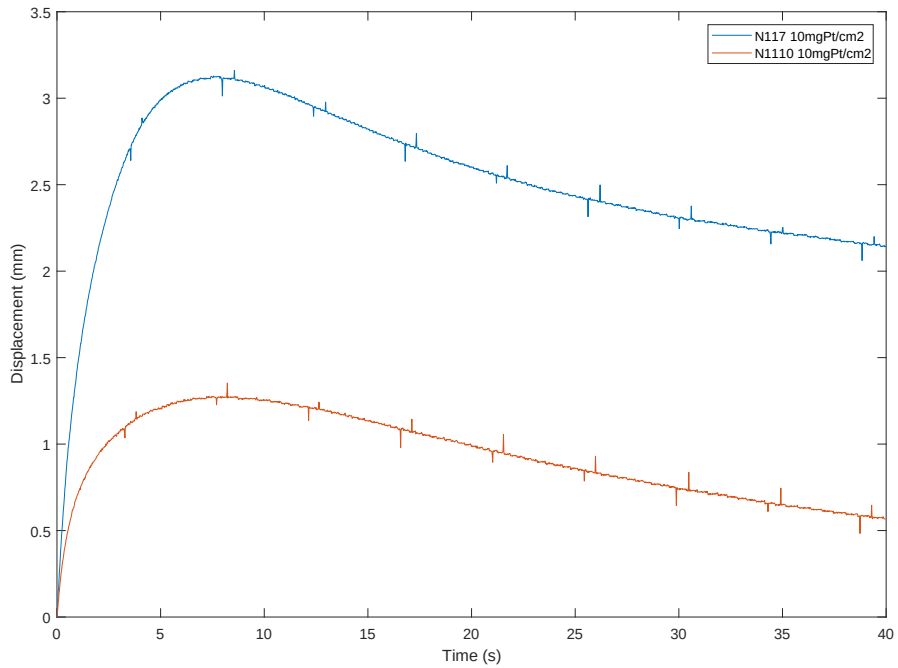

Figure 5.64: Displacement of IPMCs with different thicknesses and a Platinum loading of 10 mgPt/cm^2

step and sine input and using the blocked force and absorbed current to determine the parameters. The model was validated by comparing the model response to a 1 V square wave and predicting the blocked force. Also predicted free displacement was compared to the actual displacement. Figure 5.67 shows the measured and simulated blocked force for a square wave input with a frequency of 0.1 Hz. The model can accurately predict the blocked force under 1 V inputs. Figure 5.68 shows the simulated and measured displacement for a 1 V step input. The maximum values correspond but due to back relaxation, which is not included into the model, the outputs only correspond for the first 5 seconds of the experiment. This back relaxation can also be seen in the force output when a dc voltage is applied and thus the model also starts to deviate from the actual measurement after a few seconds. Figure 5.69 shows the measured and simulated displacement when a 1 V sine wave with a frequency of 0.1 Hz is applied. The form is predicted correctly but the amplitude of the measured value is significantly lower than predicted. The displacement's amplitude of the sine and square waves are lower than expected for all the samples that were tested. The model's

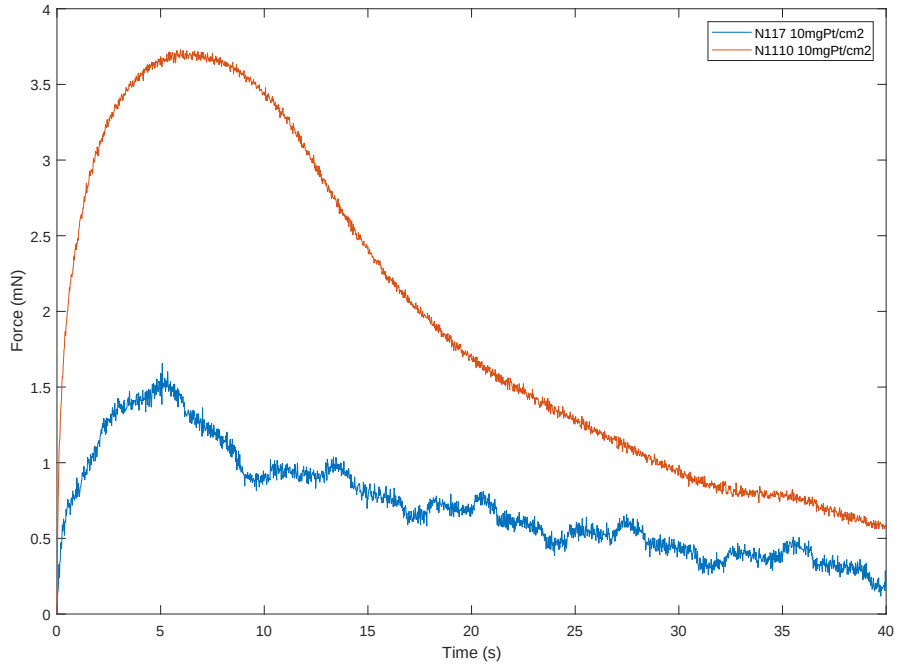

Figure 5.65: Blocked force of IPMCs with different thicknesses and a Platinum loading of 10 $mgPt/cm^2$

predicted displacement makes more sense as the peak value is achieved at around 5 s and thus the amplitude of the square waves must be close to the maximum values when a 0.1 Hz signal is applied. The model can thus predict the behaviour of the IPMC actuator. More investigations can be done to find out why the measured amplitudes of a 0.1 Hz sine and square wave are much lower than the dc amplitude.

5.3 Conclusion

In this chapter the 7 different samples were investigated. Samples varied in terms of the Platinum loading and the membrane thickness. Samples were tested in $20°C$ and $80\%RH$ as most samples started to curl when used in room conditions. The samples with the thickest loading where the least effected by testing in room conditions. Tests were also done at different humidities and temperatures to investigate the effect that it has on the response of the IPMC. It was seen that the displacement changes expo-

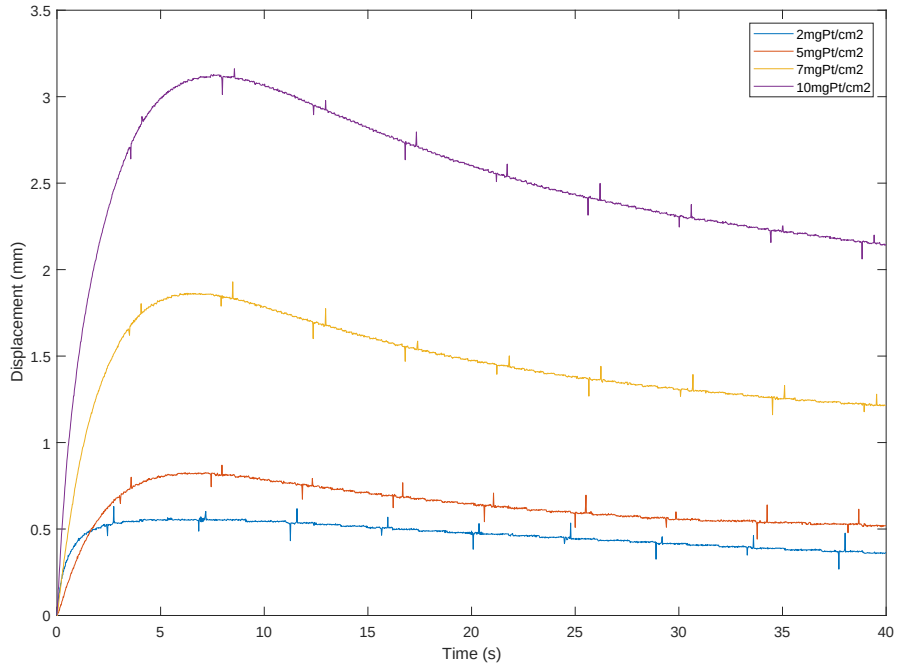

Figure 5.66: Displacement of IPMCs with different Platinum loadings for a Nafion N117 membrane

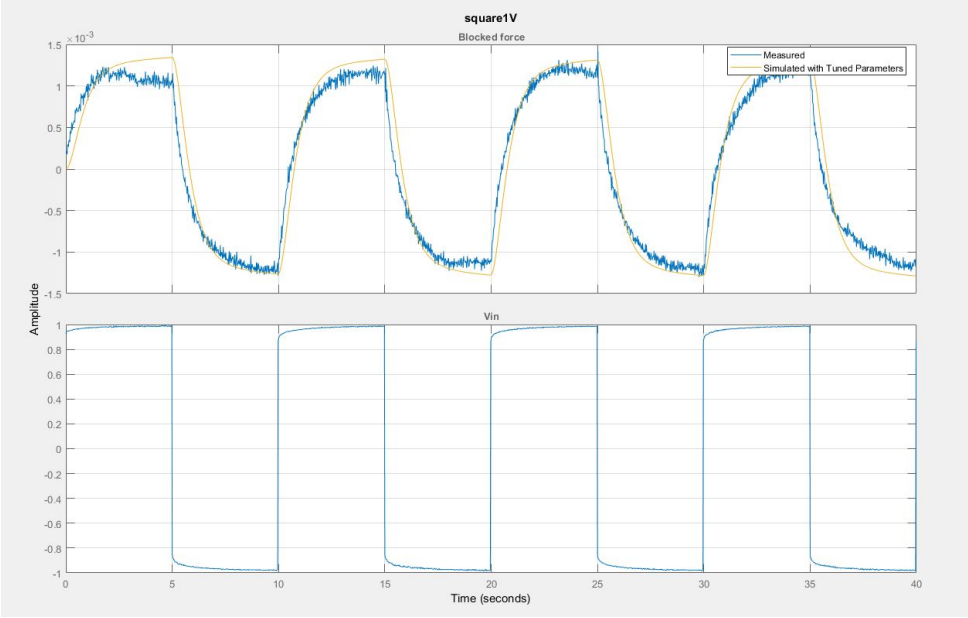

Figure 5.67: Simulated and measured force for sample 2 when a 1 V square input voltage is applied

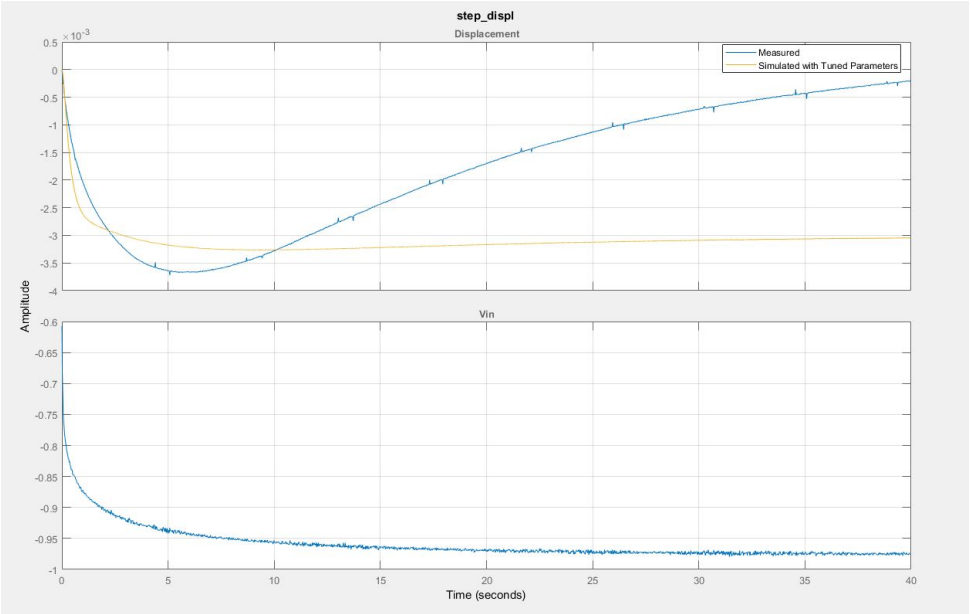

Figure 5.68: Simulated and measured displacement for sample 2 when a 1 V step input signal is applied

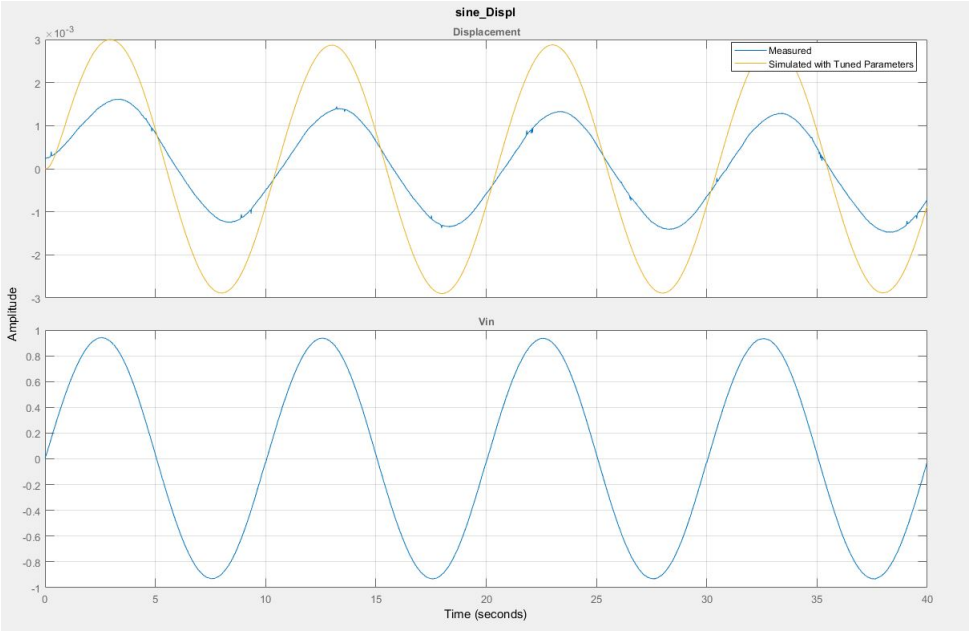

Figure 5.69: Simulated and measured displacement for sample 2 when a 1 V sine input signal with a frequency of 0.1 Hz is applied

nentially with both the humidity and the temperature. The blocked force also has an exponential increase with an increase in humidity. The response for different amplitudes and frequencies of the input voltage were also investigated.

The effect of the Platinum loading on the IPMC samples were investigated. It showed an approximately linear relationship, except for the difference between the 2 and 5 $mgPt/cm^2$ samples. The effect of thickness was also investigated and showed that an increase in thickness results in an increase in blocked force and a decrease in displacement as expected. The model discussed in the previous chapter was validated with experimental results. The model can sufficiently predict the force and displacement of the actuator when a 1 V signal is applied. The amplitude of the predicted displacement differs from the actual values for a sine wave. In all the displacement and force outputs back relaxation can be seen. Due to back relaxation that is not included in the model, the model can only correctly predict the first few seconds (until the peak) of the response for step inputs.

Chapter 6

Conclusion

In this chapter concluding remarks from the study are made. The results from the modelling and experimental characterization are discussed. Some recommendations for future work is given.

6.1 Discussion

This study consisted of a literature survey to see what research has been done on IPMCs and to gain more knowledge thereof. There are a wide variety of categories in which research has been done on IPMCs which includes improving the IPMC properties, modelling and control of IPMCs and using them in applications. In each of these categories there are various methods that have been proposed and that have shown successful results.

An experimental setup was designed to be able to apply a voltage signal to an IPMC and measure the absorbed current, applied voltage, tip displacement, and the blocked force. The main components of this setup are a data acquisition system, a load cell, a laser displacement sensor and the IPMC clamp. The laser sensor used is a optoNCDT1420-

25 from micro-epsilon. The load cell used is the GSO-10 from Transducer Techniques that is used together with the LCA-RTC load cell amplifier. A clamp was manufactured from aluminium. A NI cDAQ-9174 was used with the NI 9205,NI 9263 and NI 9217 modules. The experimental setup is placed inside the Espec SH-262 environmental chamber to be able to test at various temperatures and humidities.

To model the IPMC actuator a grey box model that makes use of an electrical equivalent circuit was used. The model consists of two parts, an electrical equivalent circuit and an electromechanical model. The model was implemented in Simulink and was verified with data from literature. Some parameters in the model must be determined from experimental data and for this the parameter estimation in Simulink was used. Simulated data was used as to verify that the parameter estimation delivers sufficient results. From this the model was developed for a 30 mm x 5 mm N117 sample with a Platinum loading of 10 mgPt/cm^2. The model could determine the electrical parameters to find a good fit to the experimental absorbed current. The model could fit the data sufficiently to the blocked force.

Seven different samples were used throughout this study. The samples varied in terms of the Platinum loading and the membrane thickness. Samples were tested in 20°C and 80 %RH as most samples started to curl when used in room conditions when no voltage was applied. The samples with the thickest loading where the least effected by testing in room conditions. Tests were also done at different humidities and temperatures to investigate the effect that it has on the response of the IPMC. It was seen that the displacement changes exponentially with both the humidity and the temperature. The blocked force also has an exponential increase with an increase in humidity. The response for different amplitudes and frequencies of the input voltage were also investigated. The effect of the Platinum loading on the IPMC samples was investigated. It showed an approximately linear relationship, except for the difference between the 2 and 5 mgPt/cm^2 samples. The effect of thickness was also investigated and showed that an increase in thickness results in an increase in blocked force and a decrease in displacement as expected.

The model used in Chapter 4 was validated with experimental results. The model can sufficiently predict the force and displacement of the actuator when a 1 V signal is applied. The amplitude of the predicted displacement differs from the actual values for a sine wave.

6.2 Future work

There are still many aspects of the IPMC that can be investigated further. The experimental data from the effect that the environmental conditions have on the actuator can be used to incorporate it into the model to be able to predict the behaviour in various environments. There were some deviations in the measured data that requires further investigations to determine the exact reason it occurs. The model can be improved by adding the nonlinear section in the electrical equivalent circuit to be able to predict behaviours at higher voltages correctly.

The work can be extended to investigate and model an IPMC as a sensor. If the model is further improved, studies can be done to use the model and implement a control system on it. The experimental setup can be used for these studies with minor changes.

The software or Matlab script used has space for improvement. Improvements like including a GUI to make it easier to use and including real time plotting can be done. With further studies it can be tested if is possible to create the same data acquisition using the Labview software as it has many possibilities for a GUI. Extra features like random signals or a signal with a changing frequency can be added as an output signal.

6.3 Conclusion

An overview and conclusion of the entire study is given in this chapter. Various results and ideas for future work was discussed. From this study it can be seen that it is

possible to model the behaviour of an IPMC actuator with a simple grey box model. In this study a linear electrical equivalent circuit is used to predict the absorbed current of the IPMC when a voltage is applied. The circuit was simplified to a linear model as it was mainly developed for predicting the behaviour at voltages lower than 1.2 V. As water electrolysis occurs at this voltage it introduces a nonlinear current absorption in the actuator.

Together with the electrical equivalent circuit, equations for a clamped beam was used to predict the force and displacement. The equations use the current calculated in the electrical circuit together with physical parameters to determine the displacement and force for an input voltage. Experimental data was used to determine some of the model parameters.

Experimental data was used to validate the model. The model could sufficiently predict the behaviour of the actuator under 1 V inputs. When step input voltages were applied back relaxation was seen in the displacement and blocked force. The model doesn't include back relaxation and could therefor only accurately predict the first few seconds. The experimental output had the same ramp and when the maximum output was reached the experimental output started to decrease where the simulated output stayed constant.

Various lessons were learned and there are possibilities for further studies on IPMCs. There are various ways the model can still be improved like including the nonlinear section in the electrical equivalent circuit, including components that change with the environmental conditions and including back relaxation into the model. The experimental setup was easy to use and functional but can be improved by changing the clamp to something smaller to have more space in the environmental chamber. Other sensors can be added to help improve the accuracy for large displacements.

Bibliography

[1] M. Vahabi, E. Mehdizadeh, M. Kabganian, and F. Barazandeh, "Experimental identification of
ipmc
actuator parameters through incorporation of linear and nonlinear least squares methods," *Sensors and Actuators A: Physical*, vol. 168, no. 1, pp. 140 – 148, 2011. [Online]. Available: http://www.sciencedirect.com/science/article/pii/S0924424711001634

[2] C. Bonomo, L. Fortuna, P. Giannone, and S. Graziani, "A circuit to model the electrical behavior of an ionic polymer-metal composite," *Circuits and Systems I: Regular Papers, IEEE Transactions on*, vol. 53, no. 2, pp. 338–350, Feb 2006.

[3] K. J. Kim and M. Shahinpoor, "Ionic polymermetal composites: Ii. manufacturing techniques," *Smart Materials and Structures*, vol. 12, no. 1, p. 65, 2003. [Online]. Available: http://stacks.iop.org/0964-1726/12/i=1/a=308

[4] M. Shahinpoor and K. J. Kim, "The effect of surface-electrode resistance on the performance of ionic polymer-metal composite (ipmc) artificial muscles," *Smart Materials and Structures*, vol. 9, no. 4, p. 543, 2000. [Online]. Available: http://stacks.iop.org/0964-1726/9/i=4/a=318

[5] Y. Gong, J. Fan, C. yin Tang, and C. pong Tsui, "Numerical simulation of dynamic electro-mechanical response of ionic polymer-metal composites," *Journal of Bionic Engineering*, vol. 8, no. 3, pp. 263 – 272, 2011. [Online]. Available: http://www.sciencedirect.com/science/article/pii/S1672652911600383

[6] H. Moeinkhah, J.-Y. Jung, J.-H. Jeon, A. Akbarzadeh, J. Rezaeepazhand, K. C. Park, and I.-K. Oh, "How does clamping pressure influence actuation performance of soft ionic polymermetal composites?" *Smart Materials and Structures*, vol. 22, no. 2, p. 025014, 2013. [Online]. Available: http://stacks.iop.org/0964-1726/22/i=2/a=025014

[7] C.-Y. Yu, Y.-W. Zhang, and G.-D. J. Su, "Reliability tests of ionic polymer metallic composites in dry air for actuator applications," *Sensors and Actuators A: Physical*, vol. 232, pp. 183 – 189, 2015. [Online]. Available: http://www.sciencedirect.com/science/article/pii/S0924424715300248

[8] C. Jo, D. Pugal, I.-K. Oh, K. J. Kim, and K. Asaka, "Recent advances in ionic polymermetal composite actuators and their modeling and applications," *Progress in Polymer Science*, vol. 38, no. 7, pp. 1037 – 1066, 2013. [Online]. Available: http://www.sciencedirect.com/science/article/pii/S0079670013000373

[9] J. W. Paquette, K. J. Kim, and D. Kim, "Low temperature characteristics of ionic polymermetal composite actuators," *Sensors and Actuators A: Physical*, vol. 118, no. 1, pp. 135 – 143, 2005. [Online]. Available: http://www.sciencedirect.com/science/article/pii/S0924424704005412

[10] H. Lei, C. Lim, and X. Tan, "Humidity-dependence of ipmc sensing dynamics: characterization and modeling from a physical perspective," *Meccanica*, vol. 50, no. 11, pp. 2663–2673, 2015. [Online]. Available: http://dx.doi.org/10.1007/s11012-015-0164-6

[11] K. Kikuchi and S. Tsuchitani, "Effects of environmental humidity on electrical properties of ionic polymer-metal composite with ionic liquid," in *ICCAS-SICE, 2009*, Aug 2009, pp. 4747–4751.

[12] R. Caponetto, S. Graziani, F. Pappalardo, and F. Sapuppo, "Identification of ipmc nonlinear model via single and multi-objective optimization algorithms." *ISA transactions*, vol. 53, no. 2, pp. 481–8, Mar 2014.

[13] Y. Tan, R. Dong, and H. He, "Model based hysteresis compensation for ipmc sensors," in *Control (CONTROL), 2014 UKACC International Conference on*, July 2014, pp. 268–272.

[14] R. Dong and Y. Tan, "A model based predictive compensation for ionic polymer metal composite sensors for displacement measurement," *Sensors and Actuators A: Physical*, vol. 224, pp. 43 – 49, 2015. [Online]. Available: http://www.sciencedirect.com/science/article/pii/S0924424715000175

[15] D. Q. Truong and K. K. Ahn, "Modeling of an ionic polymer metal composite actuator based on an extended kalman filter trained neural network," *Smart Materials and Structures*, vol. 23, no. 7, p. 074008, 2014. [Online]. Available: http://stacks.iop.org/0964-1726/23/i=7/a=074008

[16] B. Samaranayake, D. Preethichandra, A. Alahakoon, and K. Kaneto, "Modeling simulation and design of ionic polymer metal composite soft actuators," in *Industrial and Information Systems, 2007. ICIIS 2007. International Conference on*, Aug 2007, pp. 455–460.

[17] J. Simpson, R. Lumia, and M. Martinez, "Force and deflection modeling of ipmc fingers," in *Networking, Sensing and Control (ICNSC), 2013 10th IEEE International Conference on*, April 2013, pp. 136–140.

[18] C. Bonomo, L. Fortuna, P. Giannone, S. Graziani, and S. Strazzeri, "A nonlinear model for ionic polymer metal composites as actuators," *Smart Materials and Structures*, vol. 16, no. 1, p. 1, 2007. [Online]. Available: http://stacks.iop.org/0964-1726/16/i=1/a=001

[19] K. M. Newbury and D. J. Leo, "Linear electromechanical model of ionic polymer transducers -part i: Model development," *Journal of Intelligent Material Systems and Structures*, vol. 14, no. 6, pp. 333–342, 2003. [Online]. Available: https://doi.org/10.1177/1045389X03034976

[20] ——, "Linear electromechanical model of ionic polymer transducers -part ii: Experimental validation," *Journal of Intelligent Material Systems and*

Structures, vol. 14, no. 6, pp. 343–357, 2003. [Online]. Available: https://doi.org/10.1177/1045389X03034977

[21] L. Shi, S. Guo, and K. Asaka, "Modeling and experiments of ipmc actuators for the position precision of underwater legged microrobots," in *Automation and Logistics (ICAL), 2012 IEEE International Conference on*, Aug 2012, pp. 415–420.

[22] A. J. McDaid, K. C. Aw, E. Haemmerle, and S. Q. Xie, "A conclusive scalable model for the complete actuation response for ipmc transducers," *Smart Materials and Structures*, vol. 19, no. 7, p. 075011, 2010. [Online]. Available: http://stacks.iop.org/0964-1726/19/i=7/a=075011

[23] M. Diab, N. Al Awar, M. Atieh, R. Abou Marak, M. Salloum, O. Mustapha, and N. Mobayed, "Electromechanical model of ipmc artificial muscle," in *Computer Applications Research (WSCAR), 2014 World Symposium on*, Jan 2014, pp. 1–5.

[24] L. Hao, Y. Chen, and Z. Sun, "The sliding mode control for different shapes and dimensions of ipmc on resisting its creep characteristics," *Smart Materials and Structures*, vol. 24, no. 4, p. 045040, 2015. [Online]. Available: http://stacks.iop.org/0964-1726/24/i=4/a=045040

[25] S. Kang, W. Kim, H. Jin Kim, and J. Park, "Adaptive feedforward control of ionic polymer metal composites with disturbance cancellation," *Journal of Mechanical Science and Technology*, vol. 26, no. 1, pp. 205–212, 2012. [Online]. Available: http://dx.doi.org/10.1007/s12206-011-0916-8

[26] W. Liao, T. Yan, A. Wang, S. Wen, and X. Chen, "Robust nonlinear control design for an ipmc by using abc-based operator approach," in *Society of Instrument and Control Engineers of Japan (SICE), 2015 54th Annual Conference of the*, July 2015, pp. 440–444.

[27] A. Hunt, Z. Chen, X. Tan, and M. Kruusmaa, "Control of an inverted pendulum using an ionic polymer-metal composite actuator," in *Advanced Intelligent Mechatronics (AIM), 2010 IEEE/ASME International Conference on*, July 2010, pp. 163–168.

[28] L. Fu, A. McDaid, and K. Aw, "Control of an ipmc actuated robotic surgical tool with embedded interaction sensing," in *Advanced Intelligent Mechatronics (AIM), 2013 IEEE/ASME International Conference on*, July 2013, pp. 1255–1259.

[29] C. Gonzalez and R. Lumia, "An ipmc microgripper with integrated actuator and sensing for constant finger-tip displacement," *Smart Materials and Structures*, vol. 24, no. 5, p. 055011, 2015. [Online]. Available: http://stacks.iop.org/0964-1726/24/i=5/a=055011

[30] R. Lumia and M. Shahinpoor, "Ipmc microgripper research and development," *Journal of Physics: Conference Series*, vol. 127, no. 1, p. 012002, 2008. [Online]. Available: http://stacks.iop.org/1742-6596/127/i=1/a=012002

[31] S.-M. Cho and D.-W. Lee, "A biomimetic micro-collector based on an ionic polymer metal composite," *Microelectronic Engineering*, vol. 86, no. 4, pp. 916–919, 2009.

[32] R. K. Jain, S. Majumder, and A. Dutta, "Scara based peg-in-hole assembly using compliant ipmc micro gripper," *Robotics and Autonomous Systems*, vol. 61, no. 3, pp. 297–311, 2013.

[33] R. Jain, S. Datta, and S. Majumder, "Design and control of an ipmc artificial muscle finger for micro gripper using emg signal," *Mechatronics*, vol. 23, no. 3, pp. 381 – 394, 2013. [Online]. Available: http://www.sciencedirect.com/science/article/pii/S0957415813000408

[34] G.-H. Feng and S.-C. Yen, "Micromanipulation tool replaceable soft actuator with gripping force enhancing and output motion converting mechanisms," in *Solid-State Sensors, Actuators and Microsystems (TRANSDUCERS), 2015 Transducers-2015 18th International Conference on*. IEEE, 2015, pp. 1877–1880.

[35] S. Bhattacharya, B. Bepari, and S. Bhaumik, "Novel approach of ipmc actuated finger for micro-gripping," in *Informatics, Electronics Vision (ICIEV), 2015 International Conference on*, June 2015, pp. 1–6.

[36] R. Chattaraj, S. Bhattacharya, B. Bepari, and S. Bhaumik, "Design and control of two fingered compliant gripper for micro gripping," in *Informatics, Electronics Vision (ICIEV), 2014 International Conference on*, May 2014, pp. 1–6.

[37] S. Guo, L. Shi, N. Xiao, and K. Asaka, "A biomimetic underwater microrobot with multifunctional locomotion," *Robotics and Autonomous Systems*, vol. 60, no. 12, pp. 1472–1483, 2012.

[38] M. Yamakita, N. Kamamichi, T. Kozuki, K. Asaka, and Z.-w. Luo, "Control of biped walking robot with ipmc linear actuator," in *Advanced Intelligent Mechatronics. Proceedings, 2005 IEEE/ASME International Conference on*. IEEE, 2005, pp. 48–53.

[39] K. Takagi, M. Yamamura, Z.-W. Luo, M. Onishi, S. Hirano, K. Asaka, and Y. Hayakawa, "Development of a rajiform swimming robot using ionic polymer artificial muscles," in *Intelligent Robots and Systems, 2006 IEEE/RSJ International Conference on*, Oct 2006, pp. 1861–1866.

[40] Y. chu Chang and W.-J. Kim, "Aquatic ionic-polymer-metal-composite insectile robot with multi-dof legs," *Mechatronics, IEEE/ASME Transactions on*, vol. 18, no. 2, pp. 547–555, April 2013.

[41] L. Shi, S. Guo, S. Pan, Y. He, and P. Guo, "A multifunctional underwater microrobot for mother-son underwater robot system," in *Robotics and Biomimetics (ROBIO), 2013 IEEE International Conference on*, Dec 2013, pp. 1007–1012.

[42] Z. Chen, T. I. Um, and H. Bart-Smith, "A novel fabrication of ionic polymermetal composite membrane actuator capable of 3-dimensional kinematic motions," *Sensors and Actuators A: Physical*, vol. 168, no. 1, pp. 131 – 139, 2011. [Online]. Available: http://www.sciencedirect.com/science/article/pii/S0924424711000963

[43] D. N. C. Nam and K. K. Ahn, "Design of an ipmc diaphragm for micropump application," *Sensors and Actuators A: Physical*, vol. 187, pp. 174 – 182,

2012. [Online]. Available: http://www.sciencedirect.com/science/article/pii/S0924424712005092

[44] V. K. Nguyen, J. W. Lee, and Y. Yoo, "Characteristics and performance of ionic polymermetal composite actuators based on nafion/layered silicate and nafion/silica nanocomposites," *Sensors and Actuators B: Chemical*, vol. 120, no. 2, pp. 529 – 537, 2007. [Online]. Available: http://www.sciencedirect.com/science/article/pii/S0925400506001912

[45] G.-H. Feng and S.-Y. Hou, "A digital tactile actuator array with normal and shear contact force controllability for refreshable braille display application," in *Solid-State Sensors, Actuators and Microsystems (TRANSDUCERS), 2015 Transducers - 2015 18th International Conference on*, June 2015, pp. 835–838.

[46] G. D. Pasquale, S. Graziani, A. Pollicino, and S. Strazzeri, "A vortex-shedding flowmeter based on ipmcs," *Smart Materials and Structures*, vol. 25, no. 1, p. 015011, 2016. [Online]. Available: http://stacks.iop.org/0964-1726/25/i=1/a=015011

[47] P. Brunetto, L. Fortuna, P. Giannone, S. Graziani, and F. Pagano, "A small scale viscometer based on an ipmc actuator and an ipmc sensor," in *Instrumentation and Measurement Technology Conference (I2MTC), 2010 IEEE*, May 2010, pp. 585–589.

[48] S. Park, J. Ahn, J. Lee, S. Park, H.-M. Kim, K. Park, G. Hwang, M. Kim, S. Baek, and G.-S. Byun, "An ionic polymer metal composite based electrochemical conversion system in the ocean," *International Journal of Electrochemical Science*, vol. 9, no. 12, pp. 8067–8078, 2014, cited By 1. [Online]. Available: http://www.scopus.com/inward/record.url?eid=2-s2.0-84908690029&partnerID=40&md5=2d42e443e4f64d8c2136b576fb8c1d86

[49] K. Kruusamäe, A. Punning, A. Aabloo, and K. Asaka, "Self-sensing ionic polymer actuators: A review," *Actuators*, vol. 4, no. 1, p. 17, 2015. [Online]. Available: http://www.mdpi.com/2076-0825/4/1/17

Appendix A

Matlab scripts

A.1 Model setup

```
% RUN SCRIPT BEFORE SIMULATING MODEL

% physical parameters
Lt = 25e-3;      %Length of unclamped part verander na lf
Lc = 5e-3;       %Length of clamped part
b = 5e-3;        %Width of sample
h = 0.245e-3;    %Thickness of sample
Ls = Lt - 4e-3 ; %Length where measurements are taken

% electrical parameters
% Any values to start parameter estimation with
e1 = 0.1694;        %permitivity of C1
e2 = 0.0285;        %permitivity of C2
p1 = 104.0542;      %resistivity of Rc1
p2 = 23.9488;       %resistivity of Rc2
pdc = 43.862;       %resistivity of Rdc
```

```
% Measured surface resistance
Re = 8;                     %electrode resistance

% Determine from parameters above
R1 = pdc*h/(b*(Lt+Lc));     %dc resistance
Rc1 = p1*h/(b*(Lt+Lc));     %resistance branch 1
Rc2 = p2*h/(b*(Lt+Lc));     %resistance branch 2
C1 = (e1*b*(Lt+Lc))/h;      %capacitance branch 1
C2 = (e2*b*(Lt+Lc))/h;      %capacitance branch 2

% Mechanical parameters
density = 3.965e3;       %density of sample
Y = 1.45e9;              %Youngs modulus of sample 9.9e7 (724.36e6)
gamma = 1.875;  %Solution to characteristic equation
 %(1.875 for clamped-free beam)

% strain coefficient (d) parameters
% Any values to start parameter estimation with
Kd = 2.144e-7;           % Gain of transfer function d
Zd = 141.66;             % zero of transfer function d
P1d = 94.56;             % pole 1 of transfer function d
P2d = 101.89;            % pole 2 of transfer function d
```

A.2 Data acquisition

```
%create session
s = daq.createSession('ni');
%add input and output channels
AO0 = addAnalogOutputChannel(s,'cDAQ2Mod2',0,'Voltage');    %9263
```

```
AI0 = addAnalogInputChannel(s,'cDAQ2Mod1',0,'Voltage');     %9205
AI1 = addAnalogInputChannel(s,'cDAQ2Mod1',1,'Voltage');     %9205
%AI2 = addAnalogInputChannel(s,'cDAQ2Mod1',2,'Voltage');     %9205
AI3 = addAnalogInputChannel(s,'cDAQ2Mod1',3,'Voltage');     %9205

%setup channels select if load cell or laser sensor is going to be used
AI0.Range = [-0.2, 0.2];           %Absorbed current -200m - 200m V expected
AI1.Range = [-10, 10];             %laser sensor 2 - 10V expected
%AI2.Range = [-5, 5];              %load cell 0- 10V expected
AI3.Range = [-5, 5];               %Input voltage -5 - 5 V expected

%set sampling rate of session
s.Rate = 50;

%open file to log data
fid1 = fopen('exp1.bin','w'); %change file name for each experiment to ensure it
      %is not overwritten

%generate output data
%freq = sRate/samples in wave
%Define the output signal
%data_out = -1*linspace(1,1,500)'; %generate dc voltage
%generate sine wave frequency dependant on ratio of wave samples to sampling rate
data_out = 1*sin(linspace(0,2*pi,500))';
%data_out = 1*square(linspace(0,2*pi,500))'; % generate square wave "

%data_out = 1*cos(linspace(0,2*pi,500))'; %gx = senerate cos wave 0.1Hz
%data_out = sawtooth(linspace(0,2*pi,500),0.5)'; % generate triangular wave "



%queue data to be sent to AO0
```

```
queueOutputData(s,data_out);


%create listener to read and create data
%lhI = addlistener(s,'DataAvailable',@(src,event) plot(event.TimeStamps,
%event.Data)); live plot of data

%logging of data
lhI = addlistener(s,'DataAvailable',@(src,event)logData(src, event, fid1));

s.NotifyWhenDataAvailableExceeds = s.Rate;

%queue data
lh = addlistener(s,'DataRequired',@(src,event) src.queueOutputData(data_out));
s.IsContinuous = true;

%start generating and recording data
s.startBackground();
%Duration data is going to be generated and measured in s
pause(40);
%stop data
s.stop;
%close file and delete listeners
delete(lh);
delete(lhI);
fclose(fid1);

%READ DATA FROM BIN FILE

%open saved data file
fid2 = fopen('exp1.bin','r');
```

```
%read data
[data,count] = fread(fid2,[4,inf],'double');
fclose(fid2);

%select between ch1 and ch2 if force or displacement was measured
t = data(1,:);
ch0 = data(2,:);
ch1 = data(3,:);
%ch2 = data(3,:);
ch3 = data(4,:);

%Select if force or displacement was measured
time = transpose(t);
Current = transpose(ch0);
Volt = transpose(ch3);
Displ = transpose(ch1);
%Force = transpose(ch2);



Current = Current*1000; %Convert current measured to mA
Displ = 1*(((Displ/500)*1000)-4)/16*25; %Convert displacement measured to mm
Displ = Displ -12.3; %zero the starting displacement

% Force = 1*(Force/10)*100; % Convert voltage to Force in mN
% Force = Force - 4.48; %zero the starting force

%Comment out the unused figure when force or displacement was measured

figure;
%subplot(3,1,2);
plot(time, Current);
```

```
title('Absorbed current');
xlabel('Time (s)');
ylabel('Current (mA)');
xlim([-0 40]);
ylim([-0 120]);

%figure;
%subplot(3,1,1);
plot(time, Volt);
title('Input voltage');
xlabel('Time (s)');
ylabel('Voltage (V)');
xlim([0 40]);
ylim([-0 2]);

figure;
%subplot(3,1,3);
plot(time, Displ);
%title('Tip displacement');
xlabel('Time (s)');
ylabel('Displacement (mm)');
xlim([0 40]);
ylim([-0 5]);



% figure;
% plot(time, Force);
% title('Measured force');
% xlabel('Time (s)');
% ylabel('Force (mN)');
% xlim([0 40]);
```

```
% ylim([-10 10]);
```